VILNIUS GEDIMINAS TECHNICAL UNIVERSITY

Jūratė JANUTĖNAITĖ-BOGDANIENĖ

CONTROL OF PIEZOROBOTS' TRAJECTORIES FOR NANOSATELLITE STABILIZATION

DOCTORAL DISSERTATION

TECHNOLOGICAL SCIENCES,
MECHANICAL ENGINEERING (T 009)

VGTU
LEIDYKLA
Vilnius TECHNIKA 2019

Doctoral dissertation was prepared at Vilnius Gediminas Technical University in 2015–2019.

Supervisor

Prof. Dr Habil. Genadijus KULVIETIS (Vilnius Gediminas Technical University, Mechanical Engineering – T 009).

The Dissertation Defense Council of Scientific Field of Mechanical Engineering of Vilnius Gediminas Technical University:

Chairman

Assoc. Prof. Dr Artūras KILIKEVIČIUS (Vilnius Gediminas Technical University, Mechanical Engineering – T 009).

Members:

Prof. Dr Habil. Rimantas BARAUSKAS (Kaunas University of Technology, Informatics – N 009),

Prof. Dr Miguel Angel FERNANDEZ SANJUAN (Rey Juan Carlos University, Spain, Physics – N 002),

Prof. Dr Habil. Rimantas KAČIANAUSKAS (Vilnius Gediminas Technical University, Mechanical Engineering – T 009),

Prof. Dr Vytautas TURLA (Vilnius Gediminas Technical University, Mechanical Engineering – T 009).

The dissertation will be defended at the public meeting of the Dissertation Defense Council of Mechanical Engineering in the Senate Hall of Vilnius Gediminas Technical University at **1 p. m. on 15 November 2019**.

Address: Saulėtekio al. 11, LT-10223 Vilnius, Lithuania.

Tel.: +370 5 274 4956; fax +370 5 270 0112; e-mail: doktor@vgtu.lt

A notification of the intended defence of the dissertation was sent on 14 October 2019. A copy of the doctoral dissertation is available for review at VGTU repository http://dspace.vgtu.lt and at the Library of Vilnius Gediminas Technical University (Saulėtekio al. 14, LT-10223 Vilnius, Lithuania).

VGTU leidyklos TECHNIKA 2019-048-M mokslo literatūros knyga

ISBN 978-609-476-201-7

jurate.janutenaite@vgtu.lt

VILNIAUS GEDIMINO TECHNIKOS UNIVERSITETAS

Jūratė JANUTĖNAITĖ-BOGDANIENĖ

PJEZOROBOTŲ TRAJEKTORIJŲ VALDYMAS NANOPALYDOVŲ STABILIZAVIMUI

DAKTARO DISERTACIJA

TECHNOLOGIJOS MOKSLAI,
MECHANIKOS INŽINERIJA (T 009)

VGTU
LEIDYKLA
Vilnius TECHNIKA 2019

Disertacija rengta 2015–2019 metais Vilniaus Gedimino technikos universitete.

Vadovas

prof. habil. dr. Genadijus KULVIETIS (Vilniaus Gedimino technikos universitetas, mechanikos inžinerija – T 009).

Vilniaus Gedimino technikos universiteto Mechanikos inžinerijos mokslo krypties disertacijos gynimo taryba:

Pirmininkas

doc. dr. Artūras KILIKEVIČIUS (Vilniaus Gedimino technikos universitetas, mechanikos inžinerija – T 009).

Nariai:

prof. habil. dr. Rimantas BARAUSKAS (Kauno technologijos universitetas, informatika – N 009),

prof. dr. Miguel Angel FERNANDEZ SANJUAN (Rey Juan Carlos universitetas, Ispanija, fizika – N 002),

prof. habil. dr. Rimantas KAČIANAUSKAS (Vilniaus Gedimino technikos universitetas, mechanikos inžinerija – T 009),

prof. dr. Vytautas TURLA (Vilniaus Gedimino technikos universitetas, mechanikos inžinerija – T 009).

Disertacija bus ginama viešame Mechanikos inžinerijos mokslo krypties disertacijos gynimo tarybos posėdyje **2019 m. lapkričio 15 d. 13 val.** Vilniaus Gedimino technikos universiteto senato posėdžių salėje.

Adresas: Saulėtekio al. 11, LT-10223 Vilnius, Lietuva.

Tel.: (8 5) 274 4956; faksas (8 5) 270 0112; el. paštas doktor@vgtu.lt

Pranešimai apie numatomą ginti disertaciją išsiųsti 2019 m. spalio 14 d.

Disertaciją galima peržiūrėti VGTU talpykloje http://dspace.vgtu.lt ir Vilniaus Gedimino technikos universiteto bibliotekoje (Saulėtekio al. 14, LT-10223 Vilnius, Lietuva).

Abstract

Rapid industrial advancement requires novel ideas, new scientific approaches and effective technologies that would ensure quality and precision. Application of piezoelectric actuators in robotics opens many possibilities to create systems with extreme precision and control. A very important step in the development of autonomous robots is the formation of motion trajectories. Classical interpolation methods used for formation of the trajectories are suitable only when robots have wheels, legs or other parts for motion transmission. Piezorobots that are analyzed in this dissertation have no additional components that create motion, only contact points with the static plane. Therefore, traditional motion formation methods are not suitable and a problem arises how to define motion trajectory of such device.

The aim of this work is to create a trajectory control algorithm of multi-degrees-of-freedom piezorobot used for nanosatellite stabilization.

In order to achieve the objective, the following tasks had to be solved: to analyze constructions of precise piezorobots, their operating principles and motion formation methods; to analyze stabilization problems of satellites and application of multi-degrees-of-freedom piezorobots for nanosatellite stabilization; to create piezorobots' motion formation algorithms according to electrode excitation schemes, to perform an experimental research; to determine quantitative characteristics of the constructed piezorobots and their motion trajectories.

The introduction describes the importance and novelty of this thesis, goals of this work, its practical value and defended statements. The first chapter analyses the principals of ultrasonic devices, gives a thorough review of constructions of ultrasonic devices with multi-degrees-of-freedom. The second chapter provides a review of satellite stabilization principles and how multi-degrees-of-freedom piezorobots can be applied for nanosatellite stabilization. Motion formation methods for ultrasonic devices with multi-degrees-of-freedom are presented. The third chapter presents the detailed analysis of different piezorobots. In the fourth chapter experimental results are provided. Trajectory planning of piezorobot is shown, results are compared to numerical calculations performed in the third chapter. The conclusions about applicability of piezorobots' motion formation algorithms according to electrode excitation schemes are given. Seven articles focusing on the subject of the dissertation have been published, two presentations on the subject have been presented in conferences at international level.

The research for the dissertation has been funded by the Lithuanian State Science and Studies Foundation: European Regional Development Fund, Project No. DOTSUT-234 and Research Council of Lithuania, Project No. MIP-084/2015.

Reziumė

Spartėjanti pramonės pažanga reikalauja naujų mokslinių sprendimų ir našių, kokybę užtikrinančių technologijų. Pjezokeitiklių taikymas robotikoje leidžia sukurti didelio tikslumo ir valdymo sistemas. Kuriant autonominius robotus ypač svarbus yra judesio trajektorijų formavimo uždavinys. Trajektorijų formavimui taikomi klasikiniai interpoliavimo metodai yra tinkami tik tuomet, kai robotas turi judesį perduodančias dalis. Disertacijoje nagrinėjami pjezorobotai neturi jokių papildomų judesį generuojančių dalių, tik kontaktinius taškus su statine plokštuma. Todėl tradiciniai judesio formavimo metodai netinka ir reikalingi kitokie metodai aprašantys tokio pjezoroboto judesio trajektorijas.

Šio darbo tikslas yra sukurti kelių laisvės laipsnių pjezorobotų trajektorijų valdymo algoritmą nanopalydovų stabilizavimui.

Darbe sprendžiami šie pagrindiniai uždaviniai: atlikti pjezorobotų konstrukcijų analizę; išnagrinėti jų veikimo principus ir judesio formavimo metodus; išanalizuoti palydovų padėties stabilizavimo problemas ir pjezorobotų pritaikymo galimybes nanopalydovų stabilizavimui; sukurti pjezorobotų judesio formavimo metodą, atsižvelgiant į elektrodų žadinimo schemas; atlikti skaitinę analizę ir eksperimentinius tyrimus; nustatyti sukurtų pjezorobotų kiekybines charakteristikas ir judesio trajektorijas.

Disertaciją sudaro įvadas, keturi pagrindiniai skyriai, išvados, naudotos literatūros ir mokslinių publikacijų disertacijos tema sąrašai, ir 5 priedai. Įvade aprašyti darbo aktualumas, tikslas, metodika, tyrimų uždaviniai, mokslinis naujumas, praktinė reikšmė ir ginamieji teiginiai. Pirmame skyriuje apžvelgiami pjezokeitiklių veikimo principai, daugiamačių pjezokeitiklių konstrukcijų analizė. Antrame skyriuje apžvelgiami palydovų padėties stabilizavimo principai bei su stabilizavimu susijusios problemos. Pristatomi judesio formavimo metodai daugiamačiams pjezorobotams. Trečiame skyriuje pateikiama išsami pjezorobotų skaitinė analizė. Skaitinė analizė atlikta naudojant baigtinių elementų metodą. Pateikiami pjezorobotų judesio trajektorijų formavimo algoritmai atsižvelgiant į elektrodų segmentų žadinimo schemas, bei kontaktinių taškų judėjimo trajektorijos. Ketvirtame skyriuje pristatomi eksperimentų rezultatai. Pateikiamas trajektorijų planavimas, palyginami skaitinės analizės ir eksperimentų rezultatai. Pateikiamos išvados apie pjezorobotų judesio formavimo algoritmų pagal elektrodų žadinimo schemas pritaikomumą. Disertacijos tema paskelbti 7 straipsniai, pristatyti 2 pranešimai tarptautinėse konferencijose.

Moksliniai tyrimai buvo finansuoti Europos regioninės plėtros fondo, projektas Nr. DOTSUT-234 ir Lietuvos mokslo tarybos, projektas MIP-084/2015.

Notations

A – amplitude of oscillation;
α, β – angles;
b – minor axis;
$[C]$ – elasticity matric;
$[\boldsymbol{c^E}]$ – matrix of stiffness tensor for a constant electric field;
$\{\delta\}$ – displacement vector;
$[\boldsymbol{e}]$ – matrix of piezoelectric constants;
E – Young's modulus;
h – height;
k – longitudinal vibration.
$[\boldsymbol{\zeta^S}]$ – matrix of dielectric constants at permanent deformations;
l – length;
m_{jk}^n – domination coefficient;
$[\boldsymbol{M}]$, $[\boldsymbol{K}]$, $[\boldsymbol{T}]$, $[\boldsymbol{S}]$ – structural matrices of a finite element;
ν – Poison's ratio;
n – number of eigenfrequency;
$\boldsymbol{n}$ – number of degrees of freedom;
P_i – driving torque acting at the *i*-th joint;
$\boldsymbol{q}$ – joint coordinates of manipulator;
$\{\boldsymbol{Q}\}$ – vector of electrical charge;

ρ – density;
$\{\sigma\}$ – mechanical stress vector;

Abbreviations

FEM – finite element method;
MEMS – micromechanical systems.

Contents

[1] The annexes are supplied in the enclosed compact disc.

Introduction

Problem formulation

Due to the technological advancement robots are being applied more often and in various fields. It is desired to make processes autonomous and to create robots that are smaller, faster, requiring less production costs. New materials, control methods, technologies are being applied and various scientific experiments are being conducted in creation of piezorobots. Piezoelectric actuators are one of the most efficient technologies applied in control of piezorobots.

Piezoelectric actuators are known for their small size, light weight, high precision, no electromagnetic interference, simple design. Researchers like Zhao C., Ragulskis K., Uschino K., Ikeda T., Tzou H. S. and many more have made great contributions in research of these devices and their possible application areas. Piezoelectric actuators are widely applied in industrial, medical, automotive, aviation, aerospace and consumer electronics. They are also used in cryogenic and vacuum environments, because piezoelectric actuators require no lubrication to operate.

Piezorobots are used in various devices for precision positioning and control problems. They can be successfully applied for the stabilization and positioning of nanosatellites. However, traditional motion formation methods are not suitable for piezorobots and a problem arises how to plan and control trajectories.

Scientists have presented different constructions that ensure motion in desired direction, but most of the proposed solutions have additional components such as hinges or levers. This leads to an increased size of the device.

In this thesis a multi-degrees-of-freedom piezorobots which do not have any additional motion generating components are presented. Motion formation algorithms are created to ensure the precise movement of the piezorobot.

Relevance of the thesis

The analyzed piezorobots do not have additional structures that generate the motion. They only have contact points with the static plane or a manipulated object. Linear motion is created when one electrode segment is excited and rotational motion is created when all electrodes are excited at the same time. When two electrodes are excited at the same time a continuous linear motion is generated. Therefore, traditional trajectory planning algorithms are not suitable and such piezorobots require different trajectory formation algorithm.

These piezorobots have low mass, low energy consumption and operate in high precision. Due to these favourable properties, piezorobots can be successfully applied in nanosatellites where functionality must be maintained regardless of the reduced size. The motion formation algorithm according to electrode schemes presented in this work ensures that multi-degrees-of-freedom piezorobot moves accordingly to trajectory planning algorithm.

The object of research

The object of the investigation is motion trajectories of piezorobots' contact points under different excitation schemes.

The aim of the thesis

The aim of this work is to create a trajectory control algorithm of multi-degrees-of-freedom piezorobot used for nanosatellite stabilization.

The objectives of the thesis

1. To analyze operating principles of ultrasonic motors, to analyse their constructions for creating precision devices and precise piezorobots.

2. To analyze stabilization problems of satellites and application of multi-degrees-of-freedom piezorobots for nanosatellite stabilization, to deduce motion formation methods for precise piezorobots.
3. To create a mathematical model of analyzed kinematic pairs, perform numerical analysis and create piezorobots' motion formation algorithms according to electrode excitation schemes.
4. To perform an experimental research, determine quantitative characteristics of constructed piezorobots and their motion trajectories, compare the experimental results with results of numerical analysis.

Research methodology

The research was done by applying analytical, theoretical and experimental results. Literature analysis was done to analyse the operating principles of piezorobots, their constructions, application of piezorobots for nanosatellite stabilization and motion formation methods for piezorobots. Mathematical modeling techniques have been applied to compile and analyze numerical algorithms. Comparative analysis methods were applied to investigate qualitative characteristics of contact points motion trajectories of piezorobot.

Numerical analysis was done using finite element method, ANSYS software, MATLAB software. Experiments were conducted using National Instruments software and hardware, MATLAB software, impedance analyzer Wayne Kerr 6500B laser vibrometer system OFV-5000/505, 3D scanning vibrometer PSV-500-3D-HV, a linear amplifier P200.

Scientific novelty of the thesis

Motion trajectories of classical robots are defined using classical interpolation methods. They describe functions which define a state of a moving object at any given time. However, these methods are not suitable for analysed robots.

The presented multi-degrees-of-freedom piezorobots do not have any additional components for motion creation; only contact points with the static plane. Any type of motion trajectory can be successfully controlled using complex electrical signals. The proposed motion formation algorithm according to electrode excitation schemes allows to determine the trajectories of contact points. Because motion direction and intensity of any point is known, trajectories of piezorobot can be planned and controlled. It is possible to stabilize a nanosatellite and to apply the proposed solution for the positioning of a nanosatellite swarm.

Practical value of the research findings

The created motion control algorithm under different excitation schemes of multi-degrees-of-freedom piezorobot can be applied for numerical analysis of other piezorobots.

A piezorobot with three contact points can be used as a basis for manipulating robots or nanosatellite stabilization. The proposed motion formation algorithms according to electrode excitation schemes enables to determine and calculate motion trajectories of contact points at any given time. This allows to plan and control trajectories of the piezorobot. Such piezorobots can be applied in microscopic manipulators, positioning devices and nanosatellites.

The research results were submitted to a high-tech program “R&D of New Class of Trunk Like Robots: Theory and Investigation (SmartTrunk)” funded by the Reasearch Council of Lithuania (No. DOTSUT-234 and No. MIP-084/2015). Project supervisor prof. dr habil Ramutis Bansevičius.

The defended statements

1. Piezorobots with cylindrical and hemispherical actuators are a suitable choice for solving nanosatellite stabilization problems.
2. Numerical analysis has verified that the proposed mathematical model is suitable for dynamic analysis.
3. Results of the numerical analysis of cylindrical and hemispheric actuators corresponds to the results of experimental analysis.

Approval of the research findings

7 scientific papers have been published on the subject of the thesis: 5 papers have been published in journals included in “Clarivate Analytics Web of Science” database and 2 papers have been published in “Clarivate Analytics Web of Science” database Conference Proceedings.

The author has made 2 presentations at 2 scientific conferences:

- Open conference of Electrical, Electronic and Information Sciences (eStream) April 27, 2017, Vilnius, Lithuania.
- Mechanika 12–13, May, 2016, Kaunas, Lithuania.

The structure of the dissertation

The thesis is composed of introduction, four chapters, general conclusions, a list of references, author's list of publications on the topic of the dissertation.

The thesis consists of 98 pages excluding annexes, 18 numbered formulas, 64 figures and 6 tables.

1

Analysis of precise ultrasonic motors with multi-degrees-of-freedom

Traditional motors based on electromagnetic principle have been successfully used in many fields. However, due to advanced technologies such as spaceships, launch vehicles, satellites, precision instruments, new requirements have arisen which cannot be fulfilled using traditional solutions. It is required that devices would be small sized, light weight, without any electromagnetic interference, etc. Motors which satisfy these requirements are ultrasonic motors. They utilize inverse piezoelectric effect of piezoelectric materials and resonance frequencies of the stator. These motors are compact, flexible, have large torque density. Various vibrations (longitudinal, torsional, bending) can be excited thus a device needs less components. Loads are directly driven by high torque at low speed and do not require gear. A rotor has small inertia, fast response, self-locking, and a high holding torque. It is easy to control position or velocity; such motors ensure high resolution of displacement having micro or nano-scale precision. Other advantages are no electromagnetic interference, low noise, operating in extreme environmental conditions. Regardless of all these advantages, it is necessary to know drawbacks before applying ultrasonic motors. They have small power output and low efficiency, especially in case of inverse piezo effect. Their operational life is quite short due to friction and wear between stator and rotor; therefore, performance is reduced after long continuous operation. A circuit is

complex, because stator resonance excitation requires specific amplitude, frequency and phase, which change when the temperature varies. Regardless of these disadvantages ultrasonic motors are widely applied, an ongoing research is trying to minimize the negative effects. They are very useful as actuators in MEMS, have a great potential in biomedical engineering for cell manipulation. New frictional and piezoelectric materials are being developed so that motors could be applied in extreme environments. This is very important since ultrasonic motors are being increasingly applied in aerospace engineering.

Various researchers (Bansevicius et al. 1996; Zhao 2011; Ragulskis et al. 1988; Uchino and Giniewicz 2003, etc.) have analyzed piezoelectric actuators. They are successfully applied in positioning devices (Chen *et al.* 2014; Guo *et al.* 2015; Zhang and Xu 2018, etc.), as piezoelectric transformers (Carazo 2016), for optogenetic control of neural activity (Rizzo *et al.* 2018) and many other solutions. Their favorable properties as light weight, high precision, rapid movement lead to applications in satellites and nanosatellites (Allegranza *et al.* 2014). A problem that is encountered and can be successfully solved using piezorobots is stabilization of nanosatellite; various authors have proposed their solutions to address this (Bansevicius *et al.* 2015a; Navickaitė *et al.* 2015; Bručas *et al.* 2012). In this paper, the analyzed piezorobots do not have any additional components that create motion; therefore, traditional motion formation and trajectory planning algorithms are not suitable. It is possible to control such piezorobots with complex electrical signals, but this becomes a difficult problem. Trajectory planning algorithms have been proposed (Drukteiniene 2011; Bansevicius *et al.* 2018; Bansevicius *et al.* 2016a; Bansevicius *et al.* 2016b).

In this chapter the analysis of ultrasonic motors is given. Their operating principles are explained in detail, construction examples are presented and their applications are given. A large number of researches is analyzed and examples of scientists' works are shown. This chapter answers the question why the discussed ultrasonic motors are suitable for piezorobots used for stabilization of nanosatellites.

1.1. Principles of ultrasonic motors for piezorobots

One or several components of the ultrasonic motor are made from piezoelectric materials. Currently there are three types of categories – inorganic piezoelectric materials, organic piezoelectric materials and piezoelectric composites. The first group of materials are known for their strong piezoelectricity, high dielectric constant, a feature to be formed into various shapes, but lacking mechanical quality factor, having poor stability and large electric loss. Mostly inorganic piezoelectric materials are used as high power transducers. Single crystals can be

used in devices for frequency control, high selectivity filters, high temperature ultrasonic transducers, etc. The second group of materials possess excellent flexibility, low density, small impedance, however due to their low piezoelectric strain constant, they are not so actively used as piezoelectric actuators. The final group of materials combine ceramics and polymers. They have better properties than their initial components and may even possess features that are non-existent in components. Due to these exceptional properties, piezoelectric composites are widely used in ultrasonic motors. All piezoelectric materials are dielectrics which means that in an electric field they produce net dipole moments. When choosing a material, it is necessary to check their properties – dielectric constant (describes a dielectric constant of the material in a static electric field), dielectric loss, electrical quality factor, elastic properties, electric parameters. Ultrasonic motors are based on inverse piezoelectric effect of piezoelectric ceramic elements. An elastic body is excited by stress or strain and produces a forced vibration response. This response is then transformed into motion. Functioning of ultrasonic motors is based on modes of elastic bodies. Mode is defined by natural frequency ω_n and shape φ_n. In a system, which is an elastic body with an infinite number of degrees-of-freedom, an infinite number of modes exist. Modal parameters depend on mass, stiffness distribution and boundary conditions. Ultrasonic motors utilize longitudinal vibrations of bars, torsional vibrations of shafts, bending vibrations of beams (The strain modes of bending vibration of beams), natural vibrations of plates, and natural vibration of cylindrical shells. Vibrations of plates can be divided into out-of-plane (bending) and in-plane (extension-contraction) vibrations. The most complex to analyze and to apply are cylindrical shells because they vibrate in three directions. As it has been proposed by Love (Zhao 2011), these are the assumptions for cylindrical shells:

- The thickness of a shell is smaller than other dimensions.
- Both strain and displacement are sufficiently small, so that the second and higher order variables can be neglected in strain-displacement relations.
- Normal stress along the Z direction in comparison with that of other directions can be neglected.
- A straight line normal to the neutral surface before the deformation remains the straight and perpendicular to the neutral surface after the deformation.

Excited vibrations in ultrasonic motors depend on material properties, geometrical parameters, boundary conditions, electrode schemes, polarization direction of used components. Depending on these parameters, longitudinal, torsional, bending, shear vibrations are excited. Ultrasonic motors differ by wave propagation methods. They are divided into standing and travelling wave types. A standing wave is a form of vibration when some points undergo zero amplitude

and others reach maximum amplitudes. These points (or nodes) remain fixed all the time. A standing wave motor directly utilizes the modes whereas travelling wave motor utilizes the rotation mode synthesized by two standing waves. Waves that occur in elastic bodies are plane and spherical waves, longitudinal waves, shear waves, surface waves. A detailed explanation is given in (Zhao 2011), where the author describes a standing wave as two superposed plane waves with the same amplitude but opposite directions in the transmissions. A combination of two travelling waves makes certain points in elastic body stationary at any time and other points reach a maximum amplitude. It is quite simple to generate a standing wave unlike travelling wave. The later can be created by using vibrator and absorber or synthesized by standing waves. Sashida proposed the first method, when two Langevin vibrators were used. One vibrator creates the travelling wave and the other absorbs it, so that the wave reflection is avoided. The second method is based on the excitation of two electrodes with the same voltage but different phase. Travelling wave ultrasonic motors are known for their high torque (Chen *et al.* 2006; Renteria-Marquez *et al.* 2018). A combination of standing and travelling waves can be used to drive a mobile micro-robot when one wave type creates a translational motion and the other creates a rotational motion (Bansevicius *et al.* 2013). A unimorph actuator with legs is used for motion of miniature mobile robots. A standing wave is used to generate bidimensional motion (Hariri *et al.* 2015). Resonant gyros operate with a specific wave type such as presented by authors (Xiang *et al.* 2012). In this case a cylindrical resonant gyro functionality is based on a standing wave.

Ultrasonic motors can be classified by their operational principles. They can be divided as proposed by (Ragulskis *et al.* 1988):

- Ultrasonic motors with oblique collision of high frequency. (Viscous friction hypothesis) These are based on superposition of tangential components of the impact pulse. Tangential component of the impact pulse is defined by an instantaneous friction of the impact and is independent of the magnitude of its normal component. (Dry friction hypothesis) Tangential component is proportional to its normal component. Coefficient of proportionality is equal to the coefficient of dry friction.
- Ultrasonic motors with frictional anisotropy of contacts. In these type of motors additional periodic actions of converters and the moving component are superposed. Contact anisotropy is achieved by locking the converter in a specified segment of trajectory by superimposing vibrations of higher frequencies.

- Ultrasonic motors based on wave motion. Frictional interaction of wave motion between the elastic body and a driven member is the operating principle for this type of motors. Flexural, shear, torsional and longitudinal vibrations of the travelling wave type of the translational vibration converters can be realized.
- Ultrasonic motors with asymmetrical vibration cycles. They are based on asymmetry of inertia forces, forces of dry friction or the nonlinear speed deformation. Their main advantage compared to other ultrasonic motors is higher resolution. Longitudinal or torsional vibrations with an asymmetrical acceleration during one vibration cycle are excited. This creates a sliding motion in the contact zone. It is a complicated process, because non-harmonic vibrations are hard to excite in high-frequency converters.
- Ultrasonic motors with controllable constraint in the contact zone. These motors are based on the periodical variable coupling between the vibrating element and the moving component. Electrorheological and magnetorheological liquids usually show the best results for such coupling. These liquids consist of a nonpolar dispersing medium and a solid disperse phase with high dielectric permittivity. Active ionic or non-ionic substances achieve the stability of properties.
- Ultrasonic motors with external torque. The driving force comes from outside; the motion nature of the driving component is defined by coupling between the them and stationary component. Such motors are applied when start-stop, stepping and motion at a constant speed is required.

It is possible to classify ultrasonic motors by other properties, such as presented in Table 1.1 or Fig. 1.1.

Different configurations of ultrasonic motors enable to achieve different functionality; therefore, they have been widely applied in many areas. Piezoelectric transformers are used to transform electrical energy into electrical energy by means of a mechanical vibration (Carazo 2016). Piezoelectric stacks are used to ensure translational and rotational movement. Such devices usually have the same number of actuators as the number of degrees-of-freedom as shown in Fig. 1.2b. One actuator is responsible for movement to one direction. An example of the piezoelectric stack application is mechanism of antenna positioning (shown in Fig. 1.2a). A platform responsible for antenna positioning has 4 piezoelectric actuators. Each of them is a piezoelectric stack and when the voltage is applied, piezoelectric stack expands and bridge type amplification mechanism generates displacements (Chen *et al.* 2014). Piezoelectric stacks usually display non-linear dynamic behavior; therefore, control mechanisms must

be implemented to control the motion (Gozen and Ozdoganlar 2012a; Gozen and Ozdoganlar 2012b).

Table 1.1. The proposed classification of ultrasonic motors (Ragulskis *et al.* 1988)

Motion type	Translational, rotational, complex motion
Conditions of motion	No loss of contact, disrupted contact
Nature of motion	Continuous or vibratory motion of moving component, stepping, start-stop
Method of speed control of moving components	Amplitude modulation of vibrations, phase modulation of vibrations variation of parameters of controllable nonlinearity
Motion synchronization	Asynchronous, synchronous
Number of degrees-of-freedom	1 DOF, 2–5 DOF, 6 DOF, unlimited
Feedback presence	Open, closed with feedback by position, speed, acceleration, or forces in the contact zone
Type of vibration converter	Piezoelectric, piezomagnetic, electrodynamic, electromagnetic, pneumatic

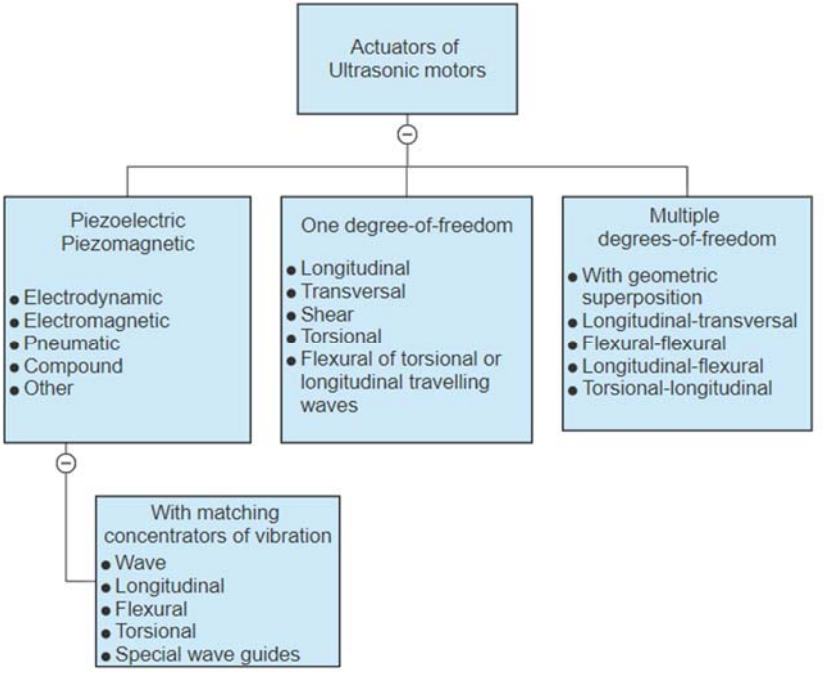

Fig. 1.1. Classification of ultrasonic transducers (Ragulskis K. *et al.* 1988)

Although the voltage input is the most common way to drive a piezoelectric actuator it leads to non-linear hysteresis and creep. They lead to errors, which is evident in positioning applications. Various methods have been proposed for hysteresis and creep elimination such as using charge input or inserting a capacitor for a piezoelectric actuator driven by a voltage input (Minase *et al.* 2010). A large number of degrees-of-freedom in a system leads to an increased size of the mechanism and a more complex control algorithm. Usually this leads to complex mechanisms that use additional components such as levers, hinges, screws, etc. A motion created by actuator is transferred to those components.

A piezoelectric ultrasonic linear motor that has a specific shape, which creates elliptical motion when excited has been presented by authors (Lee *et al*. 2011). Such movement is generated by combining a couple of vibration modes at a certain frequency range. In this case, it was carried out by combining longitudinal and transverse vibration modes.

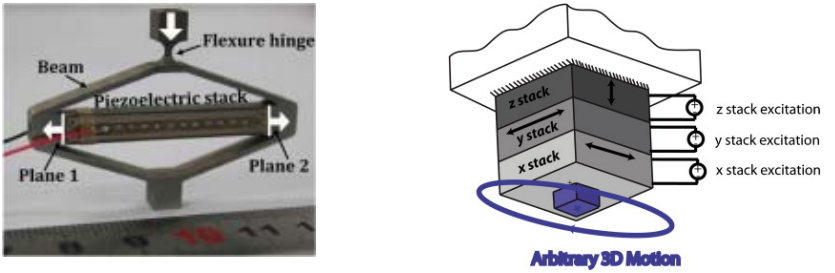

a) b)

Fig. 1.2. Examples of piezoelectric stack application: a) piezoelectric actuator for antenna positioning (Chen *et al.* 2014); b) general description of a three-axis piezo-stack actuator (Gozen and Ozdoganlar 2012a)

A square tube actuator rotates about *X* and *Y* axes depending on excited electrodes (Park *et al.* 2012). When opposing electrodes are applied a sinusoidal voltage, one electrode shrinks and the other expands thus creating motion. It is transferred through tube endpoints, which create reciprocating diagonal trajectories. Modes do not necessarily have to be resonant as shown by (Xu *et al.* 2017). An actuator can work in both resonance and non-resonance modes. A resonance mode is excited under alternating current and non-resonance mode under direct current signal. Elliptical movements at the driving feet are generated by two orthogonal bending vibration modes. When direct current is applied driving, feet produces a displacement with micro-scale under the static friction force between the driving foot and the mover. Image stabilization for compact

space camera has been achieved by using a two-axis moving platform (Janschek *et al.* 2007). A platform is driven by two piezo motors or piezo actuators, which use a combination of piezo-electric and friction forces to generate a progressive motion of an output element. Such motors or actuators are currently available for space application and have been applied in scanning mechanism of ROSETTA probe.

1.2. Constructions of ultrasonic devices with multi-degrees-of-freedom

A structure of an ultrasonic motor is made from simple components. These components can be classified by their shape into bars, beams, plates (uniform plates, rectangular plates, circular plates, circular ring plates), shells (cylindrical, hemispheric, etc.) as shown in Fig. 1.3.

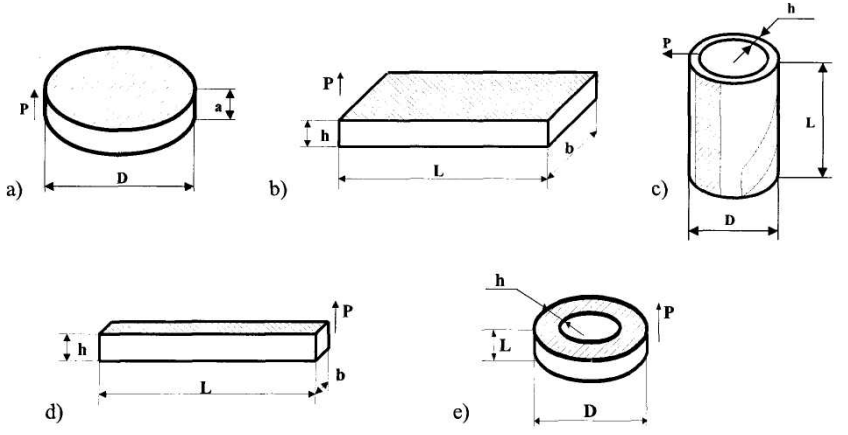

Fig. 1.3. Types of components for ultrasonic motors: a) disk; b) plate; c) cylinder; d) bar; e) ring (Tumasonienė 2009)

An interesting and complex type is an actuator (curved piezoelectric actuator) which is constructed as a circular beam with asymmetric surface bonded piezoelectric actuators (Kuang *et al.* 2009). An example of such system is given in Fig. 1.4. As authors (Guo *et al.* 2015) have proposed, planar flexure-based mechanism uses orthogonal piezoelectric actuators to create translation in *X* and *Y* directions and rotation around *Z* axis. For driving force translation and motion decoupling, six Double Circular Hinge Linkages (DCHL) are used and Dual Leaf

Parallelogram Hinge is used for motion guidance so that damage to piezoelectric actuators could be avoided. Another 3 DOF nano-positioning stage is made from platform that is driven by piezoelectric actuators with ball tips and levers ensure construction flexibility (Zhu *et al.* 2018). These lever mechanisms are used for displacement amplification. Dual-Axis Long-Traveling Nano-Positioning Stage comprises of a ball-screw stage and a three-degrees-of-freedom piezo-stage. The first stage is responsible for long travel and piezo-stage is used for precision. The moving directions for piezo-stage are along *X* and *Y* axes and rotation around Z axis. It is composed of a base, three PZT holders, three piezoelectric actuators, four translation and rotation mechanisms and a table. A translation and rotation mechanism was additionally developed to reduce the interference (Liu *et al.* 2010).

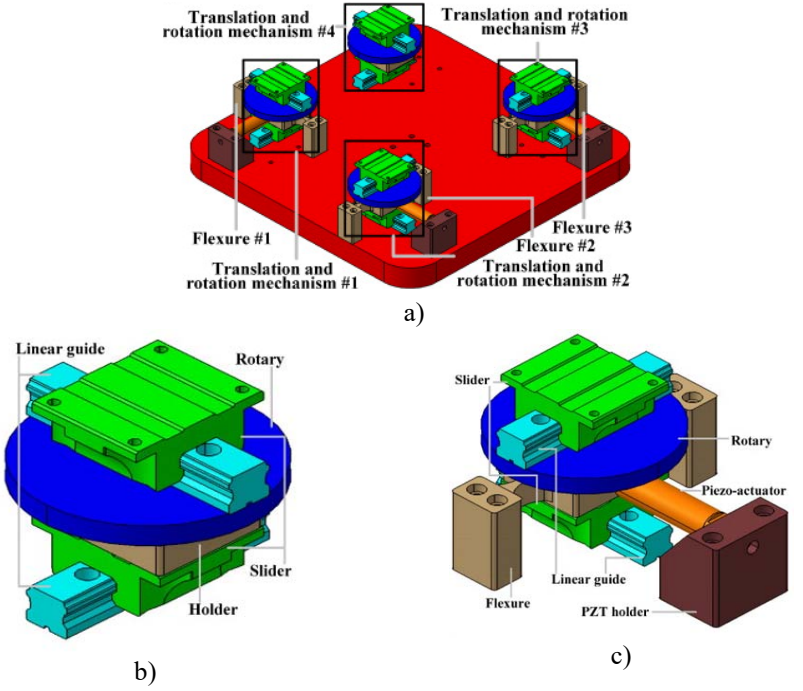

Fig. 1.4. The proposed 3 DOF low-interference nano-stage: a) the sketch of the structure; b) the translation and rotation mechanism; c) the translation and rotation mechanism with piezoactuator (Liu *et al.* 2010)

Various parallel mechanisms are used to improve the ability and performance such as a 6 DOF serial-parallel stage, which is combined of two 3 DOF

mechanisms (shown in Fig. 1.5). One 3 DOF mechanism is in-plane and provides translational X, Y and rotational θ_z movement and the second one (out-of-plane) provides one translational Z and two rotational θ_x, θ_Y movements (Cai *et al.* 2017). Mechanisms for nano manipulation were also presented in (Liaw *et al.* 2010, Liu *et al.* 2015, Zhang *et al.* 2018, Zheng *et al.* 2010, Richard *et al.* 2011). A platform for antenna positioning is driven by four piezoelectric actuators, which are constructed using a bridge type mechanism and piezoelectric stack (Chen *et al.* 2014). A piezo-actuated parallel pointing mechanism was constructed and presented (Du *et al.* 2014). A circular flexure hinge comprised of two orthogonal prismatic joints is used for piezoelectric stack protection and rotation performance.

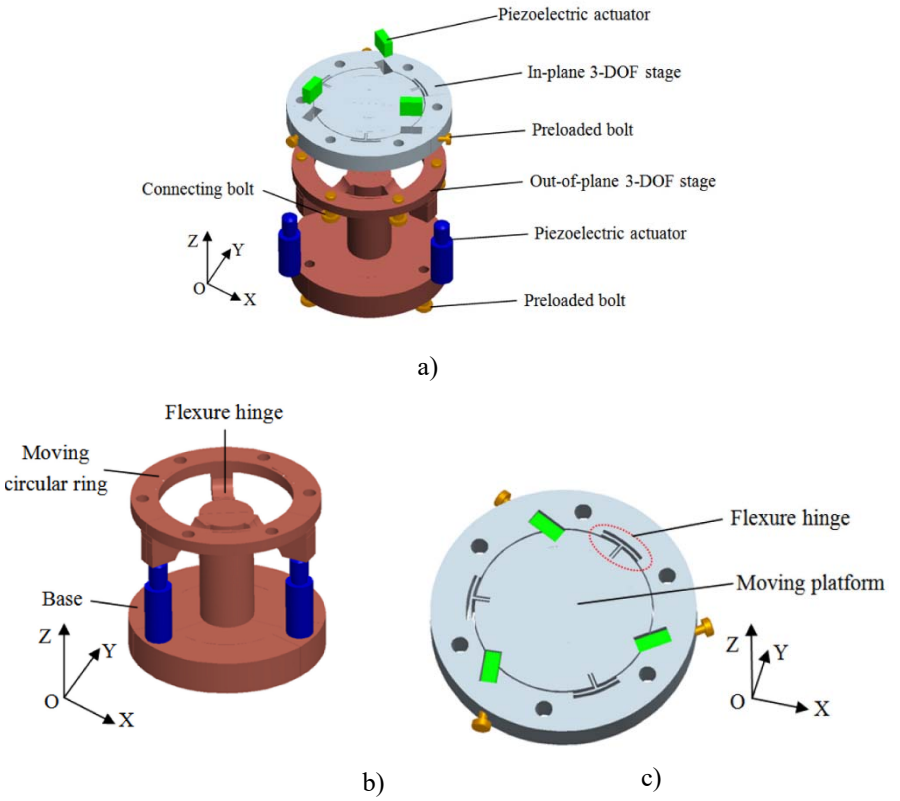

Fig. 1.5. A 6 DOF positioning system: a) exploded view;
b) the out-of-plane 3 DOF stage; c) the in-plane 3 DOF stage (Cai *et al.* 2017)

Several more flexure-based parallel mechanisms have been developed for micro/nano-manipulation (Kim and Gweon 2012, Tian *et al.* 2010, Pinskier *et al.* 2018, Kim *et al.* 2012, Qui *et al.* 2013, Shan *et al.* 2016, Choi *et al.* 2008, Choi K.B. *et al*. 2010). A piezoelectric membrane was applied in laser endoscopic device as a means of 3D imaging or ablation (Khayatzadeh *et al.* 2017a). The same authors have proposed a scanning device, which is comprised of piezoelectric cantilever, and an extended optical fiber is used for light beam scanning (Khayatzadeh *et al.* 2017b). Although only 1D movement was analyzed, it is possible to combine them in a more complex system for 2D scanning.

Due to piezoelectric material favorable properties such as small size and high accuracy, piezoelectric actuators have been applied and used in very complex problem solving such as optogenetic control of neural activity (Rizzo *et al.* 2018). Authors have proposed a four- axis piezoelectric stage for rotation and movement of tapered fiber to pattern TFs edge with complex light emission geometries. The proposed stage ensures translation in X, Y, Z directions and rotation around the taper axis and is shown in Fig. 1.6.

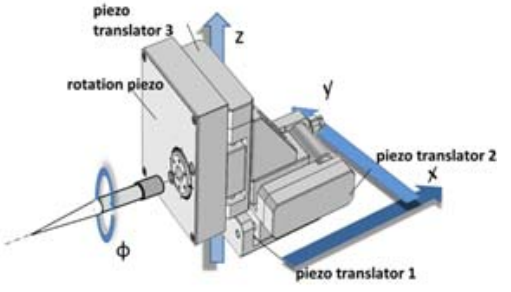

Fig. 1.6. Schematic of the four- axis piezoelectric stage for rotation and movement of tapered fiber (Rizzo *et al.* 2018)

Constructions that do not use many additional components have been analyzed and presented. A goal is to achieve a desired motion by controlling the way piezoceramic component of the ultrasonic motor deforms. An example is a linear piezoelectric transducer used in thin electronic devices. It is composed of an elastic plate, two protrusions, and two piezoelectric ceramics. Elastic plate is bent in the middle and the bent serves as tip for energy transfer (Lee *et al.* 2011). A piezoelectric substrate has 3 actuators screen-printed on to create linear motion for the slider (Bergander *et al.* 2004). Another example is a piezoceramic ring which is used to rotate the sphere positioned on top of the cylinder. The ring is

glued to a substrate and when voltage is applied, an elliptical movement is created and the sphere rotates (Gouda *et al.* 2016) as shown in Fig. 1.7. A similar ultrasonic motor has a thick-film PZT and electrode layers printed on an aluminum plate.

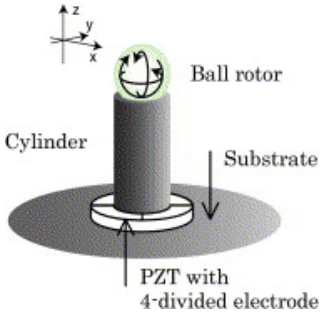

Fig. 1.7. A proposed structure of the multi-degree-of-freedom ultrasonic actuator (Gouda *et al.* 2016)

A cylinder that is placed in the center magnifies the lateral displacements of the rotor and transmits the driving force to the sphere (Aoyagi *et al.* 2002). Vibrations created by excitied piezoelectric bimorph beams are used to move a microrobot (Pan *et al.* 2010; Pan 2016). Stick and slip actuators are also successfully applied in microrobots. A 6 DOF parallel structure dedicated to the micro assembly of optical components was constructed using such components (Breguet *et al.* 1996).

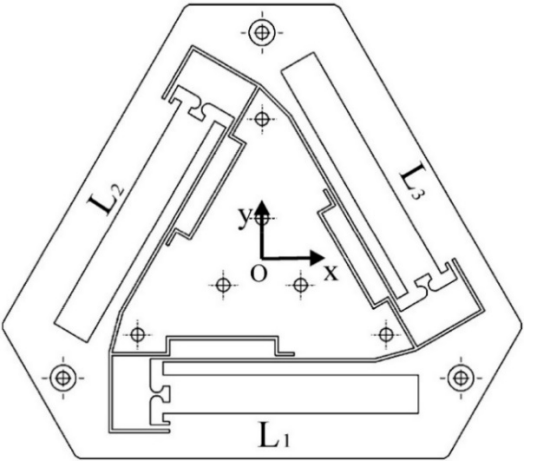

Fig. 1.8. Schematics of a 3 DOF compliant mechanism (Gan *et al.* 2017)

A piezoelectric transducer composed of 32 pieces of piezoelectric ceramics, two driving feet and one double-head flange bolt (Xu *et al.* 2017) is used for axial and vertical movement. Pieces of piezoelectric ceramics are divided in two groups and are made from different materials. Beryllium bronze sheets between the PZT plates serve as the electrodes. A square tube ultrasonic motor consists of two rotors, a shaft and a stator. PZT plates are bonded onto outside walls of the tube. There are two teeth at the opposite corners of each end of the brass tube. Two rotors are pressed against the teeth. Another 3 DOF compliant mechanism was presented by (Gan *et al.* 2017) and shown in Fig. 1.8. The platform provides translational movement in *X* and *Y* directions and rotational movement around Z axis. Three piezoelectric actuators are installed and used to create motion. The whole system additionally has micro-vision system, rapid prototyping controller board, an XE-500D controller, computer. Currently travelling wave rotary ultrasonic motor (TRUM) is used the most (Zhao 2011). The main components are stator, rotor, shell, bearing, spring, friction linear, PZT and base. Travelling wave is formed by superposition; the stator of TRUM is a ring plate of axial symmetry.

1.3. Conclusions of Chapter 1 and dissertation objectives

The analysis of ultrasonic motors and devices has shown that:

1. Ultrasonic motors work by using inverse piezo effect when an elastic body is excited and produces a forced vibration control. A forced vibration in ultrasonic motors is transformed into motion. Ultrasonic motors can be classified by various aspects such as a wave propagation method, vibration type, motion type, motion nature, the way they interact with other components in the system, etc.
2. Piezoceramic composites are usually used for the piezoceramic part of the motor. When choosing a material, it is necessary to evaluate their properties such as dielectric constant, dielectric loss, electrical quality factor, etc.
3. A choice of the device depends on the problem that is being solved. Various ultrasonic motors have been developed such as piezoelectric transformers, piezoelectric stacks, various mechanisms which are composed of levers, hinges or screws. The more degrees-of-freedom a system has, the more complex mechanism and control algorithm becomes as has been shown in this chapter. Although such mechanisms ensure high precision, rapid movement and proper operation, it is desired that they would be more compact and would have the same performance. This is

especially important in space technologies, because it is desired to reduce the costs of the spacecraft without losing any functionality.

4. Ultrasonic motors which do not use a lot of additional components have been proposed. Desired motion is achieved by controlling the way piezoceramic component of the ultrasonic motor deforms and what motion it creates. Their control is more complex; however, the benefits of reduced size and desired functionality make them a plausible choice in various problem solving and application for piezorobots.
5. The conclusions of the first chapter allow to formulate the objectives of the thesis:
    - To analyze operating principles of ultrasonic motors, to analyse their constructions for creating precision devices and precise piezorobots.
    - To analyze stabilization problems of satellites and application of multi-degrees-of-freedom piezorobots for nanosatellite stabilization, to deduce motion formation methods for precise piezorobots.
    - To create a mathematical model of analyzed kinematic pairs, perform numerical analysis and create piezorobots' motion formation algorithms according to electrode excitation schemes.
    - To perform an experimental research, determine quantitative characteristics of constructed piezorobots and their motion trajectories compare the experimental results with results of numerical analysis.

2

Application of piezorobots for nanosatellite stabilization

Space technology has become one of the most important areas of research. Various satellites are used not only for deep space exploration and analysis, but also for tasks such as weather forecasting, communication, Earth's observation. In the late 1980, the most active research direction in the field of space has become micro/nano-type satellites. They ensure functional density and technical performance, but at the same time do not require large investment and operating costs are flexible and have a short development cycle (Zheng 2017). Such satellites due to their small size and performance can not only perform various space tasks, but also can complete formation flight and virtual satellites, operate in multi-satellite network. Micro/nano satellites are now used in data communications and transition, navigation, positioning, ground and space monitoring, various scientific experiments, etc.

In this chapter satellite stabilization problems and various solutions are presented. Because current research focuses on nanosatellites, researchers have proposed solutions on how to decrease the size of some components by applying piezoelectric actuators. Further analysis shows that piezorobots can be successfully applied for nanosatellite stabilization. Because discussed piezorobots do not have additional components for motion generation, traditional trajectory planning algorithms are not suitable. At the end of the chapter, motion formation

methods for piezorobots is presented, conclusions provided. The material in this chapter was published in scientific journals (Janutėnaitė-Bogdanienė *et al.* 2017, Bansevicius *et al.* 2016a, Bansevicius *et al.* 2016b, Bansevicius *et al.* 2018, Grybas *et al.* 2016, Bansevičius *et al.* 2017, Mačerauskas *et al.* 2017).

2.1. Stabilization principles of satellites

All satellites are affected by gravity gradient, solar radiation pressure, magnetic, aerodynamic, and free molecular reaction forces. A satellite additionally may experience internal disturbances, which also affect the attitude. The most commonly known active stabilization methods are micro-thrusters, reaction wheels, and control momentum gyroscopes. Passive stabilization methods are dual spin, gravity gradient, spin stabilization, solar radiation pressure (SRP), aerodynamics, and Earth's magnetic field. Control algorithms for the satellite electromagnetic parameters allow to stabilize attitude position by geomagnetic field (Antipov *et al.* 2014). A solar radiation pressure is considered for the satellite pitch and roll stabilization while the yaw attitude is stabilized by a magneto-torque mechanism (Kumar *et al.* 2009). Attitude control of gyrostat-satellites is achieved using magnetic actuators (Doroshin 2017). It is possible to determine and control attitude of a satellite when it is passively magnetically stabilized (Burton *et al.* 2017). In such passive magnetic system, magnetically permeable rods are placed in the plane that is perpendicular to the axis, and permanent dipoles are aligned with the desired spin axis. Damping of angular motion is provided by magnetically permeable material and alignment to Earth’s magnetic field is provided by the permanent dipoles. A proposed satellite has no sensors or gyros and attitude is determined using only an estimate of the solar vector obtained from solar panel currents. Such stabilization system provides external torques, which resolve the rotational ambiguity around the single measurement vector. Some satellites include a full set of sensors and actuators for 3-axes stabilization, such as gyros, sun sensors, magnetic sensors, magnetic torque, and reaction wheels (Nakasuka *et al.* 2018). A magnetic torquer and reaction wheel are used as a combination for attitude maintenance. A reaction wheel cannot deal with its saturation and magnetic torquer cannot provide precise enough torque. There have been attempts to control using only a single type of actuator, such as using only magnetic actuation (Sofyal *et al.* 2018). This reduces the size of the satellite, but requires a more complex control mechanism and logic. Reaction spheres are also applied for satellite stabilization (Zhu *et al.* 2017). For multipoint operations a nanosatellite constellation may be used. However, their deployment is challenging due to mass, volume and power limitations. A de-orbiting mechanism using magnetic torquer interaction with space plasma has been proposed

(Park *et al.* 2018). It is also known as a plasma drag and requires no additional hardware. Atittude maneuver control and elastic mode stabilization has been realized with adaptive sliding mode theory and active vibration control technique using piezoelectric materials (Hu 2009). Most of spacecraft appendages are latched at a defined position or a deployment mechanism is used. It is usually done using various electric motors and actuators (stepper motors, brushless motors, brushed motors, electromagnetic actuators). A very common configuration for an actuator is composed by a combination of stepper motor with harmonic drive, typically monitored by a position sensor. An example of such actuator is a European Harmonic Drive Rotary Actuator developed and qualified by Sener in Spain, with the support of ESA. A similar actuator is represented by the Satellite Antenna Rotary Actuator (SARA 21) used in several scientific and telecom commercial satellites. Several examples of mentioned motors are shown in Fig. 2.1.

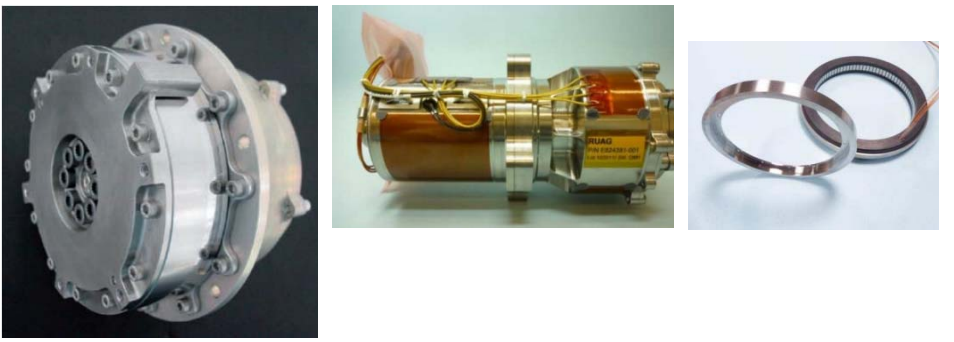

a) b) c)

Fig. 2.1. Examples of motors: a) harmonic drive rotary actuator (HDTA), b) sealed gear brush motor qualification model, c) Brushless motor qualification model for attitude control (Allegranza *et al.* 2014)

Over the past several decades, there has been an ever-increasing demand for accurate positioning systems. They must be compact, reliable, ensure high responsiveness and high efficiency. Piezorobots are often used as a solution to such problems because they can ensure high accuracy. The main component is the piezoelectric actuator which defines the main characteristics such as working resonant frequencies, mechanical properties, sensitivity, etc. Such piezorobots are small, therefore they are favorable in devices such as satellites, cameras, microscopes, spacecraft. Piezoelectric materials have been applied for space antenna vibration control (Anshul *et al.* 2015); piezoelectric transducers are used as sensors; actuators are used for attitude and control of a satellite

(Fonseca *et al.* 2017; Sabatini *et al.* 2018). Piezoelectric patches are surface-bonded in solar panels and are used to detect elastic displacements or counteract the vibration motion. Homogeneous and isotropic films of the piezoelectric actuators are attached on the surface of the flexible appendages to maintain and control satellite attitude (Cao *et al.* 2017). A hybrid control scheme using energy-based actuators switching mechanism has been proposed for spacecraft attitude control and vibration suppression (Azimi and Sharifi 2018). A 2-axis piezo-drive assembly for high precision positioning of the focal plane assembly was used for space camera (Chen *et al.* 2014). It was proposed that the focal plane motion disturbances can be compensated by a moving platform which is driven by piezo actuators or piezo motors. One must solve various problems when constructing robots or satellites and one of the major problems that is usually encountered is a proper stabilization of a device. A widely applied solution for stabilization is a gyroscope. They are applied in various areas such as medicine, mobile robots and ending with difficult solutions for satellite control or stabilization (Ahmad *et al.* 2012; Kawak 2017). Most vibratory shell gyroscopes are excited by standing wave which is the basic working mode for such devices. However due to manufacturing errors it is not possible to maintain a stable standing wave therefore additional research has to be done in order to reduce the effect of such manufacturing errors (Xiang *et al.* 2012). Gyroscopes also have unbounded drift errors (Nasir *et al.* 2012). These can be solved by combining stereo vision with gyroscope's angular velocity information. However, this leads to increased size of the mechanism since additional parts need to be added for proper functioning. Gyroscopes are successfully applied in nano-satellites for attitude determination where they are used as sensors (Shaobo *et al.* 2011). Control moment gyroscopes are applied for better performance, but exhibit high micro-vibration emission which may interfere and disrupt other spacecraft components (Kawak 2017). The most important problem related to gyroscopes is that they cannot be controlled as piezoelectric actuators. Piezoelectric actuators are used for spacecraft attitude and motion control. One of the main reasons for this choice is that such actuators are small and relatively easy to apply. They do not require large amount of hardware which can prove to be a critical factor in space applications. Shunted transducers are used to control vibrations of spacecraft containing flexible appendages (Sales *et al.* 2013). A controller to stabilize vibration modal of spacecraft can be designed using actuators (Cao *et al.* 2017). Once residual vibration is detected, it can be minimized by the same actuators.

2.2. Piezorobots with multi-degrees-of-freedom used for stabilization of nanosatellites

Attitude determination, stabilization, positioning on a large spacecraft can be performed using high performance devices as mentioned in previous section. However, this comes at a cost of mass, volume and power. Multifunctional structures allow to design systems which solve this problem (Sairajan *et al.* 2016). Nanosatellites require smaller, more compact components, therefore traditional stabilization devices are not suitable. Novel methods for stabilization and positioning are being developed to ensure proper functioning. (Burton *et al.* 2014) have proposed a model for attitude determination using low fidelity sensors. Nanosatellites themselves are passively magnetically stabilized which means that permanent dipoles are aligned with the desired spin axis. These dipoles provide alignment to the Earth ‘s magnetic field. Magnetically permeable rods are mounted in the plane perpendicular to axis and provide damping of excessive angular motions post separation. Another method proposed for nanosatellite stabilization is using propulsion system which is a cold-gas thruster (helium, nitrogen and liquefied propane are considered as propellants) (Belokonov I. *et al.* 2017). A small size ionic-plasma engine using mercury ions has been proposed for CubeSat nanosatellites (Phylonin and Belokonov 2017). The proposed construction allows to change the trajectory, compensate oscillating and rotational motions of the device. When high precision, low mass and long operational life is required, smart materials provide a great choice. Of all smart materials piezoelectric actuators are considered the most mature technology for space mechanisms and structures. Pointing mechanisms (ARTEMIS, PHARAO, EARTHCARE, SOHO), Point Ahead Angle Mechanisms (LISA), Laser control (AEOLUS, PHARAO, EARTHCARE, SWARM), Optical delay line (LISA-PF), Microvibration cancellation (PICARD, Solar orbiter), Instrumentation (ROSETTA, MISSE7, CURIOSITY), Free-floating object handling (LISA_PF, FOTON M3), Propulsion (GAIA, LISA-PF), Scanning mechanisms (Solar orbiter) have successfully applied piezoelectric actuators (Allegranza *et al.* 2014). Piezoelectric actuators are favorable due to their high operating frequency, magnetic cleanliness, high acuracy and easiness of control. Due to a low power consumption, piezoelectric actuators are also of interest for cryogenic applications.

Piezoelectric motors use friction to drive their motor and are often used for single flex camera refocusing. Such motors have been used in instrumentation (ROSETTA, SWARM), free-floating object handling (LISA-PF). Repositioning of the free-floating mass was realized using piezoelectric actuators in LISA-PF, FOTON M3/DIMAC projects. European consortium, led by TNO developed and tested a system for space called PEASSS (Piezoelectric Assisted Smart Satellite

Structure) aimed at development of technologies that would enable European space observation and in-space activities. The objective of the project was to develop, manufacture, test and qualify "smart structures" which combine composite panels, piezoelectric materials, and next generation sensors, for autonomously improved pointing accuracy and power generation in space. Smart structures enable fine angle control, thermal and vibration compensation, improving all types of future Earth observations, such as environmental and planetary mapping, border and regional imaging. Piezoelectric actuators are embedded in a composite structure so that pointing accuracy and stability can be improved. At the same time, they decrease mass and power consumption. Piezo power generation can be incorporated into structures, allowing power for distributed sensor networks.

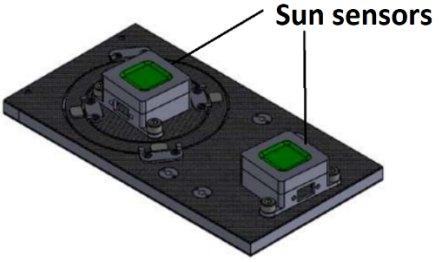

a)

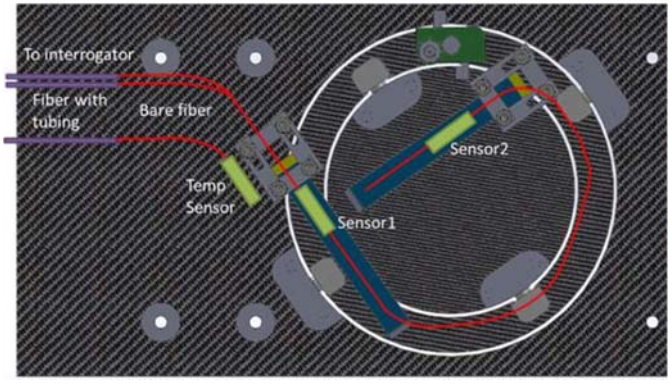

b)

Fig. 2.2. Design drawing of the Smart Structure with a fixed sun-sensor and a second sun-sensor mounted on a gimballed structure that can be tilted by means of 2 piezo bimorph actuators located at the back side of the panel: a) top view; b) bottom view (CORDIS 2018)

A CubeSat platform bus was designed, the system components include new nanosatellite electronics, a piezo power generation system, and a piezo actuated smart structure, and a fiber-optic sensor and interrogator system (CORDIS 2018). Nanosat electronic consists of Payload Data Acquisition Unit (PDAU) and an Electronic Power Supply (EPS) module. The payload consists of a pyro power generator and a smart structure. Angle of the sun-sensor body with respect to the sun is measured by sun-sensor. A second sun-sensor that is added on a fixed location of the satellite measures the tilting angle. Tilting is performed by 2 piezo bimorph actuators mounted orthogonally that move a ring and an inner disc in a gimbal setup (CORDIS 2018). The discussed smart structure is shown below in Fig. 2.2. In order to control hysteresis, a strain is measured by means of Fiber Bragg Gratings (FBG's). The pyro power generator is made from 2 sets of piezo plates which are embedded in an aluminum tray (a change in the temperature generates electrical power).

Authors (Bansevicius et al. 2015a) proposed a piezoelectric device for nanosatellite altitude control. It consists of a monolithic cylindrical piezoelectric transducer; motion is created by exciting axial travelling wave oscillations. The sphere that is mounted on top of this cylinder can be rotated around X, Y, Z axes, however this requires a more complex trajectory control. A laser beam control for nanosatellite swarm organization has been proposed and manufactured (Navickaitė *at al.* 2015). Although the problem was focused only on laser direction towards *X* axis, it shows potential that such control can be applied for more complex manipulations. As mentioned before, one of the most popular satellite attitude control method is a reaction wheel. Each axis requires a reaction wheel; therefore, a three axes attitude control needs three reaction wheels. Usually such construction is bulky and not applicable in small satellites such as CubeSat. A reaction sphere driven by piezoelectric actuators has been proposed as a solution to this problem (Bručas *et al.* 2012). Actuators are excited and rotate the sphere around three axes. MEMS and NEMS are considered for the miniaturization of space technologies (Bilhaut *et al.* 2009).

2.3. Motion formation methods for piezorobots with multi-degrees-of-freedom

Usually ultrasonic motors with several degrees of freedom use several component vibrations. It is desired that vibration amplitudes in every direction could be controlled separately and that any phase shift between the components could be implemented. This ensures that optimum operation conditions and speed reversal selection. A contact between the moving component along the plane or surface ensures that the ultrasonic motor will be powerful with high durability. Those

motors with stepping motion must have coinciding nodes in all components. Multiple-degrees-of-freedom ultrasonic motors can have controllable kinematic pairs. This means that it is possible to control a number of degrees of freedom by restrain conditions. For example, excitation of the high frequency tangential or normal vibrations in the contact zone leads to a decreased coefficient of friction. Friction forces can also be controlled by magnitude of applied force. Kinematic pair is divided into passive and active components. Active pairs generate controllable forces in each direction of each degree of freedom. A degree of mobility of the active pair describes a number of DOF in which motion is possible. Another method for controlling the number of DOF in active kinematic pair is controlling the normal component of the forces in the contact zone. Electromagnetic interactions, forces of compressed air or a liquid medium are known as one of the easiest methods. A method that is used in this work is a third method for degrees of freedom control. It is the excitation of elastic static deformations, which is achieved by using converters that are made from piezoelectric ceramic and applying a high DC. If there is a large number of degrees of freedom, it becomes difficult to use separate drives. However, ultrasonic motors enable control by exciting different modes and types of resonant vibrations. This is done by choosing the proper electrode configuration. In case when control frequencies are equal, contact points of the actuator move in elliptical trajectories, which parameters are defined by supplied voltage and phase.

The largest number of modes and vibration types can be generated by exciting proper electrodes on the bar converter. A radially polarized cylindrical actuator can have these vibrations excited: radial, flexural or several lower modes, travelling wave type, conical and barrel shaped, torsional with respect to axis X, and other complex vibrations in the form of standing or travelling wave.

Motion formation for ultrasonic devices can be categorized as following (Ragulskis *et al.* 1988):

- Using the coupling of different modes of vibration. The forces of interaction between the vibrations are evaluated by the coupling coefficients of correlation.
- Actuators of flexural and longitudinal vibrations. Greatly reduces the dimensions of actuator, because it is possible to excite independent flexural or longitudinal vibrations in the monolithic piezoceramic plate or rod. Actuators with polarization coinciding with electrical field are most frequently used.
- Actuators of torsional and translational vibrations. These are made as cylindrical rods of resonant length and use the anisotropy of elastic piezoelectric, or the magnetostriction properties. The most common are systems where longitudinal excitation allows the excitation of torsional

component of vibrations due to a certain inhomogeneity of the cross section of the rod. The main drawback is that they can be applied only in nonreversible ultrasonic motors.

- Summation of vibrations. Using two or three actuators of longitudinal and flexural vibrations it is possible to obtain closed trajectories of actuator contact points.
- Curvilinear concentrators and waveguides. Convert longitudinal vibrations into longitudinal-flexural vibrations. They can obtain the high magnitudes of tangential component of velocity in the contact zone.
- Excitation of the travelling waves and the vibration concentrators of the travelling wave type. Displacements (longitudinal, transversal, flexural, shear, etc.) corresponding to the standing waves are expressed as a solution of a linear equation of motion. The method can be simplified as excitation of the vibrations of the same frequency and mode, but in different phases.

The analyzed ultrasonic robots do not have any additional components that form the motion. Motion is created through direct impact by contact points on the actuator. Therefore, traditional motion formation methods are not suitable. The main factors for motion formation proposed by (Lavalle 2004) are:

1. Initial position of the robot (position in space, structure of the robot, etc.).
2. Time interval to perform required action.
3. Action (each action at each moment of time changes the state of device).
4. Final position.

Motion trajectories for walking piezo robots use interpolation methods such as polynomial interpolation, spline interpolation and Cornu spiral (Drukteiniene 2011). The main goal of these methods is to find a uniform function which describes all points at any given time. Polynomial interpolation usually uses 3, 4, 5, 6 rank polynomials; interpolation by splines uses cubic splines, beta splines and trigonometric splines. Cubical splines are used frequently for motion formation because trajectories are the most optimal relative to time.

Trajectories formed by trigonometric/Schoenberg polynomials are known for their little deviation from nodes. The biggest advantage of it is that due to low recalculation cost, trajectories can be adjusted in real time if an obstacle is encountered. Beta splines have the same advantage and are used for such problems. Cornu spiral, also known as Euler spiral, is used when trajectory changes from straight line to circular arc. The main drawback – a quick change is not possible and it is impossible to create a sharp turn.

A sequence of decisions must be applied over time so that a piezo robot moves in a desired trajectory. In order to control the position of the object, different type control systems are usually used. Non-rotational mobile piezo

robots must precisely replicate the given path with maximum speed (Bansevicius *et al.* 2018). Such piezorobot when only one electrode is excited moves from one point to another as presented in Fig. 2.3.

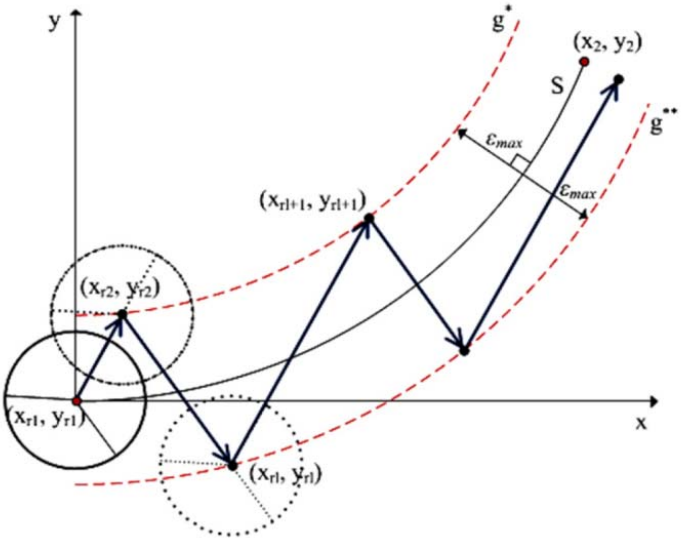

Fig. 2.3. Control and path verification system structure of piezo robot (Janutenaite J. *et al.* 2017)

If one electrode is excited in the switching contacts algorithm, then a linear movement is created. Using such algorithm motion trajectory is a broken line. Although this algorithm does not ensure precise trajectory, it is easy to control (Bansevicius *et al.* 2016a). When all three electrodes are excited, a travelling wave is generated and the piezorobot rotates around *Z* axis.

A combination of these two excitation schemes allows to create a more precise movement trajectory. Two electrodes are excited at the same time but with different voltages.

A presented fine trajectory planning algorithm describes how the piezo robot will move when two electrodes are excited with different forces (Bansevicius *et al.* 2018). In this paper, authors have presented a mathematical model for contact excitation duration. Movement trajectory is calculated using contact switching algorithm (Drukteiniene 2011). For non-mobile piezorobots trajectory planning algorithms are used to determine the position of the object that is being manipulated such as a sphere (Bansevicius *et al.* 2016b). A shaking beam type actuator is used to create an elliptical motion, which rotates the sphere (Vasiljev *et al.* 2006). Good results were achieved when a sphere is rotated by a cylindrical actuator (Bansevicius *et al.* 2016a; Bansevicius *et al.* 2017). Two electrodes are

excited at the same time but with different voltages. Such case is presented in Fig. 2.4. A more complex problem is analyzed when the piezorobot can both rotate the sphere and move on the plane (Bansevicius *et al.* 2018).

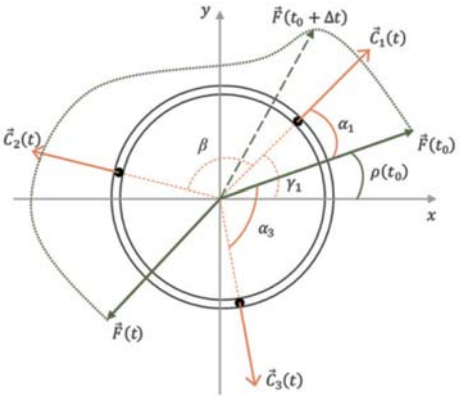

Fig. 2.4. Scheme of total force $\vec{F}(t)$ and its components $\overrightarrow{C_j}(t)$ acting at contact points, where j is the electrode number (Bansevicius *et al.* 2016a)

A triangular electrode scheme was used; two electrodes were excited at the same time. Depending on which electrodes were active, the piezorobot was either rotating the sphere or moving on the plane. The main benefit of such piezorobot is that the sphere positioning can also be controlled by changing the position of the cylinder on a plane. Trajectories of the cylinder and sphere are presented in Fig. 2.5.

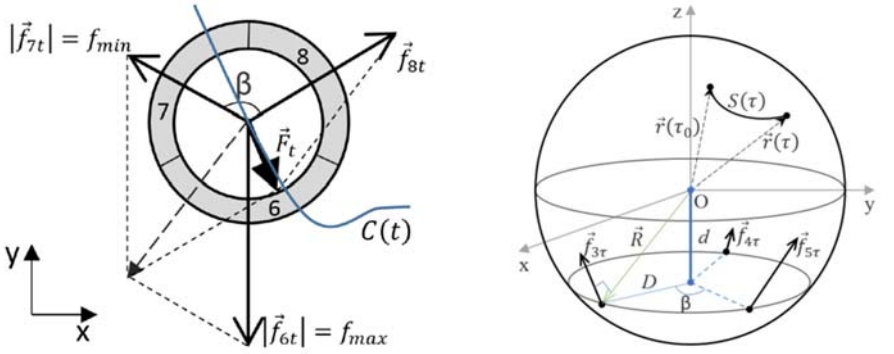

a) b)

Fig. 2.5. Motion trajectories: a) trajectory of the cylinder, b) Sphere rotation trajectory (Bansevicius *et al.* 2018)

However, the system has 6 DOF which makes control quite difficult. A standard equipment is not suitable for piezorobot trajectory measurement because movement is very small and frequent. A control system is required to ensure successful movement in desired trajectory. Such system is presented in Fig. 2.6, where control signal formation and image processing system are used to track the motion of a piezorobot. The piezorobot moves on a glass platform and control signals are amplified using high voltage amplifier. Signals are monitored using a system with oscilloscope. A video camera captures the motion of a piezorobot and this data is analyzed using LabVIEW based image processing software (Janutenaite-Bogdaniene *et al.* 2017).

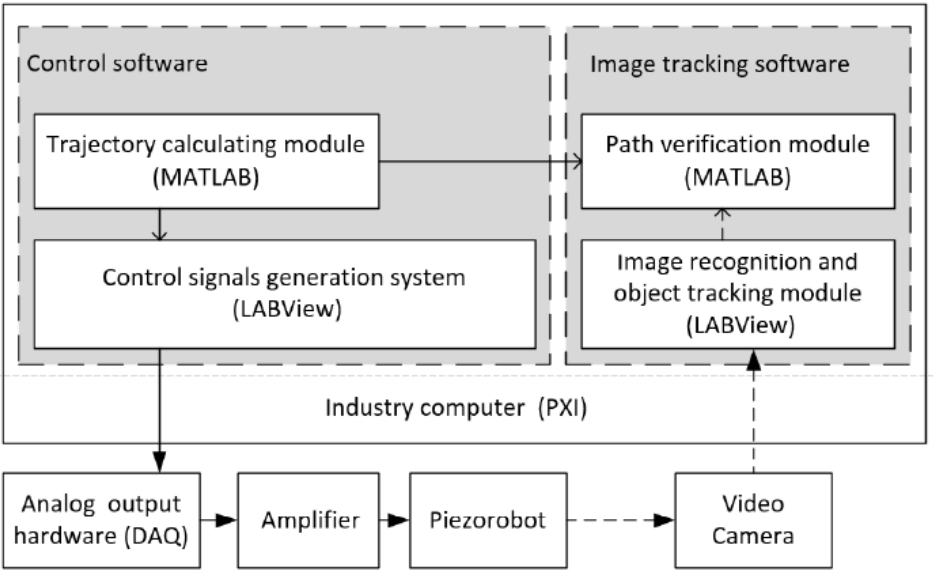

Fig. 2.6. The structure of the piezorobot control and path verification system (Janutenaite-Bogdaniene *et al.* 2017)

Interface to hardware output was set according to the technical requirements of National Instruments NI-DAQmx hardware (Shujiao *et al.* 2012; Sumathi *et al.* 2007). The trajectories planning module software is based on MATLAB and is used to calculate the trajectories of piezorobot (Drukteiniene 2011).

The functional diagram of an experiment system is shown in Fig. 2.7; hardware control system is presented in Fig. 2.8.

It is based on LabVIEW and uses MATLAB script as a mathematical module. A three sine wave generator was created with LabVIEW, it's control is defined in MATLAB script. A trajectory monitoring path data is also generated by this script.

Video camera and an image processing software is used to monitor the trajectories.

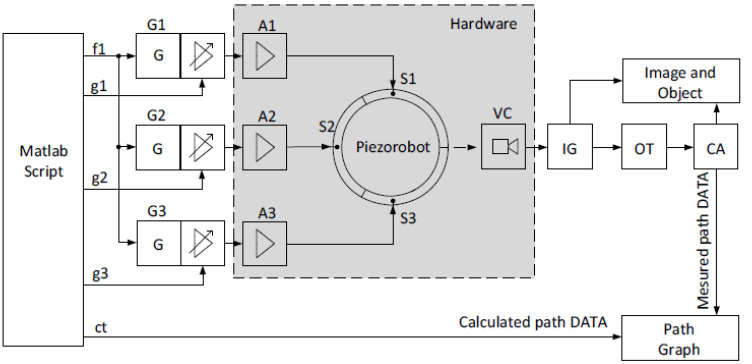

Fig. 2.7. Control of piezorobot and trajectory tracking system block diagram (Janutenaite-Bogdaniene *et al.* 2017)

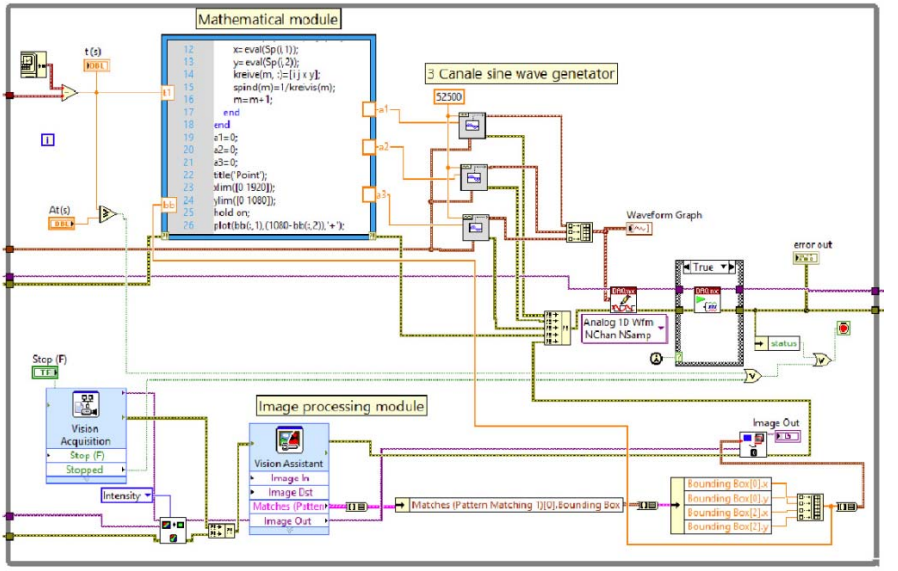

Fig. 2.8. Piezorobot's control and path monitoring software LabVIEW block diagram (Janutenaite-Bogdaniene *et al.* 2017)

Movement of the piezorobot is presented in a path graph that is generated by Image and Object modules. Theoretical coordinates are given simultaneously from MATLAB script module.

2.4. Conclusions of Chapter 2

1. Currently, the stabilization of satellites is achieved with active (micro-thrusters, reaction wheels, control momentum gyroscopes) and passive (dual spin, gravity gradient, spin stabilization, SRP, etc.) stabilization methods.
2. Although gyroscopes are used quite often, they cannot be controlled as piezoelectric actuators. They are usually chosen for their small volume, mass, accuracy and easy application.
3. Piezoelectric actuators are used for satellite stabilization, both directly or by controlling other components such as appendages. Therefore, it is logical that their favorable properties make them highly suitable for nanosatellites.
4. Piezoelectric actuators are applied in pointing mechanisms, for laser control, optical delay line, free-floating object handling, propulsion, scanning mechanisms, stabilization, etc.
5. In this thesis a multi-degrees-of-freedom piezorobot for nanosatellite stabilization was analyzed for its successful application and favorable properties such as low mass, rapid movement and precision.
6. The analyzed piezorobots do not have any additional components that form the motion and traditional motion formation methods are not suitable. Trajectory planning algorithms that were described in this chapter allow to successfully control trajectories of the piezorobot. Piezorobots motion formation algorithms according to electrode excitation scheme must be created, so that the contacts points would move in desired trajectories.

3

Mathematical model of piezorobot used for nanosatellite stabilization

In this section multi-DOF cylindrical and hemispheric resonant-type piezoelectric actuators used for satellite stabilization are analyzed. The first actuator consists of one active kinematic pair and has two different electrode schemes applied. The first electrode scheme has a rectangular shape configuration and the second electrode scheme has a triangular shape configuration. The cylindrical piezoelectric actuator has 6 DOF and can rotate a ferromagnetic sphere about three axes and simultaneously move itself on the plane. The positioning of the sphere is achieved by exciting specific electrodes, which results in the movement of contact points and direct impact on the sphere. Alternatively, the cylinder itself can be moved and positioned on the plane thus positioning the sphere. The whole positioning system is realized using a single piezoelectric actuator with high accuracy.

A mathematical model of contacting force was developed and presented in scientific articles (Bansevicius *et al.* 2016a; Bansevicius *et al.* 2016b; Janutenaite-Bogdaniene *et al.* 2017; Bansevicius et al. 2018; Bansevicius *et al.* 2017). Numerical investigation was done using ANSYS software and a working prototype has been manufactured. The presented actuator can be applied for optic beam stabilization, beam positioning in space or adaptive focusing of optical lenses in optoelectronics, laser systems and nanosatellite stabilization. The second

analyzed actuator is a hemispheric resonant-type piezoelectric actuator. This actuator has two active kinematic pairs; the surface of the hemisphere is covered with electrodes each placed at 120°. This actuator has 6 DOF and is used to rotate the sphere. Although it can move on the plane, this case is not discussed in this thesis.

Further the mathematical model and the detailed numerical analysis is presented. Harmonic and modal analysis were done, domination coefficients were calculated in order to determine resonating frequencies and suitable geometric parameters. Then contact point motion trajectories were calculated, the resultant force was determined and piezorobots' motion formation algorithms according to electrode excitation schemes were presented. At the end of the chapter conclusions are given. The material in this chapter was published in scientific journals (Janutenaite J. *et al.* 2017, Bansevicius *et al.* 2016a, Bansevicius *et al.* 2016b, Bansevicius *et al*. 2018).

3.1. Mathematical model of piezorobot

In this thesis, cylindrical and hemispheric actuators are analyzed. The piezoelectric cylinder type actuator kinematic pair is presented in Fig. 3.1a and a hemispheric type actuator with two kinematic pairs is presented in Fig. 3.3a and Fig. 3.2b. Two different electrode configurations were used to excite the vibrations of the cylindrical actuator. Dimensions of the piezoelectric cylinder are 28 mm (inner diameter) × 33 mm (outer diameter) × 20 mm (height). A cylinder that has a rectangular electrode scheme is made from a PZT-4 material and a cylinder with triangular scheme is made from a PZT-8 material.

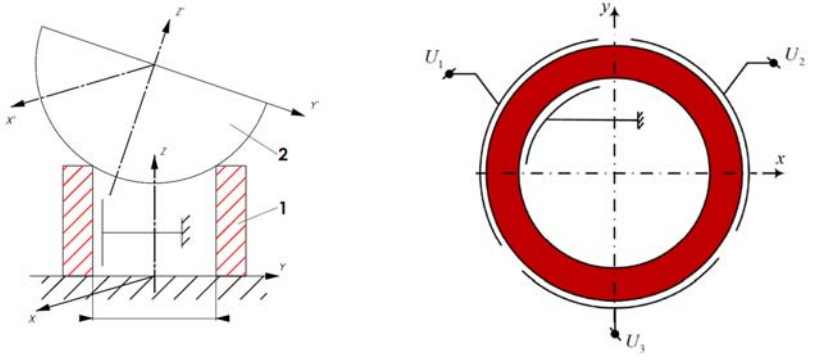

a) b)

Fig. 3.1. Cylindrical type actuator: a) the analyzed kinematic pair; b) electrode configuration

A ferromagnetic sphere is positioned on the top of the cylinder. Outer surface of the cylinder is covered with electrodes and the inner surface has a single electrode which is grounded. The analyzed electrode schemes are presented in Fig. 3.2. Material properties for PZT-4 and PZT-8 are given accordingly at Table 3.1 and Table 3.2. Dimensions of the hemisphere are 28 mm (inner diameter) × 30 mm (outer diameter) × 15 mm (height) and it is made from PZT-4 material. Outer surface is covered with electrodes, which are placed 120° each. The inner surface has a single electrode, which is grounded. The applied electrode scheme is presented in Fig. 3.3c. The sphere is positioned in space through a contacting force. Two electrodes are excited at the same time, but with different voltages.

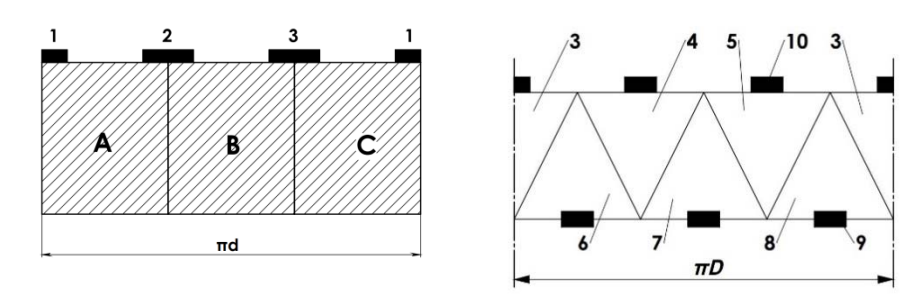

a) b)

Fig. 3.2. Electrode configuration: a) rectangular; b) triangular

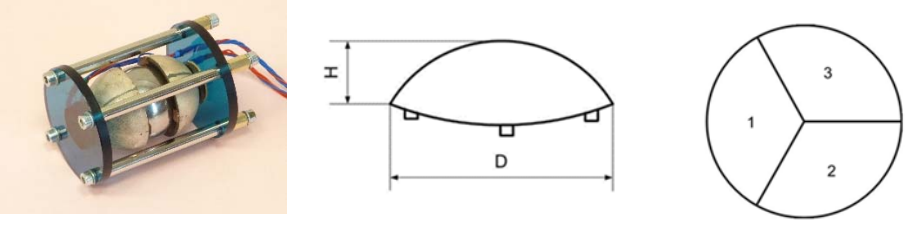

a) b) c)

Fig. 3.3. Analyzed kinematic pair: a) hemispheric actuator; b) schema of hemispheric actuator; c) electrode configiration

Higher voltages result in higher displacement amplitudes of contact points (Fig. 3.2b and Fig. 3.3b). Contact points move in elliptical trajectories; the motion causes the sphere to rotate. Motion trajectories are analyzed in the plane that goes through the contact point, radius and Z axis as shown in Fig. 3.6. However, a

problem arises, because at some moment trajectories of contact points change directions. This means that contact points might be moving in trajectories of an ellipse in opposite directions. It is important to determine such moment, because this behavior can result in improper functioning of piezorobot.

Table 3.1. Material properties of PZT-4

Property	Value
Material	PZT-4
Young's modulus, N/m^2	7.8×10^{10}
Poisson ration ν	0.31
Density, kg/m^3	7500
Relative permittivity	$\varepsilon_{11} = 1475, \varepsilon_{22} = 1475, \varepsilon_{33} = 1300$
Piezoelectric matrix, C/m^2	$e_{13} = -5.2, e_{23} = -5.2, e_{33} = 15.1,$ $e_{15} = 12.7$
Elasticity matrix, 10^{10} N/m^2	$c_{11} = 13.9, c_{21} = 7.78, c_{31} = 7.43,$ $c_{22} = 13.9, c_{32} = 7.43, c_{33} = 11.5,$ $c_{44} = 2.56, c_{55} = 2.56, c_{66} = 2.56$

Table 3.2. Material properties of PZT-8

Property	Value
Material	PZT-8
Young's modulus, N/m^2	9.9×10^{10}
Poisson ration ν	0.31
Density, kg/m^3	7600
Relative permittivity	$\varepsilon_{11} = 1290, \varepsilon_{22} = 1290, \varepsilon_{33} = 1000$
Piezoelectric matrix, C/m^2	$e_{13} = -4.1, e_{23} = -4.1, e_{33} = 14,$ $e_{15} = 10.3$
Elasticity matrix, 10^{10} N/m^2	$c_{11} = 14.69, c_{21} = 8.11, c_{31} = 8.11,$ $c_{22} = 14.69, c_{32} = 8.11, c_{33} = 13.17,$ $c_{44} = 3.29, c_{55} = 3.13, c_{66} = 3.13$

In order to ensure proper functioning of the piezorobot, it is necessary to solve these problems:

- To determine resonating frequencies;
- To calculate domination coefficients to determine which eigenforms are suitable;
- To determine which geometrical parameters are suitable;
- To analyse how the trajectories of contact points move when the voltage is applied;
- To determine when the direction of ellipses change;
- To determine which pair of voltages ensures the proper movement.

In order to determine which piezoelectric actuator is the most suitable for stabilization, an algorithm has been created. The algorithm goes as described:

- Harmonic analysis for a cylinder with specific geometric parameters r × R × h is done. Resonating eigenfrequencies are found and analyzed further;
- Eigenforms are analyzed for resonating frequencies. It is required that the largest deformations would be towards Z direction;
- Domination coefficients are calculated for resonating frequencies;
- Depending on the eigenform and domination coefficients a suitable eigenform is determined.

The cylinder and the hemisphere were modelled using ANSYS software. A solid object was divided into finite elements to perform calculations. Finite element method is one of the most popular and efficient methods in engineering for analysis of complex structures. Two types of finite elements were chosen: SOLID5 and SOLID98. The cylinder was divided into the first type finite elements and the hemisphere was divided into the second type finite elements. SOLID5 has a 3D magnetic, thermal, electric, piezoelectric, and structural field capability with limited coupling between the fields. The load for this element was voltage (ANSYS, Inc.). A cylinder is not considered a very complex structure therefore the element was suitable – it had the desired number of nodes and it was possible to divide the cylinder into these elements. In case of more complex structures a shell element type should be chosen. SOLID98 is a 10-node tetrahedral version of the 8-node SOLID5 element and is well suited to model irregular meshes. Each node has up to 6 degrees-of-freedom. Both elements are presented in Fig. 3.4; the cylinder and the hemisphere which were divided into finite elements are presented in Fig. 3.5.

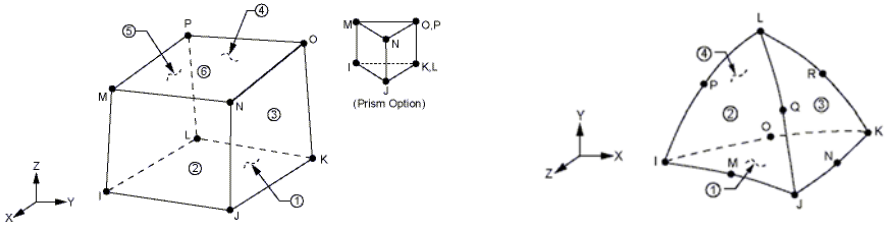

a) b)

Fig. 3.4. Finite elements chosen for the model: a) SOLID5; b) SOLID98 (Ansys14)

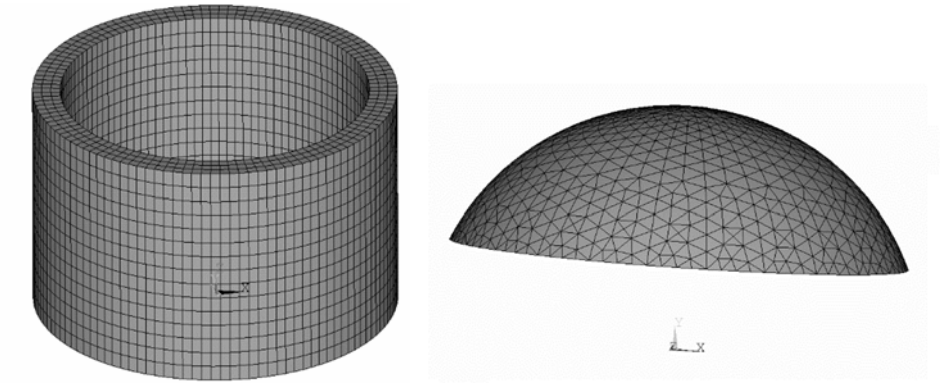

a) b)

Fig. 3.5. Analyzed objects divided into finite elements: a) cylinder divided into SOLID5 elements, b) hemisphere divided into SOLID98 elements

The complete mathematical model of a piezoelectric finite element may be expressed in the form (Kulvietis G. 1998):

$$[\boldsymbol{M}]\{\ddot{\delta}\} + [\boldsymbol{H}]\{\dot{\delta}\} + [\boldsymbol{K}]\{\delta\} - [\boldsymbol{T}]\{\varphi\} = [\boldsymbol{F}]; \qquad (3.1)$$
$$[\boldsymbol{T}]'\{\delta\} + [\boldsymbol{S}]\{\varphi\} = \{\boldsymbol{Q}\},$$

where $[\boldsymbol{M}], [\boldsymbol{K}], [\boldsymbol{T}], [\boldsymbol{S}]$ are structural matrices of a finite element (Kulvietis G. 1998):

$$\begin{aligned} [\boldsymbol{K}] &= \int [\boldsymbol{B}]'[\boldsymbol{c^E}][\boldsymbol{B}]\boldsymbol{dV}; \\ [\boldsymbol{T}] &= \int^{\boldsymbol{V}} [\boldsymbol{B}]'[\boldsymbol{e}]\,[\boldsymbol{C}]\boldsymbol{dV}; \\ [\boldsymbol{S}] &= \int_{\boldsymbol{V}}^{\boldsymbol{V}} [\boldsymbol{C}]'\,[\boldsymbol{\zeta^S}][\boldsymbol{C}]\boldsymbol{dV}, \end{aligned} \qquad (3.2)$$

where $[\boldsymbol{c^E}]$ is the matrix of stiffness tensor for a constant electric field, $[\boldsymbol{e}]$ is the matrix of piezoelectric constants, $[\boldsymbol{\zeta^S}]$ is the matrix of dielectric constants at permanent deformations, $\{\delta\}$ is the displacement vector, $\{\varphi\}$ is the vector of electrical potentials, $\{\boldsymbol{Q}\}$ is the vector of electrical charge.

Influence coefficients, based on comparison of eigen energy of the free vibrations calculated by finite element method, are used for geometry optimization. Definition of optimal excitation zones is based on the definition of angle between eigenvectors and mechanical forces with the aim to maximize the vibrations of amplitudes. The operating frequency range for ultrasonic motors is more than 20 kHz and causes qualitative differences in the operation limits as well as new phenomena that has not been observed in mechanisms before. The control of micro robots could be derived using mixed finite element method and computer algebra techniques. A dynamic model of piezorobot is (Kulvietis 1998):

$$P_i = \sum_{j=1}^{n} H_{ij}(q)\ddot{q}_j + \sum_{k=1}^{n}\sum_{l=1}^{n} C_{kl}^{i}(q)\dot{q}_k\dot{q}_l + g(q), \tag{3.3}$$

where P_i is the driving torque acting at the i^{th} joint; vector $\boldsymbol{q}$ represents joint coordinates of manipulator; **n** is number of degrees of freedom. The actuator model based on finite element method is (Kulvietis 1998):

$$[M]\{\ddot{\delta}\} + [C]\{\dot{\delta}\} + [K]\{\delta\} = \{F(\delta, \dot{\delta}, q)\} + [L]\{u(t)\}, \tag{3.4}$$

where $\{F(\delta, \dot{\delta}, q)\}$ is a nonlinear highly varying in time driving force and $\{u(t)\}$ is a control output; $\{\delta_i\} = \{\rho_i, \theta_i, z_i\}$ is a displacement vector of nodal point i in the cylindrical coordinates. This equation can be simplified using eigenvectors of the system for real-time dynamics. Criteria for complete control scheme is (Kulvietis 1998):

$$\min_{\in[0,T]} |P_i - \bar{F}_i|_{i=1,2,\ldots n}, \tag{3.5}$$

where $\bar{F}_i = \frac{\omega m}{2\pi}\int_0^{2\pi/\omega m} F_i dt$; ω is a resonant frequency; m is a number of periods. A real-time dynamic model of a robot was derived using Uicker-Khan method, because it enables the calculation of all matrices: the inertial matrix, the matrix of Coriolis and centrifugal effects, and the gravity vector. The dynamic equations of a multiple-degree-of-freedom manipulator have the following form (Kulvietis 1998):

$$P_i = \sum_{j=1}^{n}\left\{\sum_{k=1}^{j}\left[tr\left(\frac{\partial W_j}{\partial q_i}J_j\frac{\partial W_j^T}{\partial q_k}\right)\right]\ddot{q}_k + \sum_{k=1}^{j}\sum_{l=1}^{j}\left[tr\left(\frac{\partial W_j}{\partial q_i}J_j\frac{\partial^2 W_j^T}{\partial q_k \partial q_l}\right)\right]\dot{q}_k\dot{q}_l - m_j\vec{g}^T\frac{\partial W_j}{\partial q_i}\tilde{r}_{j0}\right\}, \quad (3.6)$$

where P_i is a driving torque acting at the i-th joint; q_i is a geberalized joint coordinate corresponding to the i^{th} degree-of-freedom; W_j is a transformation matrix between the i^{th} local coordinate system and the reference system; J_j is an inertia matrix of the i^{th} link with respect to a local coordinate system; m_j is a mass of the link i; $\tilde{r}_{j0}$ is a distance vector between the center of mass of the link I and the origin of the reference coordinates system, expressed in the local coordinate system of the i^{th} link; $\vec{g}$ –gravity vector. W_i can be expressed as follows (Kulvietis 1998):

$$W_i = A_0^1 A_1^2 \dots A_{i-1}^i. \quad (3.7)$$

The external torque vector placed on the gripper and rotating in the plane perpendicular to direction of the gripper (Kulvietis 1998):

$$\vec{F} = \begin{Bmatrix} F_x = m_0 r\omega^2\cos(\omega t) \\ F_y = m_0 r\omega^2\sin(\omega t) \\ 0 \end{Bmatrix}, \quad (3.8)$$

where m_0 is the mass of misbalance; r – radius; ω – angular velocity.

In order to determine suitable geometric parameters and resonating frequency, domination coefficients are calculated. It can be done by finding the sum of the amplitude squares of piezoelectric actuator oscillations in all directions of the degrees of freedom for a point, i.e., the full system energy in all directions (Tumasoniene *et al.* 2007; Kulvietis *et al.* 2005; Kulvietis *et al.* 2006):

$$S_k^n = \sum_{i=1}^{r}(A_{ik}^n)^2\,, \quad (3.9)$$

where *n* is the eigenfrequency for a system, *k* is the number of degrees of freedom in a node, A_{ik}^n is the value of the eigenform vector for the i^{th} element. Then the ratio is calculated (Tumasoniene *et al.* 2007; Kulvietis *et al.* 2005; Kulvietis *et al.* 2006):

$$m_j^n = \frac{S_j^n}{\sum_{i=1}^{k} S_i^n}\,, \quad (3.10)$$

where m_j^n is the oscillation domination coefficient that corresponds to the n^{th}eigenform. The index j of domination coefficient shows in which direction the

energy under investigation is the largest, $j = 1, 2, 3$ (1 – x coordinate, 2 – y coordinate, 3 – z coordinate). When domination coefficients in all directions of degrees-of-freedom are calculated, they can be compared to each other and dominant oscillation type can be determined. Domination coefficients calculated according to equation (3.10) are normalized so that their limits vary from 0 to 1. This way it is easier to compare them to each other. These coefficients help to differentiate eigenforms by dominating oscillations, for example, radial, tangential, axial, etc.

A piezoelectric actuator is simply a piezoceramic peace with electrodes attached to the surface. Vibrations are based on relations between polarization directions and vibration directions (Zhao 2011). For example, a longitudinal vibration is parallel to the polarization direction, transverse vibration is perpendicular to polarization direction. It is very important to choose proper electrode configuration because it allows excitation of desirable vibrations and reduction of undesirable ones. Positioning and shape of the electrodes, excitation order – all these are very important in design. By reconnecting electrodes, it is possible to create an actuator with several frequency inputs, performing in several different regimes. As given in (Kulvietis 1988) the amplitude of each harmonic is chosen by a variation of electrode area or the amplitude of the voltage $\alpha_a U_0$, supplied to the electrodes:

$$\begin{gathered} U_1 = U_0 cos\omega t; \\ U_2 = \alpha_a U_0 \cos(2\omega t + \beta); \\ U_3 = \alpha_a U_0 \cos(2\omega t + \beta + \pi), \end{gathered} \tag{3.11}$$

where α_a and β are the parameters determining the degree of asymmetry, and ω is the frequency of the first resonance of the longitudinal vibrations. A classical expression of longitudinal vibrations is this:

$$f_k = \frac{k}{2l}\sqrt{\frac{E}{\rho}}, \tag{3.12}$$

where E – Young's modulus, ρ – density, l – length, k – 1, 2, 3… longitudinal vibration.

Movement is created by exciting two electrodes at the same time. Voltage for the first electrode stays constant and the second electrode voltage is changed. Contact points move in ellipses and this motion is used to directly rotate the sphere that is placed on the cylinder or to move the cylinder into desired position. In case of the second construction, the sphere is positioned between two hemispheres. Contact points move in ellipses and rotate the sphere around three axes. It necessary to determine how the contact points move in plane. The most efficient rotation is achieved when the ellipse has a 45° angle with the *X*' axis. However,

at some point the ellipses change the direction, which may result in improper functioning of the actuator.

The force that is required for the proper motion was determined in (Drukteiniene 2011). Excitation zones of the cylinder must be simultaneously active with different force values of contact points for a resultant force calculation. Force values are obtained from harmonic analysis, where the movements of contact points are known; therefore, it is possible to calculate cumulative displacement vectors. The main task of the mathematical modelling is to calculate the length of the vectors in the time domain, when the length and direction of the force vector are given. The motion vector starting coordinates (x_0, y_0, z_0) are the coordinates of the contact point when the cylinder is not excited. The end coordinates are obtained using displacements:

$$(x, y, z) = (x_0 + ux, y_0 + uy, z_0 + uz). \tag{3.13}$$

The trajectory is analyzed in plane that goes through axis Z, radius and contact point as shown in Fig. 3.6. Firstly, the coordinate system is transformed using rotation matrix:

$$R(\theta) = \begin{bmatrix} cos\theta & -sin\theta \\ sin\theta & cos\theta \end{bmatrix}. \tag{3.14}$$

The column vectors are rotated by means of matrix manipulation:

$$\begin{bmatrix} x' \\ y' \end{bmatrix} = \begin{bmatrix} cos\theta & -sin\theta \\ sin\theta & cos\theta \end{bmatrix} \begin{bmatrix} x \\ y \end{bmatrix}. \tag{3.15}$$

The angle θ is obtained by converting Cartesian coordinates to cylindrical:

$$\rho = \sqrt{x^2 + y^2}.$$

$$\theta = \begin{cases} 0, if\ x = 0, y = 0 \\ \arcsin\left(\frac{y}{\rho}\right), x \geq 0 \\ \arcsin\left(\frac{y}{x}\right), x > 0 \\ -\arcsin\left(\frac{y}{\rho}\right) + \pi, x < 0 \end{cases}, \tag{3.16}$$

here, x stands for ux and y for uy. At any given time, the coordinates of the contact point are known, because they are defined by a sinusoidal function.

Once the transformation is done and x' values are known, equation of the ellipse is obtained from canonical equation of ellipse:

$$F(x, y) = a_{11}x^2 + 2a_{12}xy + a_{22}y^2 + 2a_{13}x + 2a_{23}y + a_{33} = 0. \tag{3.17}$$

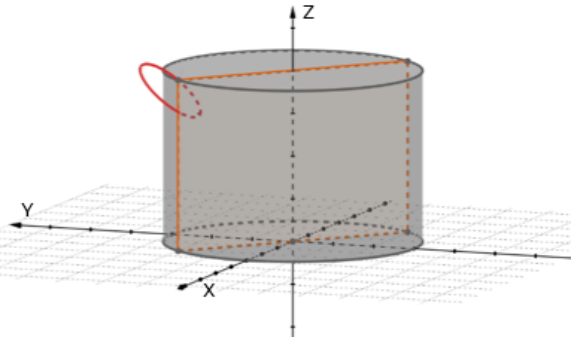

Fig. 3.6. The trajectories of the contact points are analyzed in the plane that goes through the contact point, radius and *Z* axis (shown in orange)

The coordinate system center goes through the center of the ellipse. This is done to simplify the calculations and clarify the motion of the contact point. The equation then becomes:

$$F(x,y) = a_{11}x^2 + 2a_{12}xy + a_{22}y^2 + a_{33} = 0. \quad (3.18)$$

The coefficients are then obtained by solving the equation. The length of major axis is the length of the displacement vector. Once displacement vectors of both contact points are calculated, the resultant displacement vector is obtained by vector addition.

3.2. Numerical analysis of cylindrical ultrasonic actuator used for stabilization

A kinematic pair presented in Fig. 3.1 is analyzed in this section. In total there have been 15 different cylinders modelled and analyzed. Their height and diameters vary, the thickness remains constant and equals to 2.5 mm. Harmonic analysis was done to determine resonating frequencies. For a 14 mm × 16 mm × 21 mm cylinder resonating frequencies are shown in Fig. 3.7.

It is desired that the largest deformations would occur in Z direction; therefore, it is meaningful to analyze those frequencies, which cause displacement amplitudes in Z direction to be the largest. As it can be seen from the figure, there are several frequencies of interest.

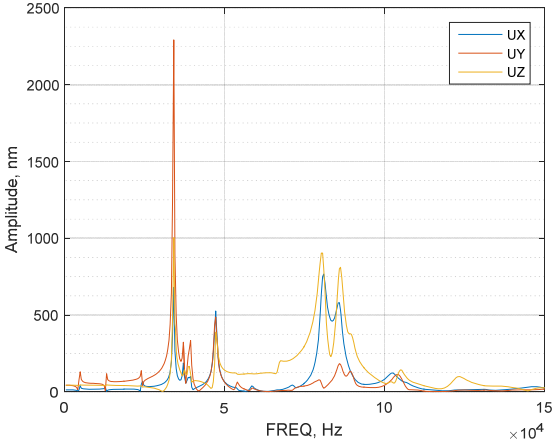

Fig. 3.7. Harmonic analysis for a 14 mm × 16.5 mm × 21 mm cylinder, it shows the amplitudes of the first contact point

Analysis showed that large displacements in Z direction occur at resonating frequencies of 39 000 Hz, 47 250 kHz, 80 250 Hz, and 86 250 Hz. Modal analysis is then required to determine eigenforms and eigenfrequencies. Domination coefficients are calculated, and we can partially determine suitable eigenforms. The number of nodal points or nodal lines for the form must be taken into account. This is defined by dimensionality of the eigenform. The number of nodal points is determined by the sign changes in oscillation amplitude for the full length of the piezoelectric actuator in the direction of coordinate axes. m_1^n represents the energy towards tangent direction, m_2^n – energy towards normal direction, m_3^n – energy towards Z direction. The first resonating frequency is not suitable because m_2^{30} is the largest and m_3^{30} is very small compared to other two domination coefficients as shown in Fig. 3.8 ($n = 30$ means it is the 30th eigenfrequency given by ANSYS software). The deformations are incorrect, therefore, this eigenfrequency is not analyzed further. The second resonating frequency corresponds to eigenform shown in Fig. 3.9a. The largest energy is towards normal direction and the lowest is towards Z direction, therefore this frequency is also not suitable. The fourth resonating frequency is not appropriate due to same reason – domination coefficients show that largest amount of energy is not towards Z direction and deformations. A proper working resonant frequency is 80 250 Hz, because it corresponds to eigenfrequency 84 319 Hz. Calculated domination coefficients show that the largest amount of energy is towards the Z direction and the second largest is towards tangent direction ($m_3^{73} > m_2^{73} > m_z^{73}$). The deformations are also appropriate as seen in Fig. 3.10a and Fig. 3.10b.

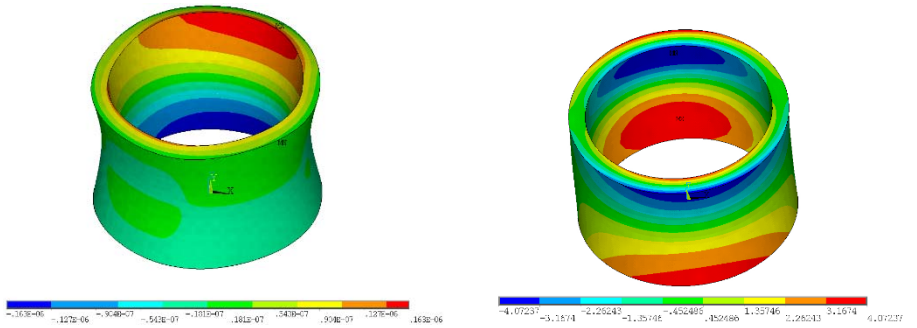

a)

$m_1^n = 0.289840223$

$m_2^n = 0.621878245$

b)

$m_3^n = 0.088281532$

$n = 30\ FREQ = 39\ 000$ Hz

Fig. 3.8. Results of harmonic and modal analysis, domination coefficients and modal shape identification: a) resonating frequency at 39 000 Hz; b) a suitable eigenform for 39 000 Hz resonating frequency; Domination coefficients show that the largest displacements are not in Z direction ($m_3^n < m_2^n < m_1^n$)

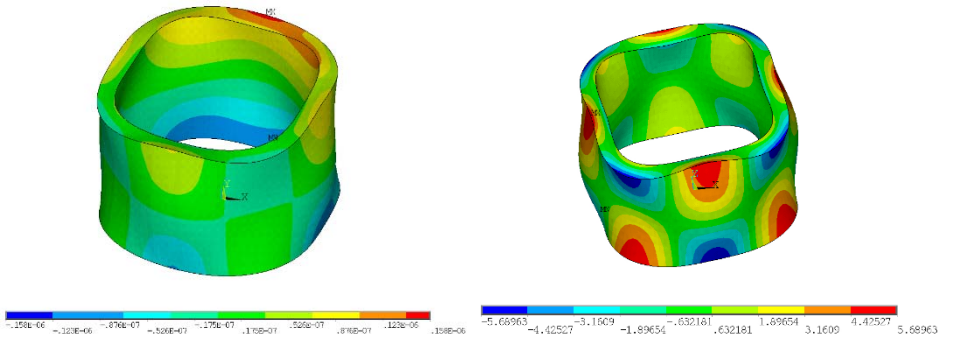

a)

$m_1^n = 0.324425258$

$m_2^n = 0.602392757$

b)

$m_3^n = 0.073181985$

$n = 37\ FREQ = 47\ 250$ Hz

Fig. 3.9. Results of harmonic and modal analysis, domination coefficients and modal shape identification: a) resonating frequency at 47 250 Hz; b) a suitable eigenform for 47 250 Hz resonating frequency

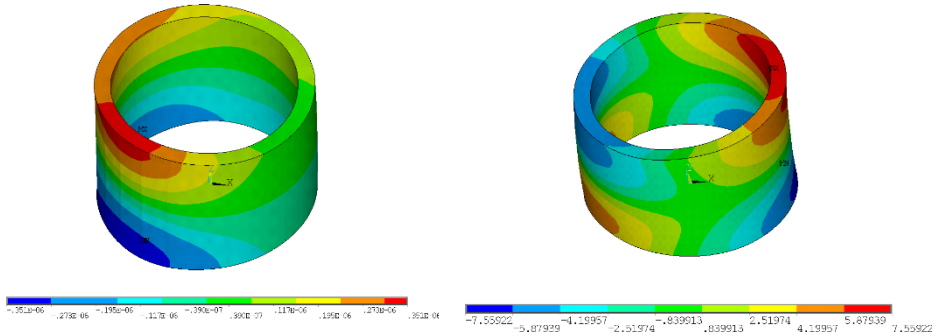

a) b)

$m_1^n = 0.377040875$ $m_3^n = 0.457270222$

$m_2^n = 0.165688904$ $n = 73\ FREQ = 80\ 250$ Hz

Fig. 3.10. Results of harmonic and modal analysis, domination coefficients and modal shape identification: a) resonating frequency at 80 250 Hz; f) a suitable eigenform for 80 250 Hz resonating frequency

In this case domination coefficients show that the largest displacements are in Z direction ($m_2^n < m_1^n < m_3^n$) and indicates that this frequency is suitable.

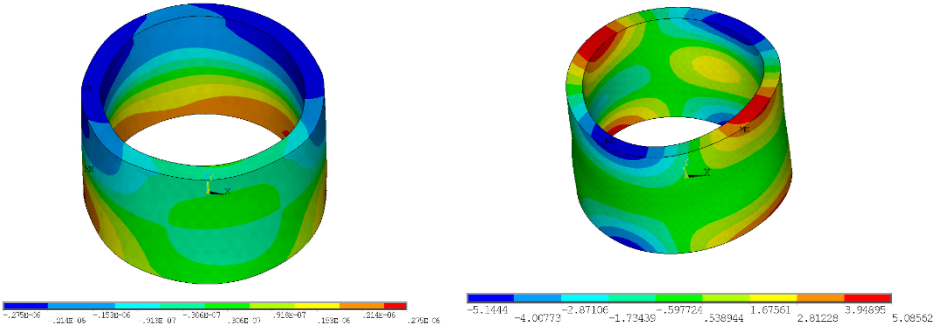

a) b)

$m_1^n = 0.61902200$ $m_3^n = 0.124837718$

$m_2^n = 0.256140221$ $n = 76\ FREQ = 86\ 250$ Hz

Fig. 3.11. Results of harmonic and modal analysis, domination coefficients and modal shape identification: a) resonating frequency at 86 250 Hz; h) a suitable eigenform for 86 250 Hz resonating frequency

A list of domination coefficients and their values are presented in Table 3.3. It can be seen how geometrical parameters affect the sequence of eigen-frequencies. The results also show, how domination coefficients change when eigenform is the same, but the frequency is different. Once proper geometrical parameters, resonating frequencies and correct eigenform have been identified, motion formation problem is addressed. Firstly, rectangular electrode scheme is analyzed. Motion is created by exciting two electrodes at the same time. Voltage for the first electrode stays a constant 100 V and voltage for the second electrode is changed each calculation. Calculations have been done when 50 V, 75 V and 100 V was applied for the second electrode. Contact points move elliptical trajectories and rotate the sphere that is positioned on top.

Table 3.3. Domination coefficients, cylinder PZT-4

Geometrical parameters ($r \times R \times h$)	Values of domination coefficients	
10 × 12.5 × 21 mm	$m_1^n = 0.456627$ $m_2^n = 0.201286$ $m_3^n = 0.342086$ N=33	$m_1^n = 0.562394$ $m_2^n = 0.143229$ $m_3^n = 0.294376$ N=57
12 × 14.5 × 21 mm	$m_1^n = 0.407486$ $m_2^n = 0.397526$ $m_3^n = 0.194988$ N=40	$m_1^n = 0.489872$ $m_2^n = 0.106050$ $m_3^n = 0.404078$ N=65
16 × 18.5 × 21 mm	$m_1^n = 0.437839$ $m_2^n = 0.090892$ $m_3^n = 0.471270$ N=83	$m_1^n = 0.437757$ $m_2^n = 0.254264$ $m_3^n = 0.307978$ N=88
12 × 14.5 × 23 mm	$m_1^n = 0.105089$ $m_2^n = 0.170812$ $m_3^n = 0.724100$ N=62	$m_1^n = 0.273364$ $m_2^n = 0.131745$ $m_3^n = 0.594891$ N=72
14 × 16.5 × 23 mm	$m_1^n = 0.176960$ $m_2^n = 0.401270$ $m_3^n = 0.421770$ N=66	$m_1^n = 0.479599$ $m_2^n = 0.101803$ $m_3^n = 0.418598$ N=73
16 × 18.5 × 23 mm	$m_1^n = 0.400504$ $m_2^n = 0.125143$ $m_3^n = 0.474352$ N=78	$m_1^n = 0.400504$ $m_2^n = 0.246405$ $m_3^n = 0.316463$ N=81

End of Table 3.3

Geometrical parameters ($r \times R \times h$)	Values of domination coefficients	
10 × 12.5 × 25 mm	$m_1^n = 0.217693$ $m_2^n = 0.576762$ $m_3^n = 0.205545$ N=26	$m_1^n = 0.249690$ $m_2^n = 0.277220$ $m_3^n = 0.473090$ N=36

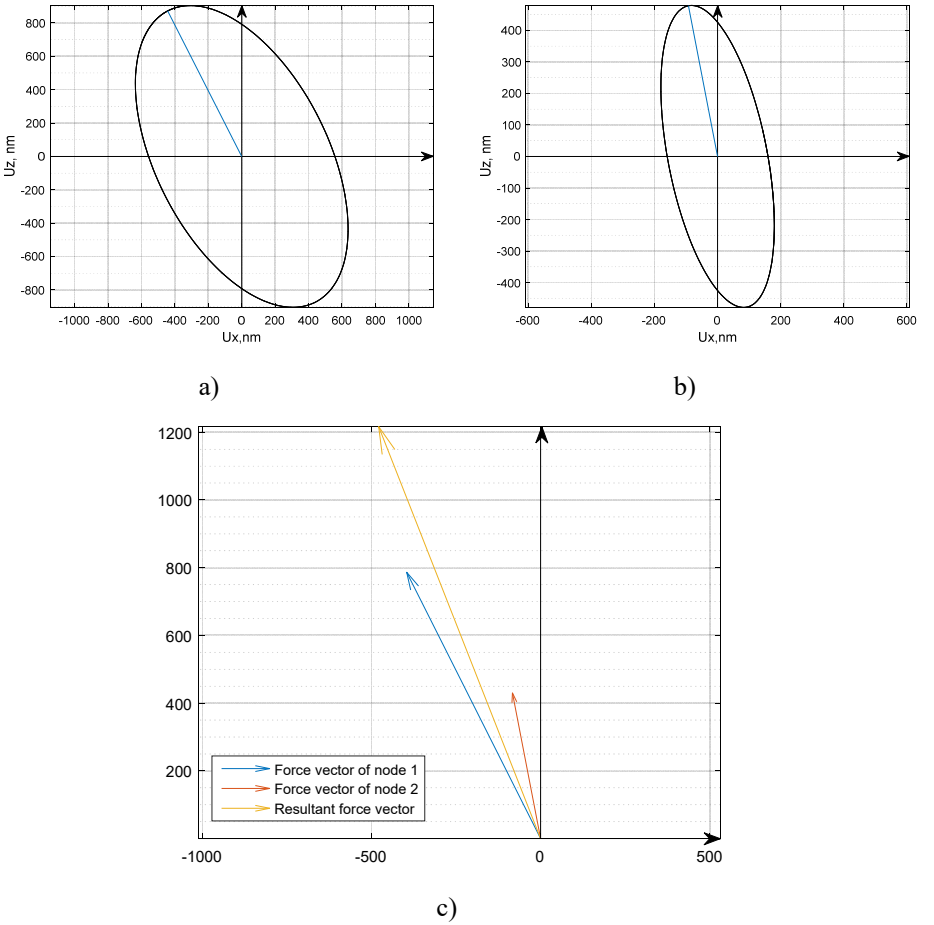

Fig. 3.12. Contact point trajectories in *XZ'* plane and their resultant force vectors. Rectangular electrode scheme used, 100 V and 50 V voltage applied to electrodes: a) motion trajectory of the first contact point; b) motion trajectory of the second contact point; c) resultant force vector

The size of contacting force is determined by calculating the resultant displacement vector. Because two contact points move at the same time, their resultant force is calculated and the angle is then found. It must be noticed that at some point the contact point trajectories change direction, which may result in improper functioning of the actuator.

The results of contact points motion trajectories are shown in Fig. 3.12 (50 V applied to the second electrode), Fig. 3.13 (75 V applied to the second electrode) and Fig. 3.14 (100 V applied to the second electrode).

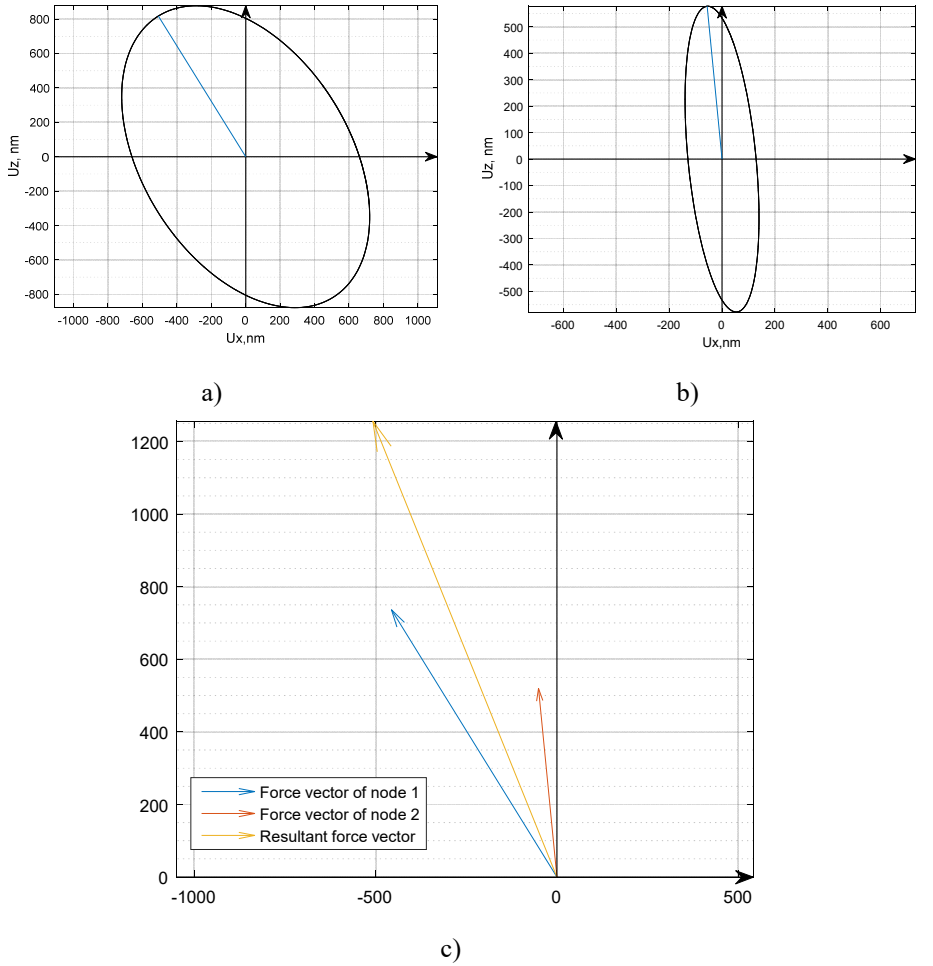

Fig. 3.13. Contact point trajectories in *XZ'* plane and their resultant force vectors. Rectangular electrode scheme used, 100 V and 75 V voltage applied to electrodes: a) motion trajectory of the first contact point; b) motion trajectory of the second contact point; c) resultant force vector

It can be seen from Fig. 3.12, Fig. 3.13 and Fig. 3.14 how motion trajectories change when the voltage for the second electrode is changed. When the applied voltage is 100 V, motion trajectories of both contact points change direction. This change is different for each analyzed object. In all cases the displacement vector is named as the force vector, because the length of the displacement vector determines the size of the force that is required for piezorobot to move in planned trajectory.

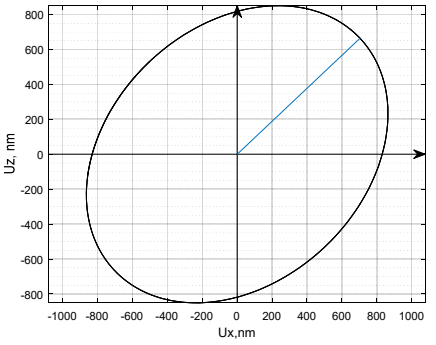

a)

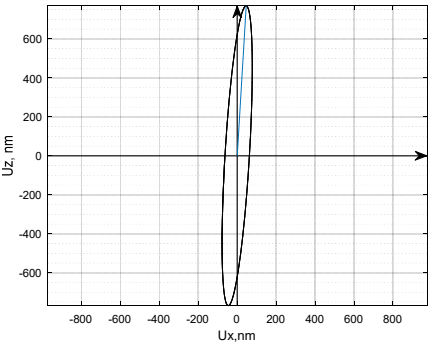

b)

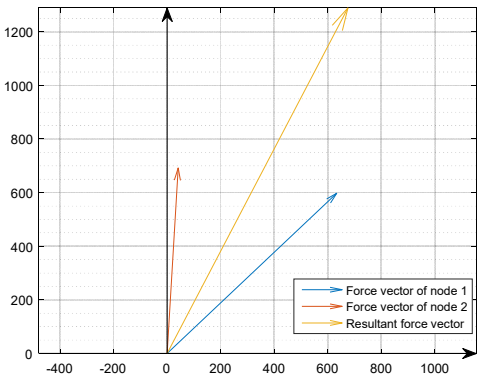

c)

Fig. 3.14. Contact point trajectories in *XZ'* plane and their resultant force vectors. Rectangular electrode scheme used, 100 V and 100 V voltage applied to electrodes: a) motion trajectory of the first contact point; b) motion trajectory of the second contact point; c) resultant force vector

When 100 V/50 V voltage is applied, both contact points move in the same direction. Their resultant force vector magnitude is $r = 1452.7$ nm with an angle of $\varphi = 68.52°$. The trajectories change when voltage to the second electrode is increased to 100 V. In this case, trajectories of both contact points have changed direction. In the following figures, motion trajectories of contact points of a cylinder with a triangular electrode scheme are presented.

All resultant force vectors are shown in polar coordinates in Fig. 3.16. The results when triangular electrode scheme was applied is shown in Fig. 3.15, Fig. 3.17, Fig. 3.18 and Fig. 3.19.

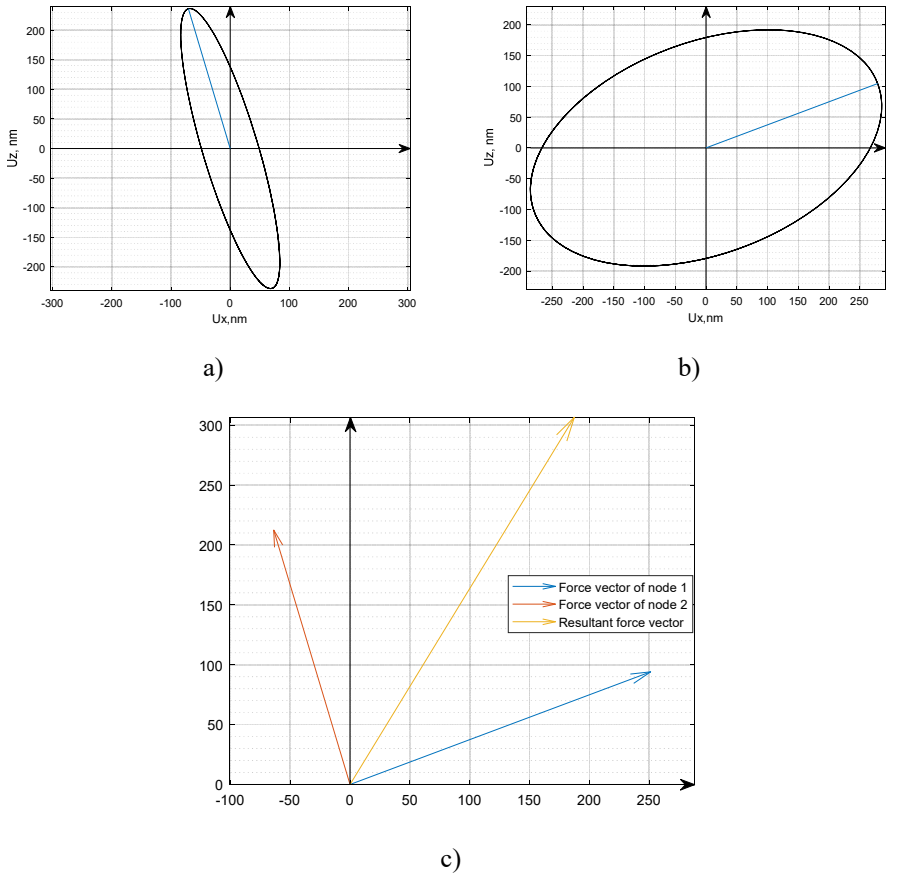

Fig. 3.15. Contact point trajectories in *XZ'* plane and their resultant force vectors. Triangular electrode scheme used, 100 V and 50 V voltage applied to electrodes: a) motion trajectory of the first contact point; b) motion trajectory of the second contact point; c) resultant force vector

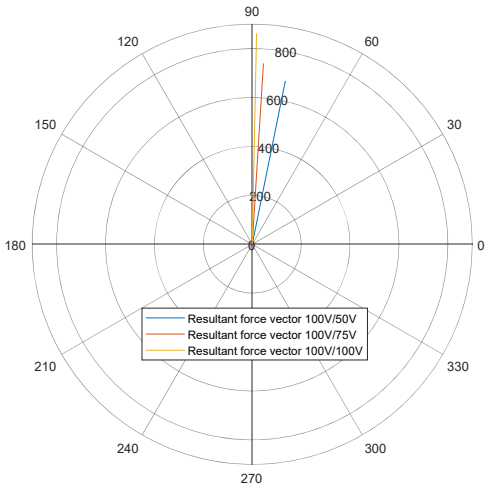

Fig. 3.16. Resultant force vectors in polar coordinates

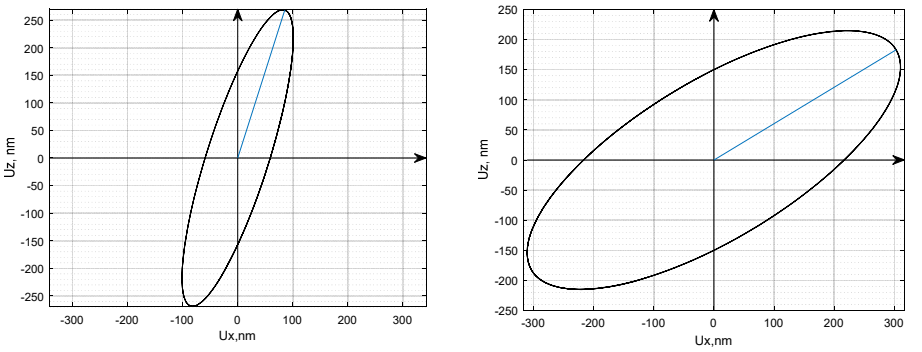

a) b)

Fig. 3.17. Contact point trajectories in *XZ'* plane and their resultant force vectors. Triangular electrode scheme used, 100 V and 75 V voltage applied to electrodes: a) motion trajectory of the first contact point; b) motion trajectory of the second contact point

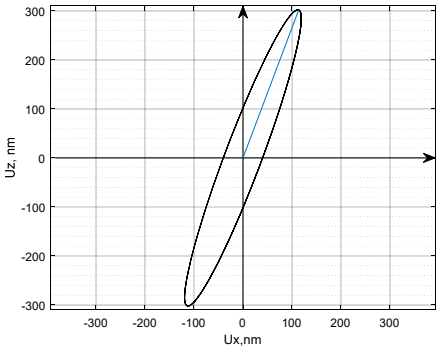

a)

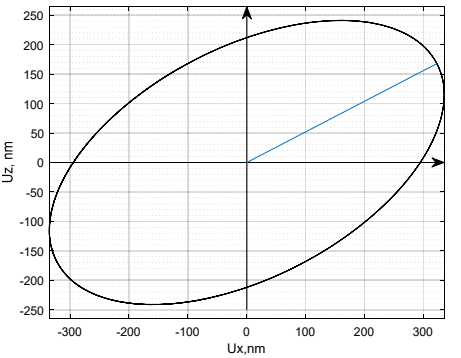

b)

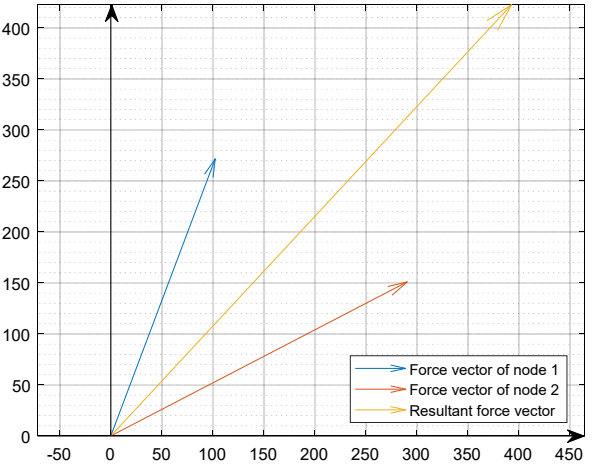

c)

Fig. 3.18. Contact point trajectories in *XZ'* plane and their resultant force vectors. Triangular electrode scheme used, 100 V and 100 V voltage applied to electrodes: a) motion trajectory of the first contact point; b) motion trajectory of the second contact point; c) resultant force vector

It can be seen from Fig. 3.15, Fig. 3.17 and Fig. 3.18 that the trajectories of the first contact point changes direction when 75 V is applied to the electrode. Higher voltages lead to an increased length of the displacement vector. The interaction of the electrodes when two electrodes are excited at the same time is complex and increased voltage does not necessarily mean that the angle of the resultant displacement vector will increase.

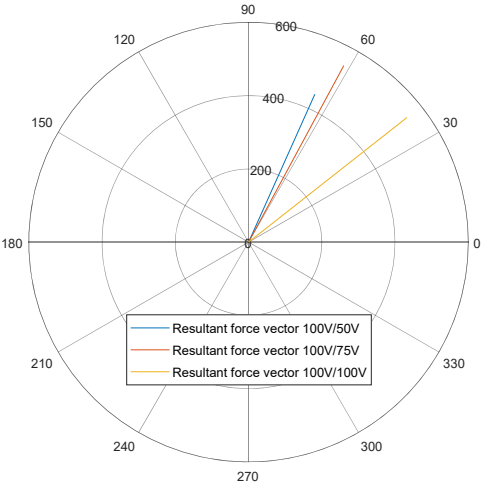

Fig. 3.19. Resultant force vectors in polar coordinates

Resonating frequencies were determined during harmonic analysis and domination coefficients were calculated for each eigenfrequency. In Table 3.3 and Table 3.4 each case has a sequence number of a suitable eigenfrequency and domination coefficients presented. As described before, two eigenfrequencies are compared by their coefficients and eigenforms in order to choose the correct one.

Table 3.4. Domination coefficients, cylinder PZT-8

Geometrical parameters ($r \times R \times h$)	Values of domination coefficients	
10 × 12.5 × 21 mm	$m_1^n = 0.124947$ $m_2^n = 0.235720$ $m_3^n = 0.639333$ N=47	$m_1^n = 0.171424$ $m_2^n = 0.140037$ $m_3^n = 0.688539$ N=51

End of Table 3.4

Geometrical parameters ($r \times R \times h$)	Values of domination coefficients	
12 × 14.5 × 21 mm	$m_1^n = 0.230435$ $m_2^n = 0.146638$ $m_3^n = 0.622927$ N = 54	$m_1^n = 0.191724$ $m_2^n = 0.371684$ $m_3^n = 0.436592$ N = 60
14 × 16.5 × 21 mm	$m_1^n = 0.184656$ $m_2^n = 0.101159$ $m_3^n = 0.714185$ N = 69	$m_1^n = 0.313729$ $m_2^n = 0.128012$ $m_3^n = 0.558259$ N = 72

Another problem that was mentioned before was that the change of geometrical parameters changes the sequence of eigenfrequencies. This can be seen in Table 3.3 and Table 3.4 by comparing N (sequence number) for different objects.

More calculated motion trajectories and domination coefficients are given in Appendix A.

3.3. Numerical analysis of hemispheric ultrasonic actuator used for stabilization

A kinematic pair presented in the Fig. 3.3 is analyzed. In total there have been 10 different hemispheres modelled and analyzed. Their height and diameters vary, the thickness remains constant and equals to 1.5 mm. The flow of analysis is analogous to the analysis of cylindrical actuator. Resonating frequencies for a 13.5 mm (inner diameter) × 15 mm (outer diameter) × 13 mm (height) hemisphere are given in Fig. 3.20.

As it can be seen from the results there are a lot of resonating frequencies that cause the largest deformation amplitudes in Z direction. The frequencies of interest are 30 750 Hz, 37 000 Hz, 43 125 Hz, 52 500 Hz, 56 625 Hz. The results of numerical analysis are given in Figs. 3.21–3.26. The first resonating frequency is not suitable because the eigenform is not correct and would create undesired motion. The second resonant frequency does not qualify the requirement that the displacements in Z direction are the largest ($m_3^n = 0.376257 < m_2^n = 0.416147$, $n = 18$). However, the difference between m_3^n and m_2^n is relatively small, and the eigenform is correct. In the case of the hemispheric actuator, it is not so obvious and easy to distinguish the suitable form with domination coefficients. The eigenforms of the third and fourth case also not

suitable. Results presented in Fig. 3.23 show that the displacements in Z direction are the largest ($m_3^n = 0.417496 > m_2^n > m_1^n$), however, the eigenform is not suitable. The same results are obtained in case presented in the Fig. 3.24 ($m_3^n = 0.392066 > m_1^n > m_2^n$). A resonating frequency at 56 625 Hz is not suitable because the deformations towards Z direction are not the largest ($m_3^n = 0.298553 < m_2^n$). Therefore, the second resonant frequency is chosen. It is worth mentioning that a suitable eigenform is also found at 77 200 Hz, although it results in small amplitudes. Ccontact point trajectories for the resonating frequency of 37 000 Hz are shown in Figs. 3.27–3.29.

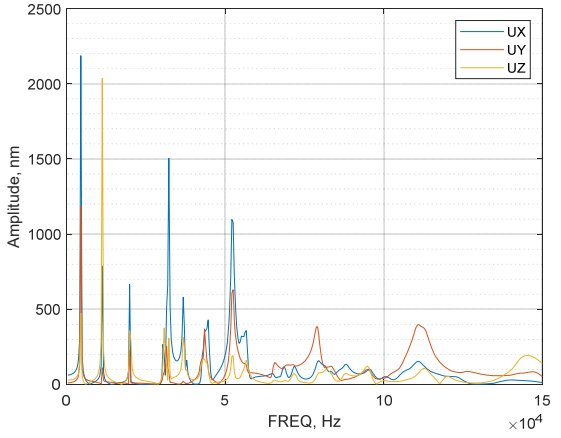

a)

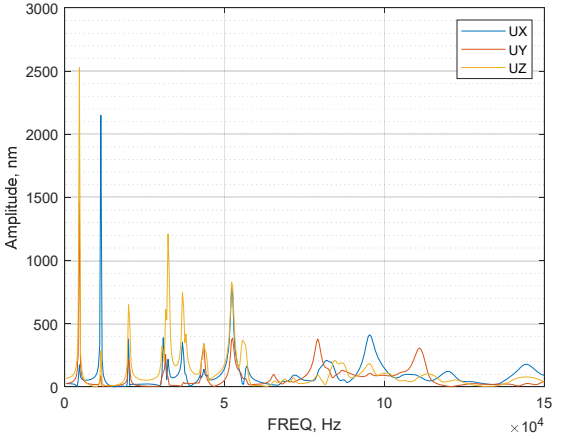

b)

Fig. 3.20. Harmonic analysis for a 13.5 mm × 15 mm × 13 mm hemisphere:
a) amplitudes of the first contact point; b) amplitudes of the second contact point

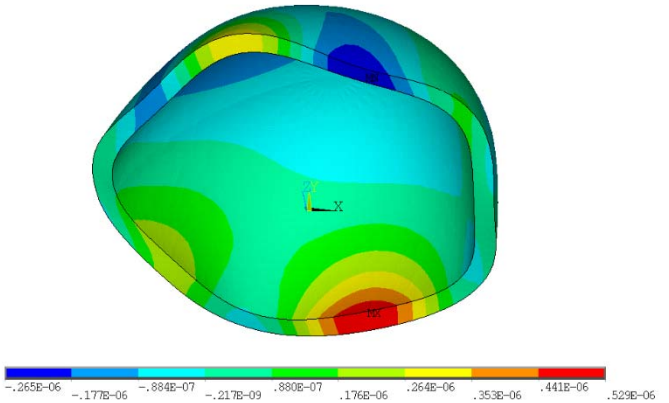

a)

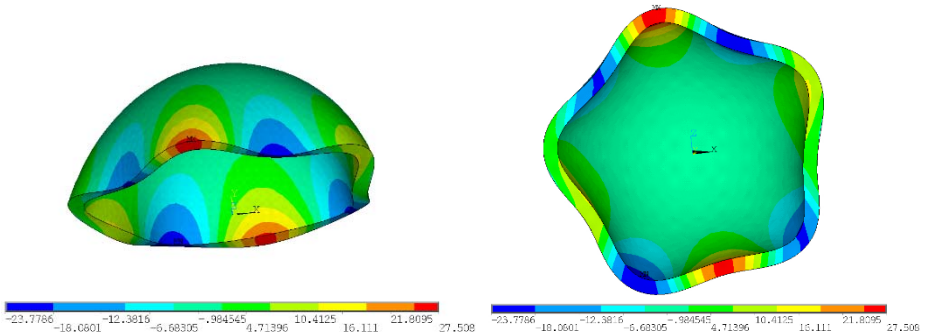

b)

$m_1^n = 0.173493$ $m_3^n = 0.410956$

$m_2^n = 0.415552$ $N = 14, FREQ = 30\ 000\ Hz$

Fig. 3.21. Results of harmonic and modal analysis, domination coefficients and modal shape identification: a) resonating frequency at 30 750 Hz; b) a suitable eigenform for 30 000 Hz resonating frequency; Domination coefficients show that the largest value is for normal ($m_1^n < m_3^n < m_2^n$) and the eigenform is not suitable

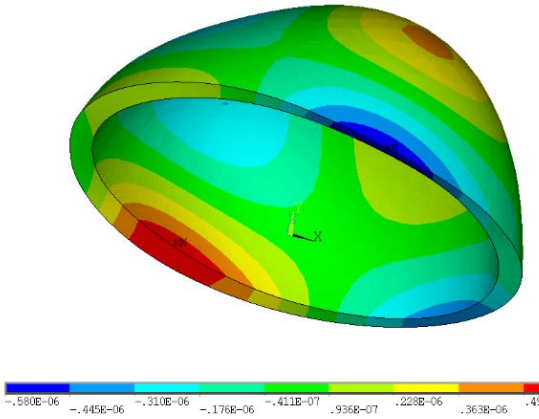

a)

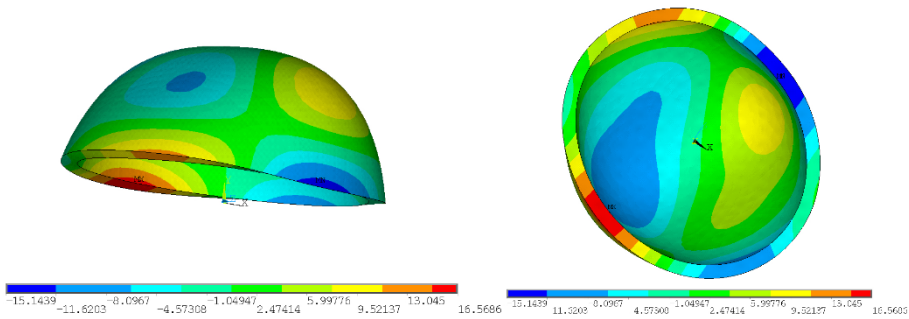

b)

$m_1^n = 0.207596$ $m_3^n = 0.376257$

$m_2^n = 0.416147$ $n = 18, FREQ = 37\ 500\ Hz$

Fig. 3.22. Results of harmonic and modal analysis, domination coefficients and modal shape identification: a) resonating frequency at 30 750 Hz; b) a suitable eigenform for 30 750 Hz resonating frequency; Domination coefficients show that the largest value is for normal ($m_1^n < m_3^n < m_2^n$), however the eigenform is suitable

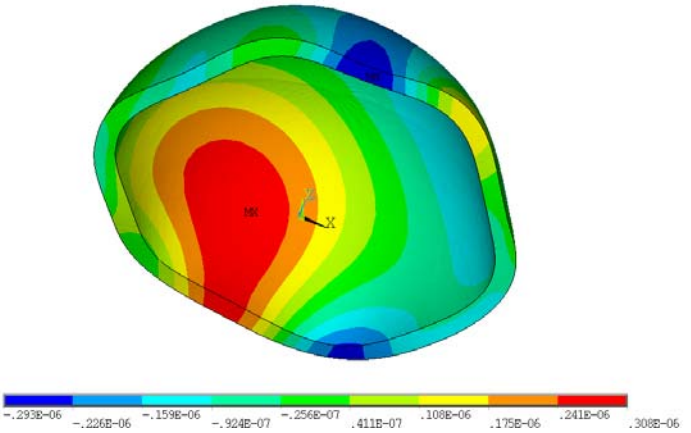

a)

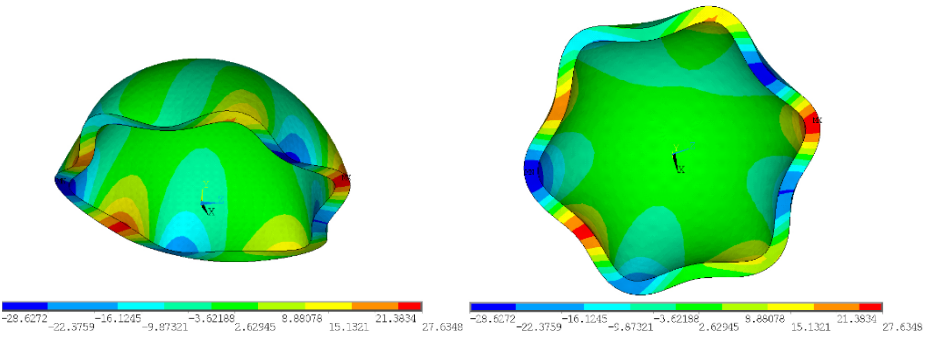

b)

$m_1^n = 0.174283$ $m_3^n = 0.417496$

$m_2^n = 0.408222$ N = 22 FREQ = 43 125 Hz

Fig. 3.23. Results of harmonic and modal analysis, domination coefficients and modal shape identification: a) resonating frequency at 43 125 Hz; b) a suitable eigenform for 43 125 Hz resonating frequency; Domination coefficients show that the largest value is for normal ($m_1^n < m_3^n < m_2^n$) and the eigenform is not suitable

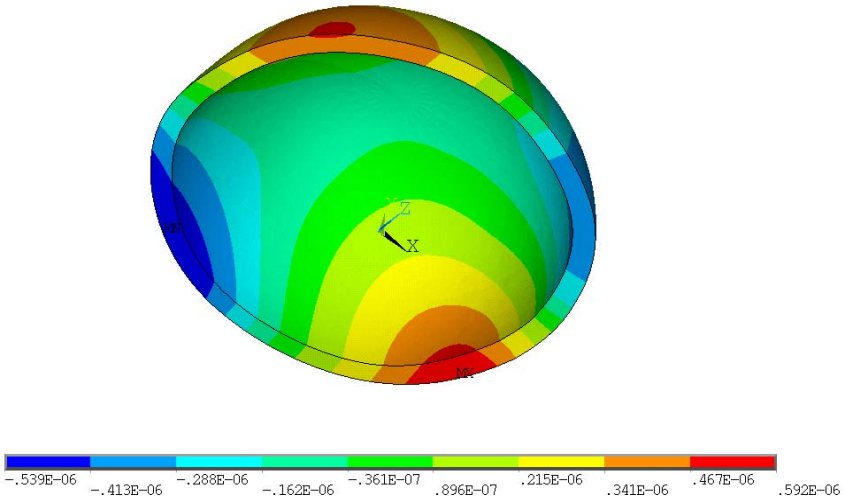

a)

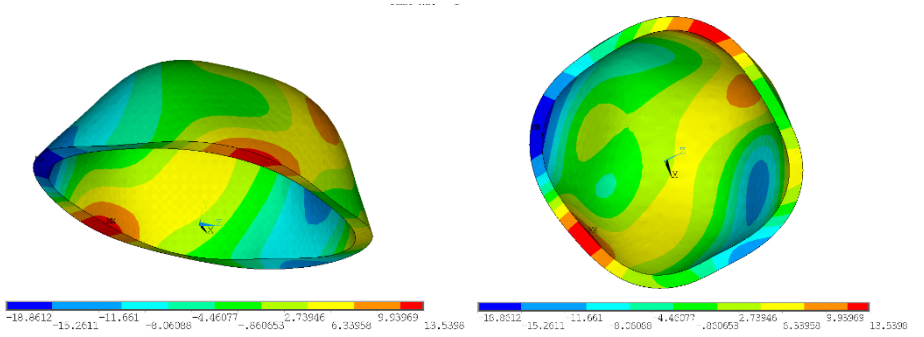

b)

$m_1^n = 0.312375$ $m_3^n = 0.392066$

$m_2^n = 0.295559$ $n = 29\ FREQ = 52\ 500\ Hz$

Fig. 3.24. Results of harmonic and modal analysis, domination coefficients and modal shape identification: a) resonating frequency at 52 500 Hz; b) a suitable eigenform for 52 500 Hz resonating frequency; Domination coefficients show that the largest value is for normal ($m_1^n < m_3^n < m_2^n$) and the eigenform is not suitable

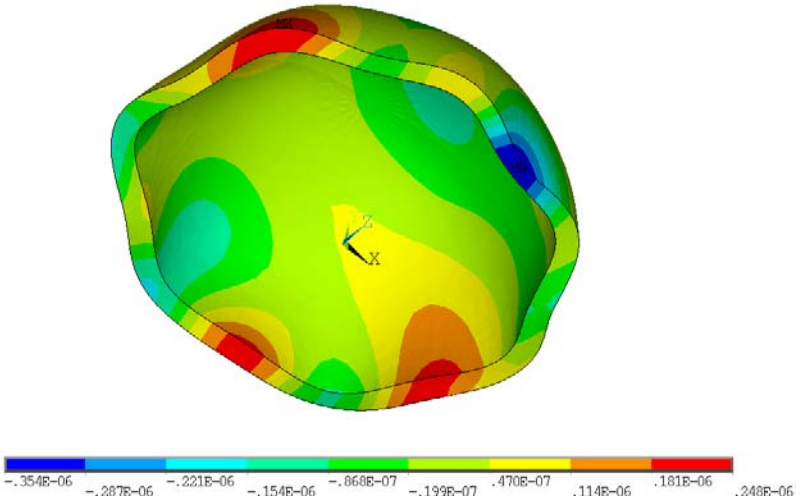

a)

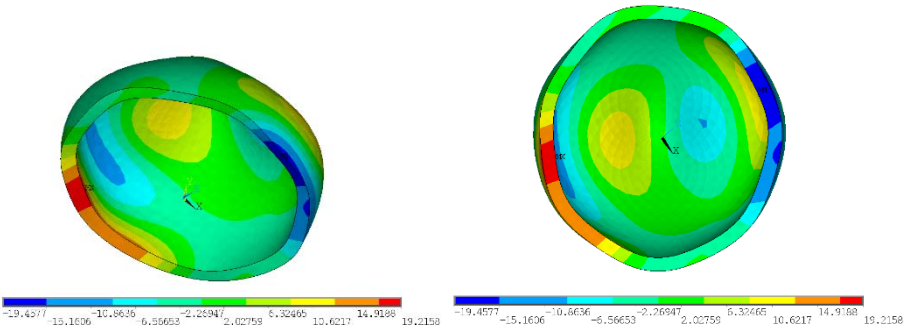

b)

$$m_1^n = 0.133170 \qquad m_3^n = 0.298553$$

$$m_2^n = 0.568277 \qquad n = 33\ FREQ = 56\,625\ Hz$$

Fig. 3.25. Results of harmonic and modal analysis, domination coefficients and modal shape identification: a) resonating frequency at 56 625 Hz; b) a suitable eigenform for 56 625 Hz resonating frequency; Domination coefficients show that the largest value is for normal ($m_1^n < m_3^n < m_2^n$) and the eigenform is not suitable

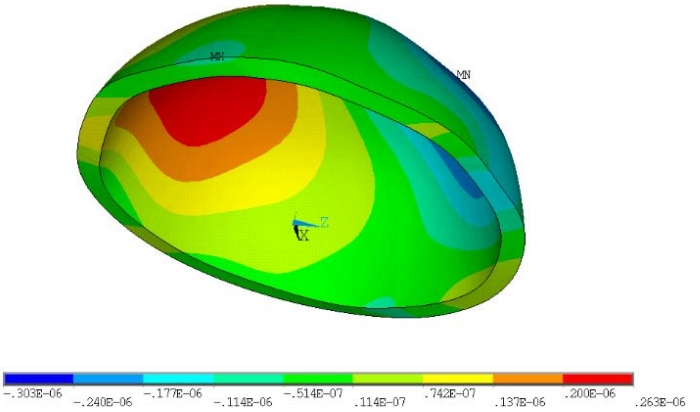

a)

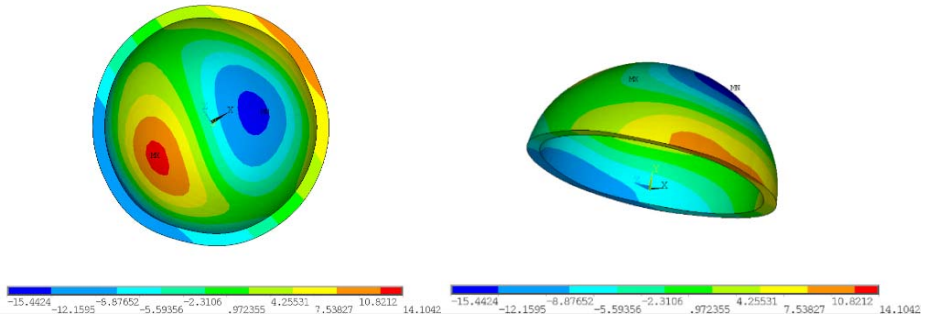

b)

$m_1^n = 0.294933$ $m_3^n = 0.490937$

$m_2^n = 0.214130$ $n = 48\ FREQ = 77\ 000\ Hz$

Fig. 3.26. Results of harmonic and modal analysis, domination coefficients and modal shape identification: a) resonating frequency at 77 000 Hz; b) a suitable eigenform for 77 000 Hz resonating frequency; Domination coefficients show that the largest value is in Z direction ($m_2^n < m_1^n < m_3^n$) and the eigenform is suitable. However, the amplitudes were too small

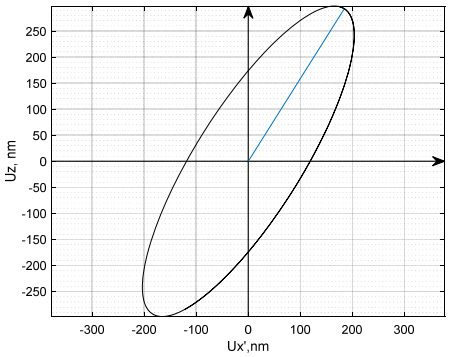

a)

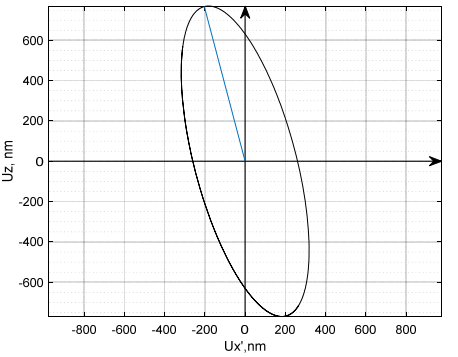

b)

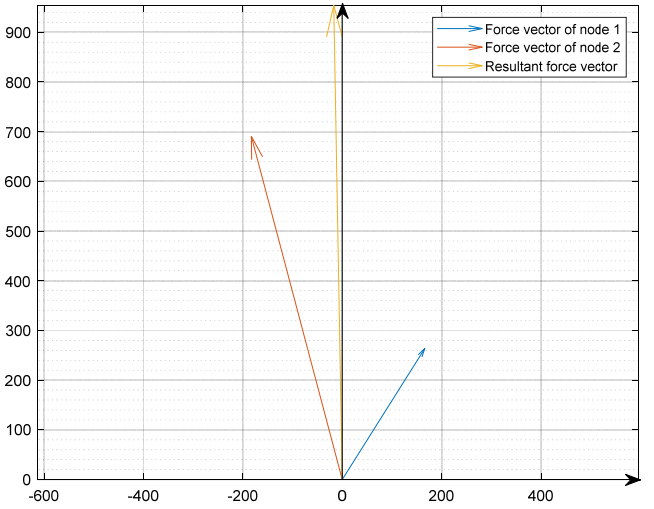

c) $r = 1060.3\ nm\ \varphi = 91.02°$

Fig. 3.27. Contact point trajectories in *XZ'* plane and their resultant force vectors. Triangular electrode scheme used, 100 V and 50 V voltage applied to electrodes: a) motion trajectory of the first contact point; b) motion trajectory of the second contact point; c) resultant force vector

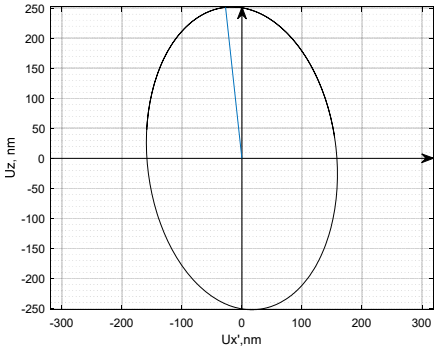

a)

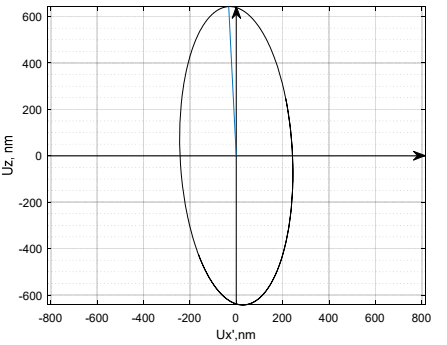

b)

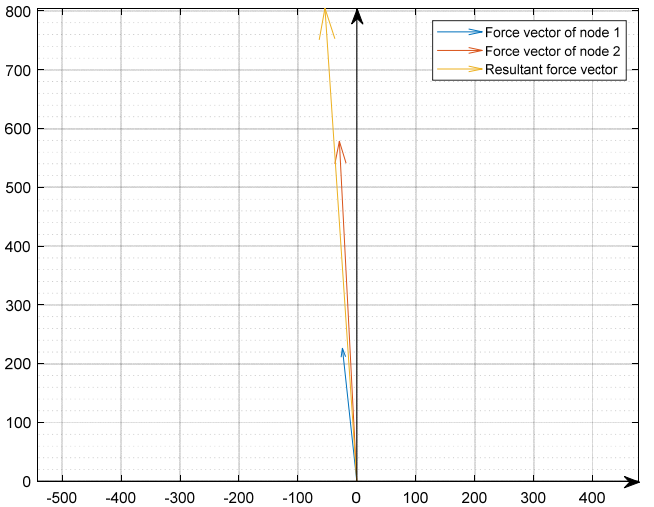

c) $r = 896.23\ nm\ \varphi = 93.85°$

Fig. 3.28. Contact point trajectories in *XZ'* plane and their resultant force vectors. Triangular electrode scheme used, 100 V and 75 V voltage applied to electrodes: a) motion trajectory of the first contact point; b) motion trajectory of the second contact point; c) resultant force vector

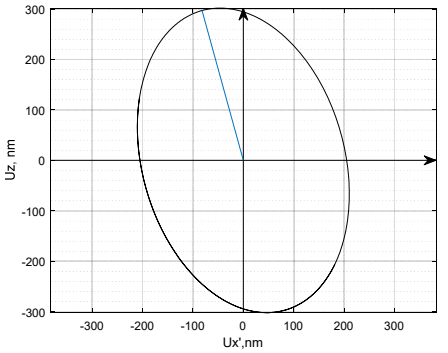

a)

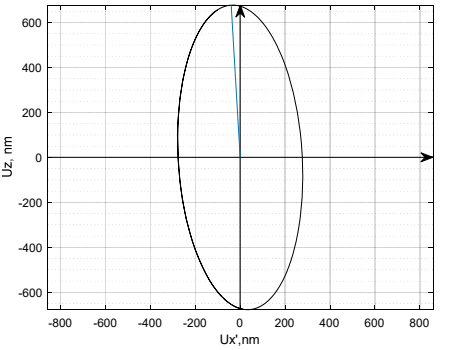

b)

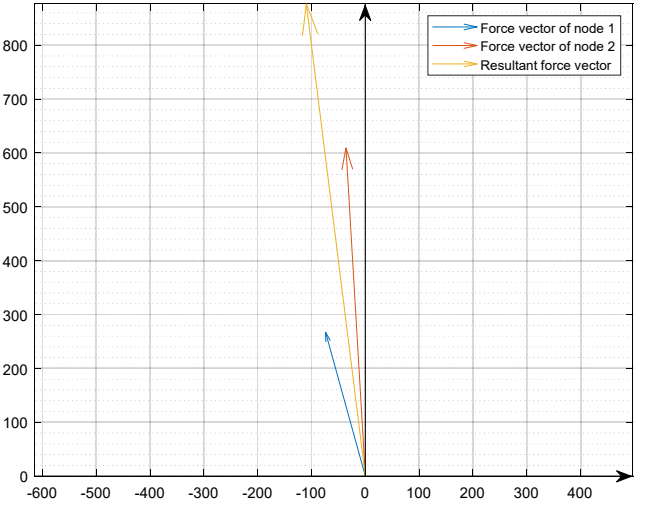

c) $r = 981.62\ nm\ \varphi = 97.13°$

Fig. 3.29. Contact point trajectories in *XZ'* plane and their resultant force vectors. Triangular electrode scheme used, 100 V and 100 V voltage applied to electrodes: a) motion trajectory of the first contact point; b) motion trajectory of the second contact point; c) resultant force vector

Fig. 3.30 shows displacement vectors of contact points and cumulative displacement vector in polar coordinates. Calculated domination coefficients for some hemispheres are given in Table 3.5.

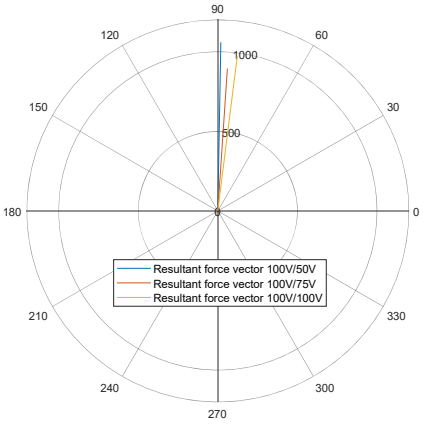

Fig. 3.30. Resultant force vectors in polar coordinates

Table 3.5. Domination coefficients, hemisphere PZT-4

Geometrical parameters ($r \times R \times h$)	Values of domination coefficients	
13.5 × 15 × 11 mm	m_1^n =0.268798 m_2^n =0.384512 m_3^n =0.346690 N = 8	m_1^n = 0.397683 m_2^n = 0.196938 m_3^n = 0.405378 N = 19
13.5 × 15 × 13 mm	m_1^n = 0.207596 m_2^n = 0.416147 m_3^n = 0.376257 N = 18	m_1^n = 0.174283 m_2^n = 0.408222 m_3^n = 0.417496 N = 22
13.5 × 15 × 15 mm	m_1^n = 0.173941 m_2^n = 0.453429 m_3^n = 0.372631 N = 13	m_1^n = 0.173941 m_2^n = 0.453429 m_3^n = 0.372631 N = 16
13.5 × 15 × 15 mm	m_1^n = 0.156675 m_2^n = 0.402229 m_3^n = 0.441096 N = 30	m_1^n = 0.143096 m_2^n = 0.238991 m_3^n = 0.617913 N = 32

It can be seen from the results that the suitable eigenform sequence number changes for each actuator. When analyzing and choosing the correct geometrical parameters for hemisphere, it is necessary to not only evaluate and compare domination coefficients, but also to check the eigenform. Numerical analysis has shown that m_3^n and m_1^n can have smaller values than m_2^n, but the eigenform can be correct.

3.4. Conclusions of Chapter 3

1. Two piezorobots with 6 degrees-of freedom have been proposed and analyzed. The results of numerical analysis have shown that by exciting two electrodes at the same time, the piezorobot can move in a continuous trajectory or rotate the sphere.
2. Harmonic analysis of cylindrical and hemispheric actuators has been performed in the frequency interval 0–150 000 Hz and it was found that resonant frequencies did not differ from eigenfrequency more than 6%. Numerical analysis has been performed for 40 objects – 15 cylindrical actuators with rectangular electrode scheme, 15 cylindrical actuators with triangular scheme, and 10 hemispheric actuators. Analysis of different geometry of the actuators has shown:
   - when the inner and outer radius changed, but the height remained the same, a suitable resonant frequency was lower each time;
   - when the inner and outer radius did not change, but the height changed, the the resonant frequency was higher.
3. The required force for the trajectories planning algorithm is determined by calculating resultant displacement vectors. Harmonic analysis showed that bigger voltage difference between the electrodes resulted in the smaller resultant displacement vector length.
4. It has been determined what voltage should be applied to each electrode so that contact points would move in such trajectories, that the resultant displacement vector would be as required for trajectories planning algorithm.

4

Investigation of quantitative characteristics

In this chapter the experimental results based on numerical analysis, that is described in Chapter 3, are presented. Firstly, an overview about motion trajectories control is given to clarify which step of a more complex problem this research solves. The trajectories of the piezorobot moving on a plane or the trajectories of the rotated sphere depend on the motion trajectories of the contact points. It is not possible to successfully control the motion without knowing what voltages should be applied and what is the length and direction of the resultant displacement vector.

Then each performed experiment is described in detail; all results have been published in press. It was verified whether the determined geometrical parameters are suitable, how much the resonating frequency differs from the frequency obtained in numerical analysis, what are the motion trajectories of contact points. Working prototypes have been created based on the problem that was being analyzed: A rotary table with cylindrical actuator with one excited electrode (Grybas *et al.* 2016), several prototypes with 3 DOF and trunk robots with 6 DOF (Bansevicius *et al.* 2017, Bansevicius *et al.* 2016a), a piezorobot for nanosatellite stabilization using a triangular electrode scheme (Bansevicius *et al.* 2018).

An experimental control system was developed to verify the trajectory planning algorithm and to verify if the piezorobots' motion formation algorithms

according to electrode excitation schemes is correct (Janutenaite-Bogdaniene *et al.* 2017, Bansevicius R. *et al.* 2016b).

The material in this chapter was published in scientific journals (Janutėnaitė-Bogdanienė *et al.* 2017, Bansevicius *et al.* 2016a, Bansevicius *et al.* 2016b, Bansevicius *et al.* 2018, Grybas *et al.* 2016, Bansevičius *et al.* 2017, Mačerauskas *et al.* 2017).

4.1. Trajectory planning for piezorobots

Mathematical models for the sphere positioning through contacting force, trajectories planning for piezorobots moving on a plane, joint trajectory planning for trunk robots have been described (Drukteiniene 2011, Bansevicius R. *et al.* 2016a, Bansevicius R. *et al.* 2016b, Bansevicius R. *et al.* 2018, Janutenaite-Bogdaniene J. *et al.* 2017, Janutenaite-Bogdaniene J. *et al.* 2018). The importance of this research and its input in the whole control problem of piezorobot can be seen in Fig. 4.1.

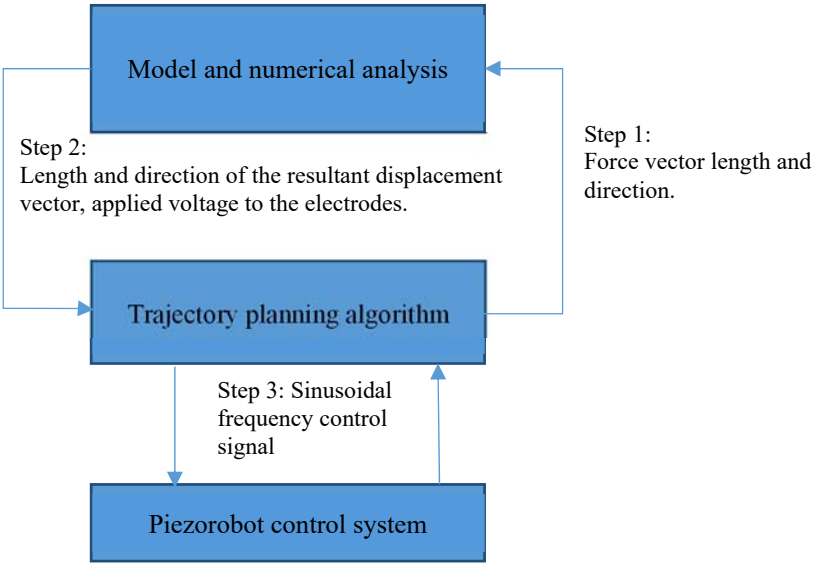

Fig 4.1. Scheme for the trajectory planning of the piezorobot

Trajectory planning consist from 3 main steps: 1) the required force vector length and direction is calculated, 2) the resultant displacement vector is

calculated accordingly to the given force vector, 3) sinusoidal control frequency is formed accordingly to the results obtained during numerical analysis.

The trajectory planning algorithm describes in what trajectory a piezorobot will move. This algorithm calculates the required force and direction for the piezorobot to move in the desired motion; the algorithm itself is described in more detail in an article (Bansevičius R. P. *et al.* 2015b). The force and its direction is determined by movement of the contact points. Because two electrodes are excited at the same time, the resultant displacement vector must be calculated. The direction and length of the resultant displacement vectors for each case are calculated during the numerical analysis. It is then known when and which electrodes must be excited, and what voltage should be applied to each electrode.

A trajectory planning MATLAB software is integrated with LabVIEW program. MATLAB software module forms a sinusoidal frequency control signal that is used to control sinusoidal signal generators. The signal is determined from the results of numerical analysis. The results of trajectory planning algorithm are presented in the next chapter, where theoretical and real trajectories are compared and the validity of algorithm is determined.

4.2. Comparison of the experimental and theoretical results

Linear motion without rotation is created by exciting two or more electrodes at the same time. As it was mentioned in the second chapter one excited electrode causes a piezorobot to move in a straight broken line. When all electrodes are excited the piezorobot rotates. A case when only one electrode is excited is presented in article (Grybas I. *et al.* 2016).

A designed rotary table consists of a cylindrical 32 mm (outer diameter) × 28 mm (inner diameter) × 14 mm (height) actuator made from PZT-4 material. The cylinder itself is placed on three equally spaced base elements that are attached to the housing. A contact with the rotor is through three contact zone elements each placed at 120°. The rotor shaft is rigidly mounted in the bearing and a magnet ensures that the pulling force between the housing and the rotor is sufficient. This causes the rotor to be in the center with respect to its rotational axis. A numerical analysis has been performed in order to determine the motion trajectories of the driven contact zone elements. It has been calculated that the correct corresponding frequency is 125 582 Hz. It has been determined that the table should function in a range 124–126 kHz. Displacements of contact points reach the highest values of 0.75 μm in X direction and 1.15 μm in Z direction. A frequency response of the actuators and average motion trajectories are shown in Fig. 4.2.

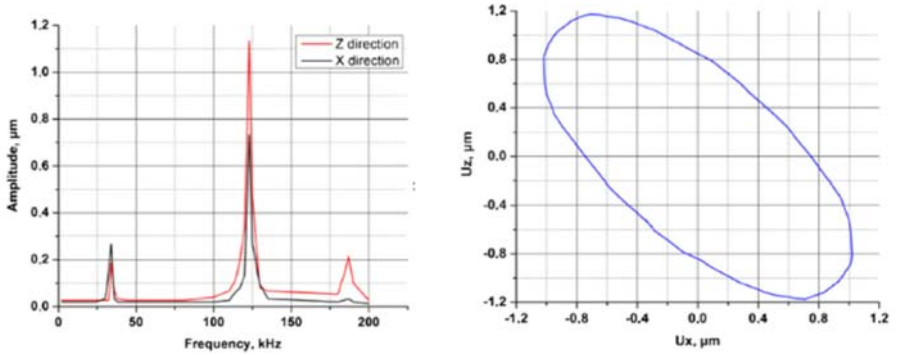

a) b)

Fig. 4.2. Dynamic characteristics of the rotary table: a) average frequency responses of the contact zone elements in the X and Z directions, b) average motion trajectory of the contact zone elements at the resonant 124 kHz frequency (Grybas I. *et al.* 2016)

The setup that was used to conduct the experiment consists of a signal generator (Agilent 33220A), rotary table, amplifier (EPA-104), Laser Dopppler vibrometer (Polytec Inc. equipment composed of laser sensor head OFV-130-3, interferometer OFV-512, and controller OFV-5000), oscilloscope (PicoScope-3424), and PC.

In order to validate the movement trajectory of the piezorobot on a plane, the whole control system was designed. A video camera was used to track the trajectory of the piezorobot so that it can be compared with the trajectory calculated mathematically. Standard image processing algorithms and coordinate tracking methods were used and are not discussed in this paper. The acquired graphical information is analyzed using automatic image processing tools. As the experiments have shown it is not possible to replicate the trajectory ideally, therefore different error values were defined. The trajectory of the cylindrical actuator is shown in Fig. 4.3 and Fig. 4.4.

The errors are smaller when the formation step is smaller. The largest errors were detected only where the trajectory makes a bend. This is because the generated force vector is not in alignment with the direction of the movement. Regardless of the errors, the required trajectory of the piezorobot has a satisfactory accuracy. The theoretical and experimental trajectories were similar which means that this method can be applied for piezorobot control. Several examples of kinematic pairs with 3 DOF have been presented in an article (Bansevicius *et al.* 2017). Rotation of the sphere around the axis corresponding to the position of a specific exciting zone is achieved by connecting a resonant frequency harmonic voltage to any of these zones (e.g., $U_1 = U_0 cos\omega t$, $U_2 = 0$, $U_3 = 0$; where ω is

the resonant frequency of a higher mode of oscillation of piezoelectric cylinder) leads to.

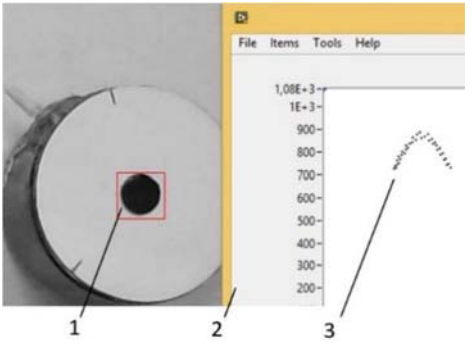

Fig. 4.3. Object tracking and path plotting window:
1 – tracking point on piezorobot, 2 – path of piezorobot,
3 – path plotting window (Janutenaite-Bogdaniene *et al.* 2017)

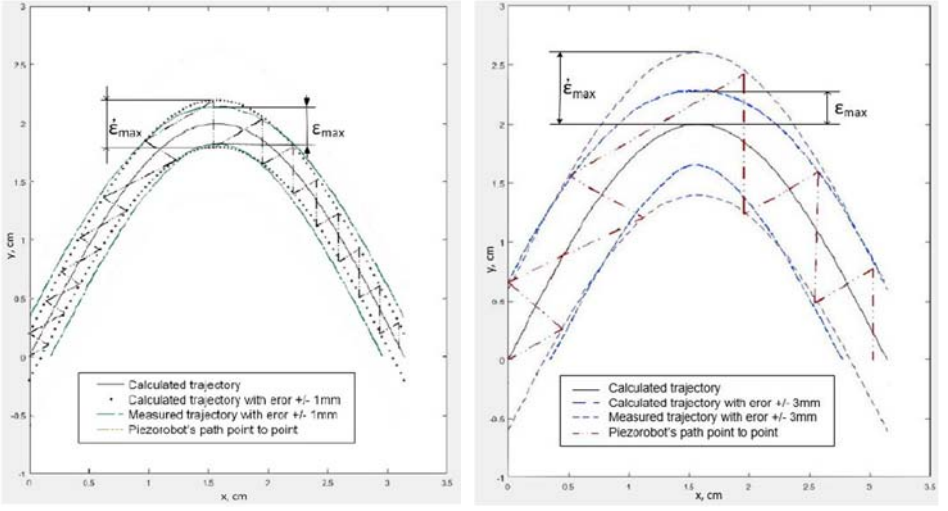

a) b)

Fig. 4.4. Trajectories of piezorobot obtained during the experiment: a) ε_{max} – calculated error ± 1 mm; b) ε'_{max} – measured error ± 3 mm (Janutenaite-Bogdaniene *et al.* 2017)

Rotation of the link around the axis z is achieved by connecting three-phase harmonic voltages to electrodes, such as $U_1 = U_0 cos\omega t$, $U_2 = U_0 \cos(\omega t + \frac{2\pi}{3})$,

$U_3 = U_0\cos(\omega t + \frac{4\pi}{3})$. In a Fig. 4.5 an example of an active kinematic pair with 3 DOFs is given. It is a piezoelectric cylinder, which moves on a plane.

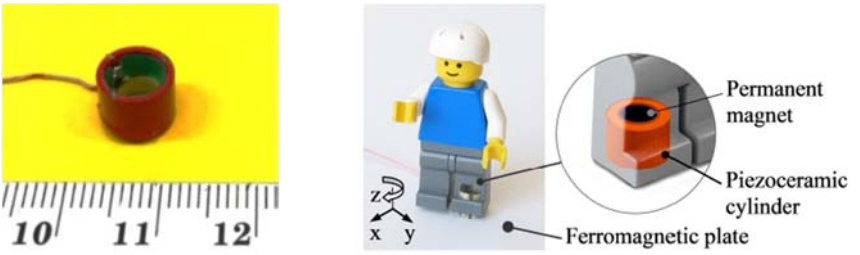

a) b)

Fig. 4.5. Several examples of piezoelectric active kinematic pairs with controllable structure: a) piezoelectric cylinder for scale; b) piezoelectric actuator used to move the figurine on the plane (Bansevicius *et al.* 2017)

This type of kinematic pair is technologically advanced and allows developing high-speed 3D positioning on a plane. Two modifications of piezoelectric robots with 6 DOF are shown in Fig. 4.6.

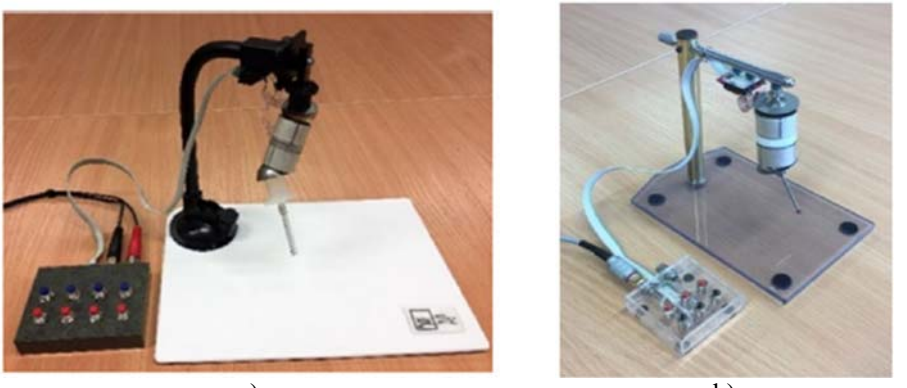

a) b)

Fig. 4.6. Two modifications of a piezoelectric robot: a) ferromagnetic spheres used as links; b) ferromagnetic cylinders used as links (Bansevicius *et al.* 2017)

Impedance-phase vs. frequency characteristics are given in Fig. 4.7. The measurements were done with impedance analyzer Wayne Kerr 6500B (Wayne Kerr Electronics Inc., USA). The motion of piezorobot was generated by using a burst type signal where $U_1 = 60\ V$ and $f = 64$ kHz.

The resolution and velocity were measured at the grip with a laser vibrometer system OFV-5000/505 (Polytec Inc., USA). The results are presented in Fig. 4.8.

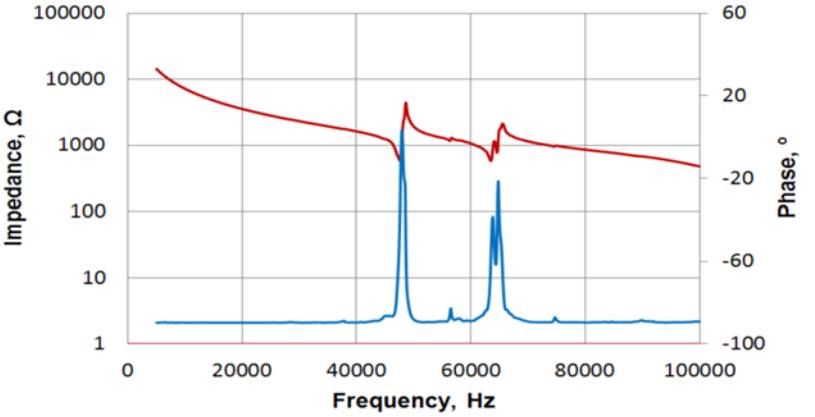

Fig. 4.7. Frequency response of impedance of piezoelectric transducer (operational frequency is 64 kHz) (Bansevicius *et al.* 2017)

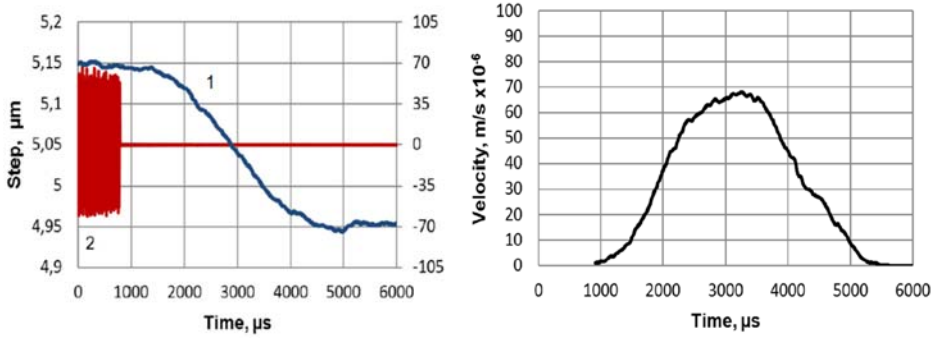

a) b)

Fig. 4.8. Results of the experiment: a) displacement; b) velocity of a robot, when burst type electric signal ($U_1 = 60\ V$) is connected to the electrodes of the piezoelectric actuator (Bansevicius *et al.* 2017)

A piezoelectric cylindrical actuator 33 mm (outer diameter) × 28 mm (inner diameter) × 21 mm (height) was manufactured and experiments were conducted. A PZT-4 type material was chosen for its suitable properties such as high resistance to depolarization and low dielectric loss. A working frequency obtained experimentally was 65 kHz, which is very close to a working frequency obtained from modal analysis (61.721 kHz). The form at this frequency ensures that the largest displacements occur towards z direction. Three identical electrodes, each

placed at 120° cover the outer surface of the cylinder. Two high frequency signals $U_1(t)$ and $U_2(t)$ are applied to the electrodes. The motion created by oscillations is conveyed through contact points. When only one electrode is excited, then the motion is passed through the contact point that is positioned in the middle of an electrode segment. When two electrodes are excited, then the motion force is a resultant force vector of two contact points. The highest displacements are between them. Different voltages are applied to obtain the required motion for trajectory planning algorithm. During this experiment proper voltage ratios were determined.

Experiments were done with both, rectangular and triangular, electrode schemes. When two electrodes are excited, the piezorobot moves in a continuous line or rotates the sphere. The results presented in the article (Bansevicius *et al.* 2016) show how multi-degree-of-freedom trunk robots can be controlled by actuating only the trunk of the robot. This allows to considerably increase the number of degrees-of-freedom, reduce the number of actuators, enable the grip to reach hardly accessible zones, simplify mechanical design and ensure low weight. The results of numerical analysis have been used for trajectory planning algorithm and the movement in desired trajectory has been tested experimentally. The trajectories of grip were realized using special software. The number of degrees-of-freedom of every kinematic pair were controlled in real time and it was possible to see the relation to the phase of external force with alternating direction. Trajectory planning algorithms for two excitation schemes were previously presented in paper (Bansevicius *et al.* 2013).

The experiments conducted were used verify it. An experimental system was developed to validate the correctness of the proposed algorithms. A piezoelectric cylinder served as a prototype of the piezorobot that moved on a glass plate and the control system was used to monitor it. The experimental system is shown in Fig. 4.9. The interface to hardware output was set according to the technical requirements of National Instruments NI-DAQmx hardware.

The trajectory planning algorithm MATLAB software was integrated into LabVIEW program. A sinusoidal frequency control signal for three sinusoidal generators is formed by MATLAB software. A sinusoidal signal generated for the piezorobot control was 52.5 kHz (compared to 49 kHz obtained during numerical analysis). Amplitude control signals change the amplitude of each signal and manage the amplifiers. This signal is then conveyed to each segment of the piezorobot. Amplitudes are managed according to the algorithm that is described by MATLAB software.

The force generated by segments of piezorobot is proportional to the control signal amplitudes which have been monitored by a digital oscilloscope.

The experiment has shown that movement trajectory of the piezorobot is very similar to the trajectory calculated mathematically. The results are shown in

Fig. 4.10 where two real-time trajectories are compared to mathematically calculated trajectories.

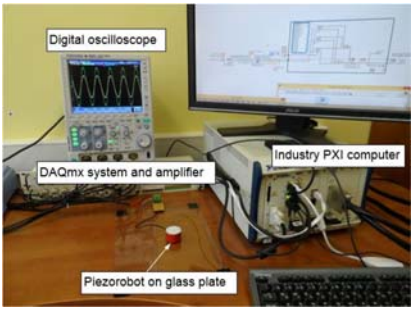

Fig. 4.9. The experimental computer based system (Bansevicius *et al.* 2016a)

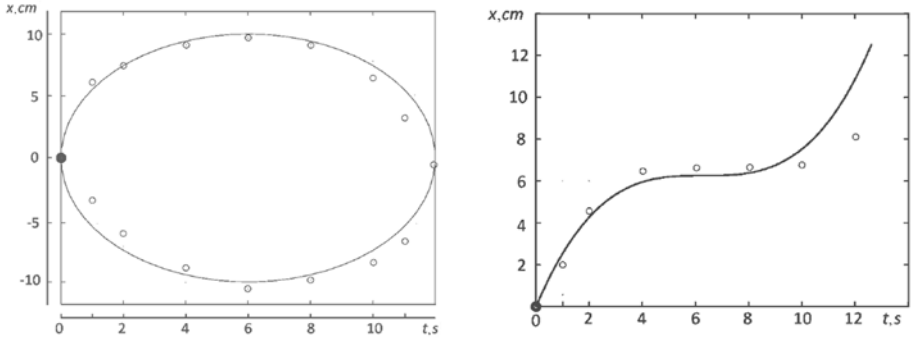

a) b)

Fig. 4.10. Real trajectories of piezorobot obtained during experiments: a) elliptical trajectory; b) curve trajectory. Here ● – starting position, ○ – a point at discrete time moment, — – programmed coordinates (Bansevicius *et al.* 2016a)

A piezoelectric transducer used for nanosatellite positioning was presented in paper (Bansevicius *et al.* 2016b). It is required to reduce the satellite spinning after launch. This can be done by orienting the payload in a precise direction. Effective attitude control system consists of a passive ferromagnetic sphere and a piezoceramic cylinder. A magnet inside the cylinder ensured that the sphere is always in contact with the cylinder. Numerical analysis done prior to experiments is described in the previous chapter. It was required that the deformations would be the largest in Z direction and the second largest would be tangential. This was determined by domination coefficients and an eigenform. The analysis also showed that the required geometric parameters should be 14 mm (inner radius) × 17 mm (outer radius) × 23 mm (height) and the material used for this experiment was PZ26. In all experiments, the radius of the sphere was $R = 17$ mm and a

distance from the center of the sphere to the force acting plane was $d = 14$ mm. Different combinations of voltage were tested: voltage in electrodes that differ 3 times, 2 times and 1.5 times. The resonating frequency with largest amplitudes was 77 kHz, but a more suitable form is at 74 kHz. Trajectory planning algorithm was designed to maximize the velocity of the sphere in any direction. Numerical analysis showed that a combination of 150 V and 50 V created the highest amplitudes and proper angle with a XZ plane. The trajectory planning algorithm was verified numerically and experimentally. The experimental system was already described and shown in Fig. 4.9. A 71 kHZ sinusoidal signal for piezorobot control was generated. This differs by 4.05% from the result obtained from numerical analysis. The voltage to the electrodes was applied the same as it was during numerical analysis. The experimental results showed that the movement of the sphere is very similar to the one that was calculated mathematically. Video frame analysis at certain discrete time points verified that the sphere rotates and in short intervals the selected surface point movement is similar to the planned trajectory.

A radially poled piezoelectric cylinder made from the hard type piezo ceramic of type PZT-8 was produced for experiments based on the results of numerical analysis. It has six triangle-shaped electrodes on the surface, which were formed by etching using nitric acid. Dimensions of the cylinder were 33 mm × 28 mm × 20 mm; measurements were performed using a 3D scanning vibrometer and an impedance analyzer shown in Fig. 4.11. Vibration modes were investigated and resonating frequencies identified.

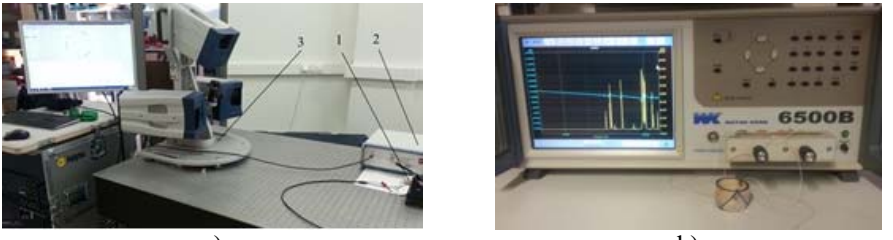

a) b)

Fig. 4.11. Experimental setup: a) setup for investigating the modes of vibration; b) impedance measurement of the piezoelectric cylinder. Here 1 – piezoelectric cylinder; 2 – linear amplifier; 3 – 3D scanning vibrometer; 4 – impedance analyzer (Bansevicius *et al.* 2018)

Equipment used for the experiment was a linear amplifier P200 (FLC Electronics AB, Sweden) which drives the actuator, a 3D scanning vibrometer PSV-500-3D-HV (Polytec GmbH, Springe, Germany) and an impedance analyzer

6500B (Wayne Kerr Electronics Ltd., West Sussex, UK) (Bansevicius *et al.* 2018).

A driving voltage of 5 V chosen for the experiment was a harmonic signal within the scanned frequency range of 10–150 kHz. The driving frequency was 93.6 kHz and vibrations were visualized with a 3D laser scanning vibrometer (Fig. 4.12).

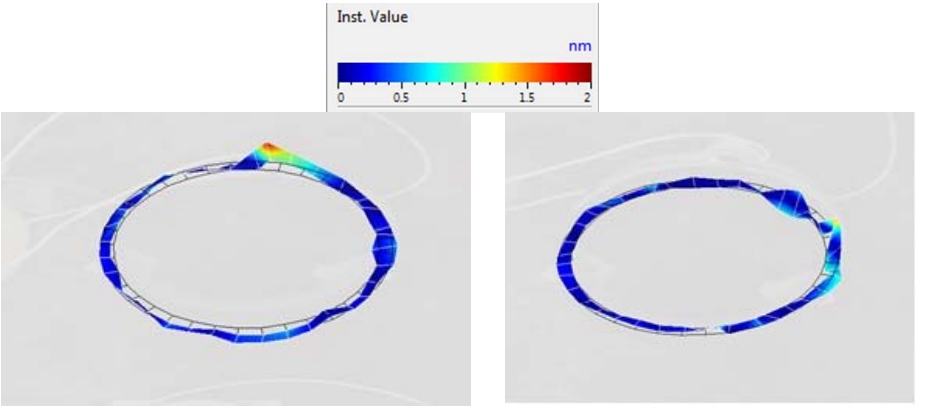

a) b)

Fig. 4.12. Deformation modes: a) the tip directed to the scanned surface; b) the tip directed backwards to the scanned surface (Bansevicius *et al.* 2018)

The area of the deflections of the top surface is about 2 times larger, when driving voltage is connected to the triangle-shaped electrode with the tip directed backwards to the scanned surface. It shows that the position of 3 contact points on each side of the cylinder should be in the middle of the triangular electrodes as it was shown in Fig. 3.2b. Dependence of the amplitude of the axial point versus applied voltage is given in Fig. 4.13.

The dashed line represents a case when the triangle-shaped electrode with the tip directed to the active contacting element is excited. The solid line represents the case when the triangle-shaped electrode with the tip directed backwards to the active contacting element is excited. Vibration amplitude is affected by electrode configuration and the way the tip is directed. Larger amplitudes are acquired when the electrode with the tip directed backwards to the active contacting element is excited. The experimental results showed that resonant vibrations are excited at a driving frequency of 93.6 kHz as shown in Fig. 4.14.

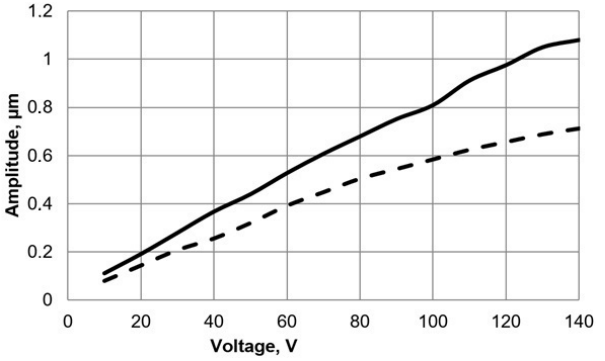

Fig. 4.13. Amplitude vs applied voltage of the axial vibrations of contacting element at the operational frequency 93.6 kHz: dashed line – when the triangle-shaped electrode tip is directed to an active contacting element; solid line – when the triangle-shaped electrode tip is directed backwards to the active contacting element (Bansevicius *et al.* 2018)

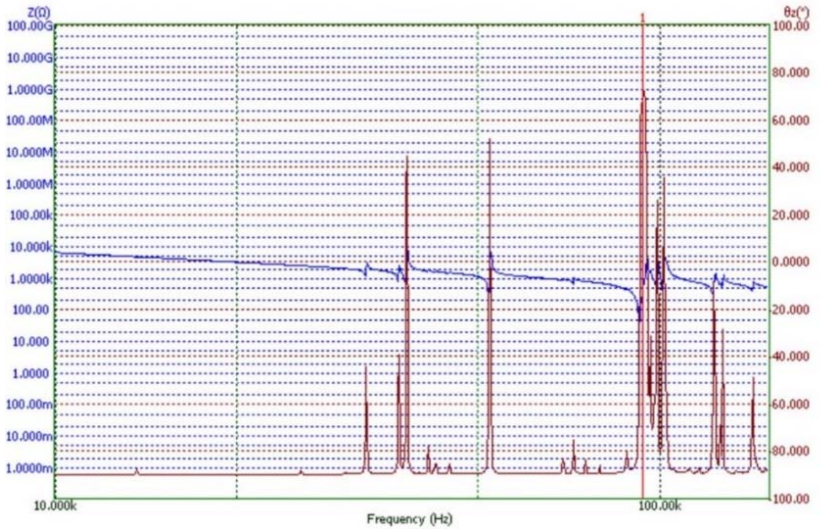

Fig. 4.14. Impedance/phase diagrams of the piezoelectric cylinder. A resonant frequency for driving a transducer is 93.6 kHz (Bansevicius R. *et al.* 2018)

These vibrations generate the lateral motion of the piezo cylinder placed on the horizontal plane. They also can generate the angular rotation of the sphere placed on 3 contact points of the piezo cylinder. Measurements of the sphere ‘s rotation angle about *X* axis are shown in Fig. 4.15.

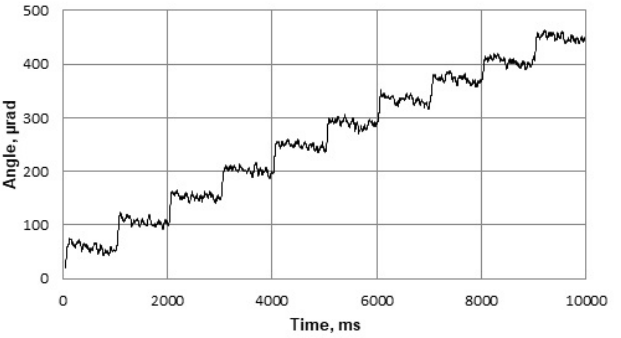

Fig. 4.15. Measured stepped rotation of the sphere (Bansevicius R. *et al.* 2018)

A case when one electrode of the cylindrical actuators was excited with the harmonic electric signal containing 10 periods was tested. The excitation frequency was 93.6 kHz, the voltage amplitude was 40 V. Such electric signal was applied in steps every second. A minimal resolution of 50 rad was obtained; average rotation speed was 42.5 rad/s. Compared to the results of FEM analysis, the difference of driving frequency differed only by 5.5% (88 361 Hz compared to 93 600 Hz). Fig. 4.16 shows how the prototype looks – a hollow sphere is placed on top of the cylindrical actuator.

Fig. 4.16. Cylindrical actuator with the sphere positioned on top

Experiments with the second kinematic pair were also conducted. Several prototypes of hemispheric actuators are given in Fig. 4.17 and Fig. 4.18.

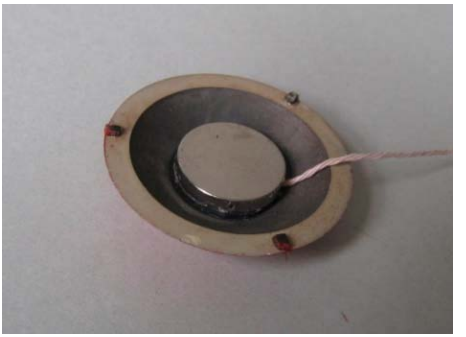

Fig. 4.17. A hemispheric actuator with a magnet attached to it

a) b)

Fig. 4.18. Prototypes of hemispheric actuators: a) hemispheric actuators with different geometrical parameters; b) hemispheric actuator with a sphere positioned on top

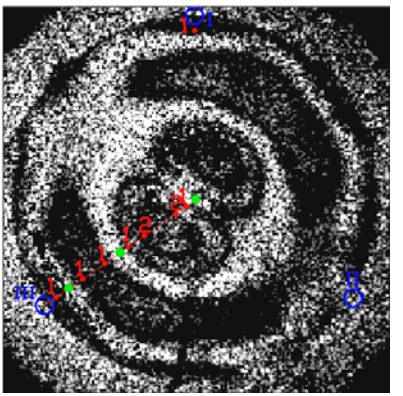

Fig. 4.19. Vibrational form of a hemispheric actuator at 42 kHz excitation

The proposed actuator rotates the sphere around three axes. The results of numerical analysis have been verified experimentally. Fig. 4.19 shows the results of interferometer. It can be seen that the form is very similar to form obtained with

numerical analysis. Resonating frequency is also very close. When one actuator is used for the rotation of the sphere, then the required working frequency is higher. In a case when sphere is rotated by two hemispheres as shown in Fig. 3.3a, the working resonant frequency is lower.

A trajectory planning algorithm has been created and tested. As with cylindrical piezoelectric actuator the trajectories of contact points were determined for every voltage pair. Both a moving on a plane piezorobot, and piezorobot for sphere rotation have been observed. The results showed that the trajectory is correct and results obtained during numerical analysis ensure a proper functioning.

4.3. Application of trajectory planning algorithm for nanosatellite swarm

The analyzed piezorobots are very compact and as results have demonstrated are also very precise, ensuring nanometric resolution. The cylindrical piezorobot can move on the plane and change the positiong of the sphere, or it can directly rotate the sphere. Through the positioning of the sphere, a nanosatellite can be stabilized and maintain its position in space. Similarly, hemispheric piezorobot can rotate the sphere and thus position the nanosatellite.

Furthermore, these piezorobots can be applied for nanosatellite swarm. Each nanosatellite would have a proposed device and all of them could be rotated to a desired direction at the same time. They could be adjusted depending on the position of Earth, each other and other celestial objects.

4.4. Conclusions of Chapter 4

1. Several different prototypes of piezorobots with mutli-degrees-of-freedom have been constructed and tested. Working frequencies that were determined during numerical analysis were very close to those during the experiment (The difference was less than 6%):
   - Frequency obtained for cylinder 32 mm (outer diameter) × 28 mm (inner diameter) × 14 mm (height) was 125 kHz (numerical analysis) and 124 kHz (experimental analysis). The difference was 0.8%.
   - Frequency obtained for cylinder 34 mm (outer diameter) × 28 mm (inner diameter) × 23 mm (height) was 74 kHz (numerical analysis) and 71 kHz (experimental analysis). The difference was 4.05%.

- Frequency obtained for cylinder 33 mm (outer diameter) × 28 mm (inner diameter) × 21 mm (height) was 50 kHz (numerical analysis) and 52.5 kHz (experimental analysis). The difference was 5%.
- Frequency obtained for cylinder 33 mm (outer diameter) × 28 mm (inner diameter) × 20 mm (height) was 88.4 kHz (numerical analysis) and 93.6 kHz (experimental analysis). The difference was 5.5%.

2. The trajectories of contact points have also been measured. The results showed that:
   - when the calculated error ε_{max} is estimated to be ±1 mm, measured error ε'_{max} acquires values ± 1.36 mm;
   - when ε_{max} is ±3 mm, measured error is $\varepsilon'_{max} = \pm 4.6$ mm.
3. Object tracking and path plotting allows to compare the mathematically calculated trajectory with the experimental trajectory. It can be seen visually that the piezorobot replicates the required trajectory.
4. The resolution and velocity of the piezorobot was measured using a 3D laser vibrometer system OFV-5000/505, impedance was measured with impedance analyzer Wayne Kerr 6500B, linear amplifier P200 was for the actuator driving. The control software is based on LabVIEW and designed to operate on industry PXI computer system. Image tracking subsystem is also based on LabVIEW, high resolution industry camera (Basler Scout SCA 1600-14 gm) is used to track the piezorobot. Interface to hardware output was set according to the technical requirements of National Instruments NI-DAQmx hardware.
5. The experimental results have shown that the proposed piezorobot's motion formation algorithm according to electrode excitation scheme is correct and such piezorobots can be successfully applied for nanosatellite stabilization. The proposed method can be successfully used for future calculations and research.

General Conclusions

1. Analysis of ultrasonic motors has shown that due to their feasible properties they are applied in various ultrasonic devices where high precision is needed. An active research of such devices is going on and ultrasonic motors have proven to be a suitable choice.
2. Analysis of satellites has shown the main problems of satellite stabilization and how piezorobots can be successfully applied for solving nanosatellite stabilization problems by decreasing the size of the object, but maintaining the required functionality. Motion formation methods for piezorobots have been presented, because traditional trajectory planning and control methods are not suitable.
3. Two piezorobots with 6 degrees-of freedom have been proposed and analyzed. The results of numerical analysis have shown that by exciting two electrodes at the same time, the piezorobot moves in a continuous trajectory or rotates the sphere. Harmonic and modal analysis were conducted in order to determine resonating frequency which results in the highest displacement amplitudes in Z direction. After analysing dynamics of 45 piezoelectric actuators with different geometric parameters, a suitable frequency range has been determined: 60 kHz–90 kHz for cylindrical actuator and 37 kHz–

55 kHz for hemispheric actuator. It has been determined that resonating frequency sometimes might not generate the largest displacements, but it should be as close as possible to the required eigenfrequency.

4. Numerical analysis has shown that a change of geometrical parameters leads to a change of sequence of eigenfrequencies. In order to avoid excitation of improper eigenfrequency, domination coefficients were calculated and a proper eigenform has been chosen. Such algorithm allows to choose proper geometrical parameters and proper eigenforms. A relation between a change of geometrical parameters and a change of required eigenfrequency have been shown – increase in height leads to a higher resonating frequency; increase in radius decreases the resonating frequency.
5. Using steps of the numerical analysis described in this thesis it is possible to determine cumulative displacement vectors at any given time when the direction and length of the force vector are known. Trajectory planning algorithm calculates the force using cumulative displacement vectors. Numerical analysis has allowed to determine the motion trajectories of contact points when the voltage is changed.
6. Experimental analysis has verified the validity of the numerical analysis. The experiments have shown that the resonating frequency differs no more than 6% between the experiment and calculations.
7. Numerical and experimental analysis have shown that piezorobots are controlled and function as desired. Their high precision and small size are a preferable choice for nanosatellite stabilization and can be successfully implemented.

References

Allegranza, C.; Gaillard, L.; Le Letty, R.; Patti, S.; Scolamiero, L.; Toso, M. 2014. Actuators for Space Applications: State of the Art and New Technologies, in *ACTUATOR 2014, 14th International Conference on New Actuators*, Bremen, 2014, 283–288.

Aoyagi, M.; Beeby, S. P.; White, N. M. 2002. A novel multi-degree-of-freedom thick-film ultrasonic motor, *IEEE Transactions on Ultrasonics, Ferroelectrics, and Frequency Control* 49(2): 151–158.

Anshul, S.; Rajeev, K.; Rahul, V.; Vishal S. C. 2015. Active vibration control of space antenna reflector over wide temperature range, *Composite Structures* 128: 291–304.

Antipov, K. A.; Tikhonov, A. A. 2014. On satellite electrodynamic attitude stabilization, *Aerospace Science and Technology* 33(1): 92–99.

Azimi, M.; Sharifi, G. 2018. A hybrid control scheme for attitude and vibration suppression of a flexible spacecraft using energy-based actuators switching mechanism, *Aerospace Science and Technology* 82–83: 140–148.

Bansevicius R.; Parkin R.; Jebb A.; Knight J. 1996. Piezomechanics as a subsystem of mechatronics: present state of the art, problems, future developments, *IEEE Transactions on Industrial Electronics* 43(1): 23–29.

Bansevicius R.; Drukteiniene A.; Kulvietis G.; Tumasonienė I. 2013. Design of mobile microrobot based on standing and travelling waves, *International Journal of Advanced Robotic Systems: Mechatronics* 10(219): 1–7.

Bansevicius, R.; Kulvietis, G.; Mazeika, D.; Drukteiniene, A.; Tumasoniene, I.; Bakanauskas, V. 2015a. The Synthesis of Trajectories in Piezoelectric Attitude Control Devices for Nanosatellites, *Journal of vibration engineering & technologies* 3(3): 345– 353.

Bansevičius R. P.; Drukteinienė A.; Jūrėnas V.; Kulvietis G.; Mažeika D. 2015b. Fine trajectory planning method for mobile piezorobots, in *12th International Workshop on Piezoelectric Materials and Applications in Actuators,* Vilnius, 2015.

Bansevicius R. P.; Mazeika, D.; Kulvietis, G.; Tumasoniene, I.; Drukteiniene, A.; Jurenas, V.; Bakanauskas, V. 2017. Investigation of sphere trajectories of a rotational type piezoelectric deflector, *Mechanical Systems and Signal Process*, 1–8.

Belokonov, I.; Ivliev, A. 2017. Development of a Propulsion System for a Maneuvering Module of a Low-orbit Nanosatellite, *Procedia Engineering* 185: 366–372.

Bergander A.; Driesen W.; Varidel T.; Breguet J. M. 2004. Monolithic piezoelectric actuators for miniature robotic systems, in *Actuator 2004, 9th International Conference on New Actuators, Bremen, Germany*, 114–117.

Bilhaut, L.; Duraffourg, L. 2009. Assessment of nanosystems for space applications, *Acta Astronautica* 65(9–10): 1272–1283.

Breguet J. M.; Pernette E.; Clavel R. 1996. Stick and slip actuators and parallel architectures dedicated to microrobotics, *Proceedings of the SPIE* 2906:13–24.

Bručas D.; Bansevičius, R.; Domeika, A.; Tomkus, V.; Bakanauskas, V. 2012. Novel attitude control devices for CubeSat satellites, *Journal of Vibroengineering* 14(3): 849.

Burton, R.; Rock, S.; Springmann, J.; Cutler, J. 2014. Dual attitude and parameter estimation of passively magnetically stabilized nano satellites, *Acta Astronautica* 94(1): 145–158.

Burton, R.; Rock, S.; Springmann, J.; Cutler, J. 2017. Online attitude determination of a passively magnetically stabilized spacecraft, *Acta Astronautica* 133: 269–281.

Cai, K.; Tian, Y.; Wang, F.; Zhang, D.; Liu, X.; Shirinzadeh, B. 2017. Design and control of a 6-degree-of-freedom precision positioning system, *Robotics and Computer-Integrated Manufacturing* 44: 77–96.

Cao, X.; Yue, C.; Liu, M. 2017. Flexible satellite attitude maneuver via constrained torque distribution and active vibration suppression, *Aerospace Science and Technology* 67: 387–397.

Carazo, A. V. 2016. Piezoelectric transformers: A Historical Review, *Actuators* 5: 12.

Chen, Y.; Liu, Q. L.; Zhou, T. Y. 2006. A traveling wave ultrasonic motor of high torque, *Ultrasonics* 44: 581–584.

Chen, J.; Xu, M. L.; Feng, B.; Tian, Q. G. 2014. A novel positioning stage using piezoelectric actuator for antenna pointing, in *Recent Advances in Structural Integrity Analysis - Proceedings of the International Congress APCFS/SIF 2014*, Sidney, 2014, 437–441.

Choi, Y. J.; Sreenivasan, S. V.; Choi, B. J. 2008. Kinematic design of large displacement precision XY positioning stage by using cross strip flexure joints and over-constrained mechanism, *Mechanism and Machine Theory* 43(6): 724–737.

Choi, K. B.; Lee, J. J.; Hata, S. 2010. A piezo-driven compliant stage with double mechanical amplification mechanisms arranged in parallel, *Sensors Actuators A: Physical* 161 (1–2): 173–181.

Doroshin, A. V. 2017. Attitude dynamics of gyrostat–satellites under control by magnetic actuators at small perturbations, *Communications in Nonlinear Science and Numerical Simulation* 49: 159–175.

Drukteiniene A. 2011. Trajectories' Formation for Mobile Multidimensional Piezorobots with Nanometer Resolution. PhD dissertation. Vilnius Gediminas Technical University, Vilnius. 150 p.

Du, Z; Shi, R.; Dong, W. 2014. A piezo-actuated high-precision flexible parallel pointing mechanism: conceptual design, development, and experiments, *IEEE Transactions on Robotics* 30(1): 131–137.

Fonseca, I. M.; Rade, A. D.; Goes, L. C. S.; Sales, T. P. 2017. Attitude and vibration control of a satellite containing flexible solar arrays by using reaction wheels, and piezoelectric transducers as sensors and actuators, *Acta Astronautica* 139: 357–366.

Gan, J.; Zhang X.; Li, H.; Wu H. 2017. Full closed-loop controls of micro/nano positioning system with nonlinear hysteresis using micro-vision system, *Sensors and Actuators A: Physical* 257: 125–133.

Gouda, Y.; Nakamura, K.; Ueha, S. 2006. A miniaturization of the multi-degree-of-freedom ultrasonic actuator using a small cylinder fixed on a substrate, *Ultrasonics* 44: 617–620.

Gozen, B. A.; Ozdoganlar, B. 2012a. A method for open-loop control of dynamic motions of piezo-stack actuators, *Sensors and Actuators A: Physical* 184: 160–172.

Gozen B. A.; Ozdoganlar B. 2012b. Characterization of three-dimensional dynamics of piezo-stack actuators, *Mechanical Systems and Signal Processing* 31: 268–283.

Guo, Z.; Tian, Y.; Liu, C.; Wang, F.; Liu, X.; Shirinzadeh, B.; Zhang, D. 2015. Design and control methodology of a 3-DOF flexure-based mechanism for micro/nano-positioning, *Robotics and Computer-Integrated Manufacturing* 32: 93–105.

Hariri, H. H.; Soh, G. S.; Foong, S. H.; Wood, K. L.; Otto, K. 2015. Miniature piezoelectric mobile robot driven by standing wave, in *14th IFToMM World Congress,* Taipei, 2015, IMD–123.

Hu, Q. 2009. A composite control scheme for attitude maneuvering and elastic mode stabilization of flexible spacecraft with measurable output feedback, *Aerospace Science and Technology* 13(2–3): 81–91.

Janschek, K.; Tchernykh, V.; Dyblenko, S. 2007. Performance analysis of opto-mechatronic image stabilization for a compact space camera, *Control Engineering Practice* 15(3): 333–347.

Kawak, B. J. 2017. Development of a low-cost, low micro-vibration CMG for small agile satellite applications, *Acta Astronautica* 131: 113–122.

Khayatzadeh, R.; Civitci, F.; Ferhanoglua, O. 2017a. A 3D scanning laser endoscope architecture utilizing a circular piezoelectric membrane, *Optics Communications* 405: 222–227.

Khayatzadeh, R.; Civitci, F.; Ferhanoglua, O. 2017b. Optimization of piezo-fiber scanning architecture for low voltage/high displacement operation, *Sensors and Actuators* 255: 21–27.

Kim, H.; Gweon, D. G. 2012. Development of a compact and long range XYθz nano-positioning stage, *Review of Scientific Instruments* 83 (8): 085102.

Kim, H.; Ahn, D. H.; Gweon, D. G. 2012. Development of a novel 3-degrees of freedom flexure based positioning system, *Rev Sci Instrum* 83 (5): 055114.

Kuang, Y. D.; He, X. Q.; Chen, C. Y.; Li, G. Q. 2009. Modelling and deformation characteristics of a circular beam with asymmetric piezoelectric actuators, *Composite Structures* 90(3): 263–269.

Kulvietis, G.; Mazeika, D.; Tumasoniene, I. 2005. The identification of resonance eigenfrequencies for multicomponent ultrasonic actuators, *WSEAS Transactions on Systems* 12 (4) 2300–2307.

Kulvietis, G.; Mazeika, D.; Tumasoniene, I. 2006. Eigenfrequency identification for optimization of multicomponent ultrasonic actuators, *WSEAS Transactions on Systems* 3(5): 558–564.

Kumar, K. D.; Tahk, J.; Bang, H. C. 2009. Satellite attitude stabilization using solar radiation pressure and magnetotorquer, *Control Engineering Practice* 17(2): 267–279.

Lavalle, S. M. 2004. *Planning Algorithms.* Cambridge University Press, 842 p.

Lee, W. H.; Kang, C. Y.; Paik, D. S.; Ju, B. K.; Yoon S. J. 2011. Butterfly-shaped ultra slim piezoelectric ultrasonic linear motor, *Sensors and Actuators A: Physical* 168(1): 127–130.

Kulvietis G. 1998. Dynamics and Control of Precision Microrobots, *Vibroengineering* Science *and Arts of Lithuania,* 322–337.

Liaw, H. C.; Shirinzadeh, B. 2010. Constrained motion tracking control of piezo-actuated flexure-based four-bar mechanisms for micro/nano manipulation, *IEEE Transactions on Automation Science and Engineering* 7(3): 699–705.

Liu, C. H.; Jywe, W. Y.; Jeng, Y. R.; Hsu, T. H.; Li, Y. T. 2010. Design and control of a long-traveling nano-positioning stage, *Precision Engineering* 34(3): 497–506.

Liu, P.; Yan, P.; Zhang, Z.; Leng, T. 2015. Modeling and control of a novel X-Y parallel piezoelectric-actuator driven nanopositioner, *ISA Trans* 56: 145–154.

Minase J.; Lu T.; Cazzolato B.; Grainger S. 2010. A review, supported by experimental results, of voltage, charge and capacitor insertion method for driving piezoelectric actuators, *Precision Engineering* 34(4): 692–700.

Nakasuka, S.; Miyata, K.; Tsuruda, Y.; Aoyanagi, Y.; Matsumoto, T. 2018. Discussions on attitude determination and control system for micro/nano/pico-satellites considering survivability based on Hodoyoshi-3 and 4 experiences, *Acta Astronautica* 145: 515–527.

Nasir, A. K.; Hulle, C.; Roth, H. 2012. Data fusion of stereo vision and gyroscope for estimation of indoor mobile robot orientation, *IFAC Proceedings Volumes* 45(4): 163–168.

Navickaitė, S.; Bansevičius, R.; Jūrėnas, V.; Bakanauskas, V.; Dragašius, E. 2015. Piezoelectric Laser Scanning/Deflecting Manipulator for Organizing the Swarm of the Nanosatellites, *Ferroelectrics* 480(1): 77–84.

Pan, C. H.; Tzou, S. S.; Shiu, R. Y. 2010. A novel wireless and mobile piezoelectric micro robot, in *2010 IEEE International Conference on Mechatronics and Automation*, Xi'an, 2010, 1158–1163.

Pan, C. H. 2016. Novel mobile piezoelectric micro robots driven by traveling wave, in *International Conference on Manipulation, Automation and Robotics at Small Scales (MARSS)*, Paris, 2016, 1–6.

Park, S.; He, S. 2012. Standing wave brass-PZT square tubular ultrasonic motor, *Ultrasonics* 52(7): 880–889.

Park, J. H.; Matsuzawa, S.; Inamori, T.; Jeung, I. S. 2018. Nanosatellite constellation deployment using on-board magnetic torquer interaction with space plasma, *Advances in Space Research* 61(8): 2010–2021.

Phylonin, O.; Belokonov, I. 2017. The Small-size Ionic-plasma Engine for Nanosatellites, *Procedia Engineering* 185: 373–379.

Pinskier, J.; Shirinzadeh, B.; Clark, L.; Qin, Y. 2018. Development of a 4-DOF haptic micromanipulator utilizing a hybrid parallel-serial flexure mechanism, *Mechatronics* 50: 55–68.

Qin, Y.; Shirinzadeh, B.; Zhang, D.; Tian, Y. 2013. Design and Kinematics Modeling of a Novel 3-DOF Monolithic Manipulator Featuring Improved Scott-Russell Mechanisms, *Journal of Mechanical Design* 135(10): 101004.

Ragulskis, K.; Bansevicius, R.; Barauskas, R.; Kulvietis, G. 1988. *Vibromotors for precision microrobots*. CRC Press. 310 p.

Renteria-Marquez, I. A.; Renteria-Marquez, A.; Tseng, B.T.L. 2018. A novel contact model of piezoelectric traveling wave rotary ultrasonic motors with the finite volume method, *Ultrasonics* 90: 5–17.

Richard, M.; Clavel R. 2011. Concept of modular flexure-based mechanisms for ultra-high precision robot design, *Mechanical Sciences, Special Issue on Future Directions in Compliant Mechanisms* 2: 99–107.

Rizzo, A.; Lemma, D. E.; Pisano, F.; Pisanello, M.; Sileo, L.; Vittorio, M.; Pisanello, F. 2018. Laser micromachining of tapered optical fibers for spatially selective control of neural activity, *Microelectronic Engineering* 192: 88–95.

Sabatini, M.; Giovanni B.; Palmerini, G. P.; Ribet, M.; Gasbarri, P.; Lampani, L. 2018. Effects of a High Fidelity Filter on the attitude stabilization of a flexible spacecraft, *Acta Astronautica* 151: 260–269.

Sairajan, K. K.; Aglietti, G. S.; Mania, K. M. 2016. A review of multifunctional structure technology for aerospace applications, *Acta Astronautica* 120: 30–42.

Sales, T. P.; Rade, D. A.; Souza, L. C. G. 2013. Passive vibration control of flexible spacecraft using shunted piezoelectric transducers, *Aerospace Science and Technology* 29(1): 403–412.

Shan, J. J.; Liu, Y.; Gabbert, U.; Cui, N. G. 2016. Control system design for nano-positioning using piezoelectric actuators, Smart Materials and Structures 25 (2): 10 pp.

Shaobo, N.; Zhang, C. 2011. Attitude determination of nano satellite based on gyroscope, sun sensor and magnetometer, *Procedia Engineering* 15: 959–963.

Shujiao, J.; Yanmin L.; Wanli Z. 2012. The design of data acquisition system based on virtual instrument, in *Proceedings of 2012 2nd International Conference on Computer Science and Network Technology,* Changchun*,* 2012, 594–597.

Sofyal, A.; Jafarov, E.M.; Wisniewski, R. 2018. Robust and global attitude stabilization of magnetically actuated spacecraft through sliding mode, *Aerospace Science and Technology* 76: 91–104.

Sumathi, S.; Surekha P. 2007. *LabVIEW Based Advanced Instrumentation Systems*. Berlin, Heidelberg: Springer. 728 p.

Tian, Y.; Shirinzadeh, B.; Zhang, D. 2010. Design and dynamics of a 3-DOF flexure-based parallel mechanism for micro/nano manipulation, *Microelectronic Engineering* 87 (2): 230–241

Tumasonienė I. 2009. Determining Eigenforms of Piezo Actuators Used in High-Precision Microrobots. PhD dissertation. Vilnius Geminimas Technical University, Vilnius. 100 p.

Tumasoniene, I.; Kulvietis, G.; Mazeika, D.; Bansevicius, R. 2007. The eigenvalue problem and its relevance to the optimal configuration of electrodes for ultrasound actuators, *Journal of Sound and Vibration* 308: 683–691.

Uchino, K.; Giniewicz, J. 2003. *Micromechatronics*. CRC Press. 504 p.

Uchino, K. 2003. *Introduction to Piezoelectric Actuators and Transducers*. International Center for Actuators and Transducers, Penn State University. 40 p.

Vasiljev, P.; Mazeika, D.; Kulvietis, G.; Vaiciuliene, S. 2006. Piezoelectric Actuator Generating 3D-Rotations of the Sphere, *Solid State Phenom* 113: 173–178.

Xu, D.; Liu, Y.; Liu, J.; Yang, X.; Chen, W. 2017. Developments of a piezoelectric actuator with nano-positioning ability operated in bending modes, *Ceramics International* 43(1): S21–S26.

Zhao, C. 2011. *Ultrasonic motors: Technologies and Applications*. Beijing: Science Press; Berlin/Heidelberg: Springer. 494 p.

Zhang, X.; Xu, Q. 2018. Design, fabrication and testing of a novel symmetrical 3-DOF large-stroke parallel micro/nano-positioning stage, *Robotics and Computer-Integrated Manufacturing* 54: 162–172.

Zheng, J.; Salton, A.; Fu, M. 2011. Design and control of a rotary dual-stage actuator positioning system, *Mechatronics* 21(6): 1003–1012.

Zheng, Y. 2017. *Space Microsystems and Micro/Nano Satellites*. Butterworth-Heinemann. 440 p.

Zhu, L.; Guo, J.; Gill, E. 2017. Review of reaction spheres for spacecraft attitude control, *Progress in Aerospace Sciences* 91: 67–86.

Zhu, W.; Yang, F.; Rui, X. 2018. Robust independent modal space control of a coupled nano-positioning piezo-stage, *Mechanical Systems and Signal Processing* 106: 466–478.

Xiang, X.; Yulie W.; Xiaomei W.; Yi, T.; Xuezhong, W. 2012. Investigation on standing wave vibration of the imperfect resonant shell for cylindrical gyro, *Sensors and Actuators A: Physical* 179: 70–77.

https://cordis.europa.eu/result/rcn/238974_en.html (last visited 2018.12.20)

https://www.pi-usa.us/fileadmin/user_upload/pi_us/files/catalogs/PI-Positioning-with-Piezo-Systems_catalog.pdf (last visited 2018.12.20)

ANSYS, Inc. *Release 11.0 Documentation for ANSYS.*

List of Scientific Publications by the Author on the Topic of the Dissertation

Publications in the reviewed scientific journals

Grybas, I.; Bansevičius, R. P.; Jūrėnas, V.; Bubulis, A.; Janutėnaitė, J.; Kulvietis, G. 2016. Ultrasonic Standing Waves-driven High Resolution Rotary Table, *Precision Engineering* 45: 396–402. ISSN: 014-6359. (IF 2.685) (Clarivate Analytics Web of Science)

Bansevičius, R. P.; Janutėnaitė-Bogdanienė, J.; Jūrėnas, V.; Kulvietis, G.; Mažeika, D.; Drukteinienė, A. 2018. Single Cylinder-type Piezoelectric Actuator with Two Active Kinematic Pairs, *Micromachines* 9(11): 597. ISSN: 2072-666X. (IF 2.480) (Clarivate Analytics Web of Science)

Bansevičius, R. P.; Drukteinienė, A.; Kulvietis, G.; Mačerauskas, E.; Janutėnaitė, J.; Mažeika, D. 2016. Fine Trajectory Planning Method for Mobile Piezorobots, *Journal of Vibroengineering* 18(4): 2043–2052. ISSN: 1392-8716. (IF 0.398) (Clarivate Analytics Web of Science)

Bansevičius, R.P.; Kulvietis, G.; Jurėnas, V.; Janutėnaitė-Bogdanienė, J. 2017. Piezoelectric Kinematic Pairs with Several DOF in Miniature High-resolution

Piezoelectric Robots, *Journal of Vibroengineering* 19(7): 5182–5190. ISSN: 1392-8716. (Clarivate Analytics Web of Science)

Janutėnaitė-Bogdanienė, J.; Mačerauskas, E.; Drukteinienė, A.; Kulvietis, G.; Bansevičius, R. P. 2017. Cylindrical Piezorobot's Trajectory Planning and Control, *Journal of Vibroengineering* 19(4): 2670–2679. ISSN: 1392-8716. (Clarivate Analytics Web of Science)

Publications in other editions

Mačerauskas, E.; Janutėnaitė-Bogdanienė, J.; Kulvietis, G. Control Methods for Piezomechanical Robots Moving in Trajectories: Software and Hardware, in *2017 Open Conference of Electrical, Electronic and Information Sciences (eStream): Proceedings of the Conference.* Vilnius: Vilnius Gediminas Technical University, 1–5. ISBN: 9781538639993.

Bansevičius, R. P.; Kulvietis, G.; Mačerauskas, E.; Janutėnaitė, J.; Drukteinienė, A.; Mažeika, D. 2016. Trajectory Planning for Stabilization System of Nanosatellite, in *Mechanika'2016: proceedings of the 21th international scientific conference*. Kaunas: Kaunas University of Technology, 22–28. ISSN: 1822-2951.

Summary in Lithuanian

Įvadas

Problemos formulavimas

Vis labiau vystantis technologijoms, spartėja ir plečiasi robotų pritaikomumas. Siekiama daugiau procesų automatizuoti, sukurti ir pagaminti robotus mažesnių matmenų, greitesnius, mažesnėmis gamybos sąnaudomis. Taikomos naujos medžiagos, valdymo būdai, technologijos, atliekami moksliniai tyrimai bandant sukurti nanorobotus. Viena iš efektyvių technologijų, taikomų nanorobotų valdymui, yra pjezokeitikliai.

Pjezoeletriniai keitikliai pasižymi dideliu tikslumu, mažu svoriu, yra kompaktiški, neturi elektromagnetinių trukdžių bei yra nesudėtingos konstrukcijos. Šiuos įrenginius ir jų pritaikomumą įvairiose srityse tyrė mokslininkai kaip Zhao C., Ragulskis K., Uschino K., Ikeda T., Tzou H. S. ir daugelis kitų. Pjezoelektriniai keitikliai plačiai taikomi pramonėje, medicinoje, automobiliuose, aviacijoje, kosmoso technologijose bei plataus vartojimo elektronikos prietaisuose. Pjezorobotai naudojami sprendžiant įvairias įrenginių valdymo ir precizinio pozicionavimo problemas. Jie gali būti sėkmingai pritaikomi nanopalydovų stabilizavimui ir pozicionavimui. Tradiciniai judesio formavimo metodai nėra tinkami pjezorobotams, todėl kyla problema kaip planuoti ir valdyti jų judesio trajektorijas.

Šiame darbe nagrinėjami daugelio laisvės laipsnių pjezorobotai neturi papildomų judesį generuojančių komponentų. Sukurti judesio formavimo algoritmai užtikrina tikslų pjezoroboto judesį.

Darbo aktualumas

Šiame darbe nagrinėjami daugelio laisvės laipsnių pjezorobotai, kurie neturi papildomą judesį generuojančių komponentų. Jie turi tik kontaktinius taškus su statine plokštuma ar objektu. Pjezoroboto judesys plokštuma arba sferos sukimas sugeneruojamas perduodant judesį kontaktiniais taškais. Žadinant vieną elektrodą išgaunamas tiesiaeigis judesys, o žadinant visus elektrodus vienu metu išgaunamas sukamasis judesys. Kuomet žadinami du elektrodai vienu metu išgaunamas tiesiaeigis tolydus judesys.

Pjezorobotai yra lengvi, pasižymintys mažomis energijos sąnaudomis bei dideliu tikslumu. Dėl šių savybių jie gali būti sėkmingai pritaikomi nanopalydovuose, kuomet reikia užtikrinti precizinį veikimą ir sumažinti aparatinės įrangos dydį. Labai svarbus ir sudėtingas uždavinys – užtikrinti, kad pjezorobotas judėtų suplanuota trajektorija. Tradiciniai trajektorijų planavimo algoritmai nėra tinkami ir reikalingas kitoks trajektorijų formavimo algoritmas. Šiame darbe pristatomi pjezorobotų judesio formavimo algoritmai, atsižvelgiant į elektrodų žadinimo schemas, užtikrina daugelio laisvės laipsnių pjezoroboto judėjimą suplanuota trajektorija.

Tyrimo objektas

Disertacijos tyrimų objektas yra pjezoroboto kontaktinių taškų judėjimo trajektorijos esant skirtingoms žadinimo schemoms.

Darbo tikslas

Šio darbo tikslas yra sukurti kelių laisvės laipsnių pjezorobotų trajektorijų valdymo algoritmą nanopalydovų stabilizavimui.

Darbo uždaviniai

Darbo tikslui pasiekti buvo sprendžiami šie uždaviniai:

1. Išanalizuoti pjezoelektrinių variklių veikimo principus, išanalizuoti jų konstrukcijas precizinių įrenginių kūrimui ir pjezorobotams.
2. Išanalizuoti palydovų stabilizavimo problemas ir daugelio laisvės laipsnių pjezorobotų taikymą nanopalydovų stabilizavimui, nustatyti judesio formavimo metodus pjezorobotams.
3. Sukurti analizuojamų kinematinių porų matematinius modelius, atlikti skaitinę analizę ir sukurti judesio formavimo algoritmus atsižvelgiant į elektrodų žadinimo schemas.
4. Atlikti eksperimentinius pjezokeitiklių dinamikos tyrimus, nustatyti kiekybines sukurtų pjezorobotų charakteristikas ir jų judesio trajektorijas, palyginti eksperimentinius rezultatus su skaitinės analizės rezultatais.

Tyrimų metodika

Darbe taikyti analitiniai, skaitiniai ir eksperimentiniai tyrimų metodai. Literatūros šaltinių analizė atlikta tiriant pjezokeitiklių veikimo principus, konstrukcijas, pjezorobotų

pritaikymą nanopalydovų stablizavimui ir pjezorobotų judesio formavimo metodus. Matematinio modeliavimo metodai buvo taikomi skaitinių algoritmų sudarymui ir analizei. Lyginamosios analizės metodai taikyti tiriant pjezoroboto kontaktinių taškų judėjimo trajektorijomis kokybines charakteristikas.

Skaitinė analizė atlikta naudojant baigtinių elementų metodą, ANSYS programinę įrangą, MATLAB programinę įrangą. Eksperimentai atlikti naudojant National Instruments LABVIEW programinę ir aparatinę įrangas, MATLAB programinę įrangą, varžos analizatorių Wayne Kerr 6500B, lazerinio vibrometro sistemą OFV-5000/505, 3D nuskaitymo vibrometras PSV-500-3D-HV, stiprintuvas P200.

Mokslinis naujumas ir jo reikšmė

Dažniausiai robotų judesio trajektorijos yra apibrėžiamos naudojant klasikinius interpoliavimo metodus. Šiais metodais aprašomos funkcijos, kuriomis apibrėžiama judančio kūno būsena bet kuriuo laiko momentu. Deja, tokie metodai nėra tinkami disertacijoje analizuojamiems pjezorobotams.

Darbe nagrinėjami daugelio laisvės laipsnių pjezorobotai neturi papildomų komponentų judesio formavimui, tik kontaktinius taškus su statine plokštuma. Tokių pjezorobotų judesio trajektorija gali būti sėkmingai valdoma sudėtingais elektriniais signalais. Darbe pasiūlytas judesio formavimo algoritmas atsižvelgiant į elektrodų žadinimo schemas, leidžia valdyti kontaktinių taškų judėjimo trajektorijas pagal suplanuotą pjezoroboto judėjimo trajektoriją. Sukurtas metodas skirtas pjezoroboto kontaktinių taškų sugeneruojamiems jėgos krypčiai ir dydžiui nustatyti. Toks sprendimas leidžia ne tik stabilizuoti nanopalydovą, bet ir palydovų spiečių.

Darbo rezultatų praktinė reikšmė

Sukurti pjezoroboto judesio formavimo algoritmai atsižvelgiant į elektrodų žadinimo schemas gali būti taikomi kitų pjezorobotų skaitinei analizei ir tyrimams.

Trijų kontaktinių taškų pjezorobotas gali būti taikomas robotų valdymui ar nanopalydovų stabilizavimui. Taikant pasiūlytus judesio formavimo algoritmus atsižvelgiant į elektrodų žadinimo schemas leidžia nustatyti ir apskaičiuoti kontaktinių taškų judesio trajektorijas bet kuriuo duotuoju laiko momentu. Tai leidžia planuoti ir valdyti pjezoroboto judesio trajektorijas. Tokie pjezorobotai gali būti pritaikomi pozicionavimo įrenginiuose ar nanopalydovuose.

Gauti tyrimų rezultatai taikyti LMT aukštųjų technologijų projekte “Naujos straublio tipo robotų klasės sukūrimas, teorija ir tyrimai (SmartTrunk)” (No. DOTSUT-234 ir No. MIP-084/2015). Projekto vadovas prof. habil. dr Ramutis Bansevičius.

Darbo rezultatų aprobavimas

Disertacijos tema yra paskelbti 7 moksliniai straipsniai: 5 – mokslo žurnaluose, esančius “Clarivate Analysis Web of Science” duomenų bazėse ir 2 – “Clarivate Analysis Web of Science” Conference Proceedings duomenų bazėse.

Disertacijos atliktų tyrimų rezultatai buvo paskelbti dviejose mokslinėse konferencijose:

- Respublikinėje konferencijoje “Mechanika” 2016 m. Kaunas, Lietuva.
- Tarptautinėje konferencijoje Open Conference of Electrical, Electronic and Information Sciences (eStream) 2017 m. Vilnius, Lietuva.

Ginamieji teiginiai

1. Pjezorobotai su cilindriniais ir hemisferiniais pjezokeitikliais yra tinkami sprendžiant nanopalydovų stabilizavimo problemas.
2. Skaitinė analizė patvirtino pasiūlyto matematinio modelio tinkamumą pjezorobotų dinamikos analizei.
3. Cilindrinio ir hemisferinio pjezokeitiklių skaitinės analizės rezultatai sutampa su eksperimentinio tyrimo rezultatais.

Disertacijos struktūra

Darbą sudaro bendroji charakteristika, keturi pagrindiniai skyriai, išvados, literatūros sąrašas, autoriaus publikacijų disertacijos tema sąrašas ir trys priedai. Disertacijos apimtis (be priedų) – 98 puslapiai, 18 formulių, 64 iliustracijos ir 6 lentelės.

1. Precizinių daugialaipsnių variklių analizė

Pirmajame disertacijos skyriuje atlikta literatūros šaltinių apžvalga apie pjezokeitiklių veikimo principus, jų konstrukcijas. Pjezokeitiklių veikimas pagrįstas atvirkštiniu pjezoefektu, kai kūne yra sužadinami virpesiai, kuriais išgaunamas judesys. Pjezokeitikliai klasifikuojami pagal bangų sklidimo metodą, virpesių rūšį, judesio tipą, pagal sąveiką su kitais sistemos komponentais ir t.t. Pjezokeitikliams dažniausiai naudojami pjezokeraminiai kompozitai, jų parinkimas priklauso nuo to, kokioje aplinkoje, įrenginyje naudojami pjezokeitikliai. Darbų analizė parodė, kad kuo daugiau laisvės laipsnių turi sistema, tuo sudėtingesnis mechanizmas ir jo valdymas bei didesni gabaritai. Ir nors pasiekiamas reikiamas tikslumas, norima, kad tokie įrenginiai būtų mažesni. Tai ypač svarbu kosmoso technologijose, kuomet reikia sumažinti kosminio įrenginio dydį ir kaštus, neigiamai nepaveikiant jo funkcionalumo. Minėtam tikslui pasiekti taikomi pjezokeitikliai, kurie neturi papildomų komponentų ir reikiamas judesys sukuriamas sužadinant virpesius ir valdant pjezokeraminio komponento deformacijas ir, atitinkamai, kontaktinių taškų judėjimą.

2. Pjezorobotų taikymas nanopalydovų stabilizavimui

Šiame skyriuje pristatomos ir analizuojamos palydovų stabilizavimo problemos. Vykstantys intensyvūs tyrimai kosmoso technologijų srityje skatina ieškoti vis naujų būdų kaip sumažinti įrangos matmenis. Darbų analizė parodė, kad tam yra tinkami pjezoelektriniai keitikliai bei pjezorobotai. Dažniausiai pjezoroboto judesys plokštuma arba sferos sukimas sugeneruojamas perduodant judesį kontaktiniais taškais.

Palydovai yra veikiami išorinių ir vidinių jėgų, kurios gali sukelti trikdžius ir turėti neigiamos įtakos jo padėčiai žemės ar kito dangaus kūno atžvilgiu. Iš visų išmaniųjų

medžiagų, pjezoelektriniai keitikliai laikomi labiausiai išvystyta technologija kosmoso įrenginiams ir konstrukcijoms. Jie naudojami nukreipimo mechanizmuose (ARTEMIS, PHARAO, EARTHCARE, SOHO), lazerio valdyme (AEOLUS, PHARAO, EARTH-CARE, SWARM), optinis vėlinimas linijoje (LISA-PF), mikrovirpesių šalinimui (PICARD, Solar orbiter), įrankiams (ROSETTA, MISSE7, CURIOSITY) ir t.t.

Darbe nagrinėjamų pjezorobotų judesys perduodamas per kontaktinius taškus. Judesio trajektorijos vaikščiojantiems robotams, kuriems judesys perduodamas per kontaktinius taškus, sudaromos naudojant polinominę interpoliaciją, splainus ar Cornu spiralę. Nagrinėjamų pjezorobotų judesys yra sukeliamas žadinant elektrodus. Kuomet žadinamas vienas elektrodas, sukuriamas tiesiaeigis judesys, judėjimo trajektorija yra laužtė. Nors toks algoritmas neužtikrina visiškai tikslios trajektorijos, tačiau pjezorobotą lengva valdyti (Bansevicius *et al.* 2016a). Kai vienu metu žadinami visi trys elektrodai, sukuriama bėganti banga ir pjezorobotas sukasi apie Z ašį. Trajektorijų planavimo algoritmas, aprašantis pjezoroboto judėjimą, žadinant 2 elektrodus vienu metu, aprašytas (Bansevicius *et al.* 2018). Šio algoritmo jėgų atstojamosios ir jos komponenčių, veikiančių kontaktiniuose taškuose schema pateikta S.2.1 paveiksle. Uždavinys tampa dar sudėtingesnis, kai norime sukurti pjezorobotą, kuris gali ir judėti plokštuma, ir sukti sferą (Bansevicius et al. 2018). Šiam atvejui naudojama trikampė elektrodų schema, žadinami 2 elektrodai vienu metu. S.2.2a paveiksle pateikta tokio pjezoroboto judėjimo trajektorija plokštuma, o S.2.2b paveiksle – sferos judėjimo trajektorija).

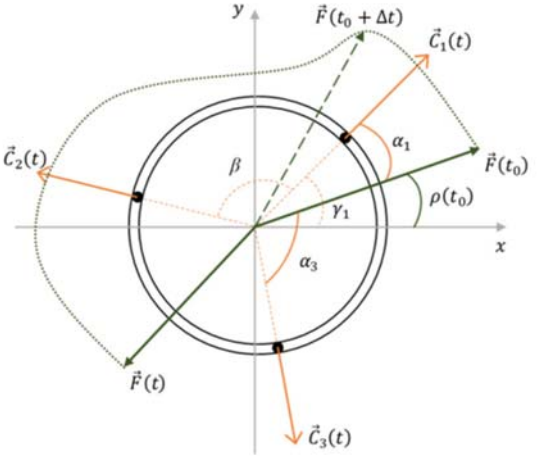

S.2.1 pav. Jėgų atstojamosios $\vec{F}(t)$ ir jos komponenčių $\vec{C_j}(t)$, veikiančių kontaktiniuose taškuose schema, j - elektrodo numeris (Bansevicius *et al.* 2016a)

Tokio pjezoroboto pagrindinis privalumas – sferos pozicionavimas gali būti atliekamas keičiant cilindro padėtį plokštumoje. Sukurta prototipinė valdymo sistema (Mačerauskas *et al.* 2017), kuri leistų užtikrinti reikiamą pjezoroboto judėjimą. Valdymo sistemos pavyzdys pateiktas S.2.3 paveiksle.

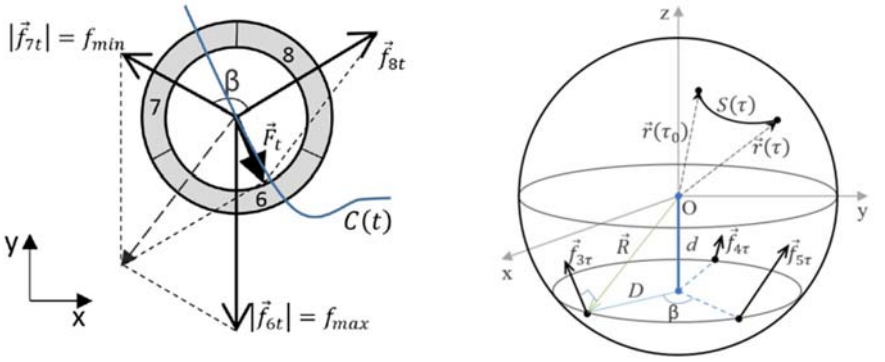

a) b)

S.2.2 pav. Judėjimo trajektorijos: a) cilindro judėjimo trajektorija; b) sferos sukimosi trajektorija (Bansevicius *et al.* 2018)

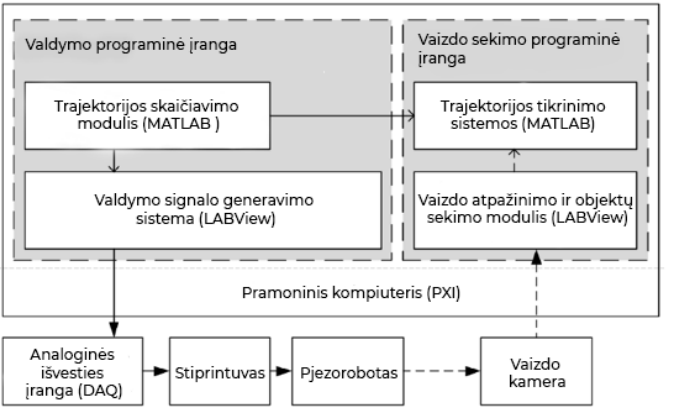

S.2.3 pav. Pjezoroboto valdymo ir trajektorijos tikrinimo sistemos struktūra (Janutenaite-Bogdaniene *et al.* 2017)

Valdymo signalo formavimas ir vaizdų apdorojimo sistema leidžia sekti pjezoroboto judėjimą. Pjezorobotas juda ant stiklinės platformos ir yra stebimas osciloskopu. Vaizdo kamera fiksuoja pjezoroboto judėjimą ir šie skaitmeniniai duomenys yra analizuojami su LabVIEW vaizdų apdorojimo programine įranga (Janutenaite Bogdaniene et al. 2017).

3. Pjezoroboto, naudojamo nanopalydovų stabilizavimui, matematinis modelis

Šioje darbo dalyje pristatomi ir analizuojami daugelio laisvės laipsnių pjezokeitikliai skirti nanopalydovų stabilizavimui. Cilindriniam pjezokeitiklio (S.3.1 pav.) judesiui išgauti naudotos 2 skirtingos žadinimo schemos (S.3.2 pav.), hemisferiniam pjezokeitikliui viena

schema (S.3.3c pav.). Cilindrinį pjezokeitiklį sudaro kinematinė pora pavaizduota S.3.1a paveiksle, hemisferinį pjezokeitiklį – dvi kinematinės poros, pavaizduotos S.3.3a paveiksle.

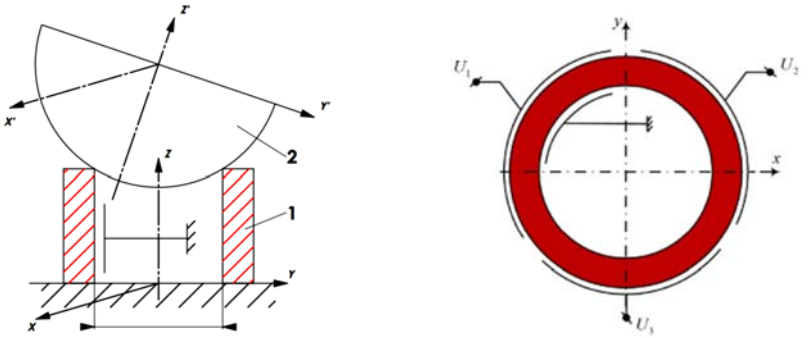

a) b)

S.3.1 pav. Cilindrinis pjezokeitiklis: a) nagrinėjama kinematinė pora; b) elektrodų konfigūracija

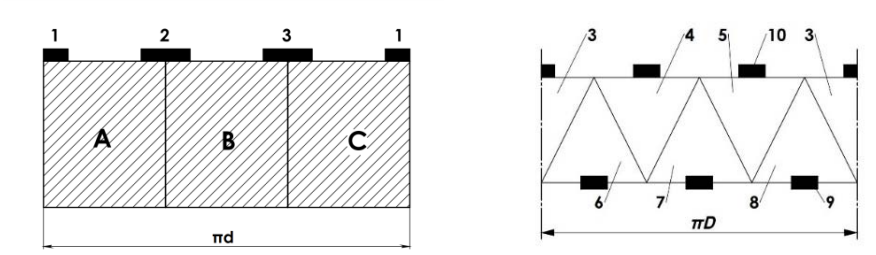

a) b)

S.3.2 pav. Elektrodų konfigūracijos: a) stačiakampė; b) trikampė

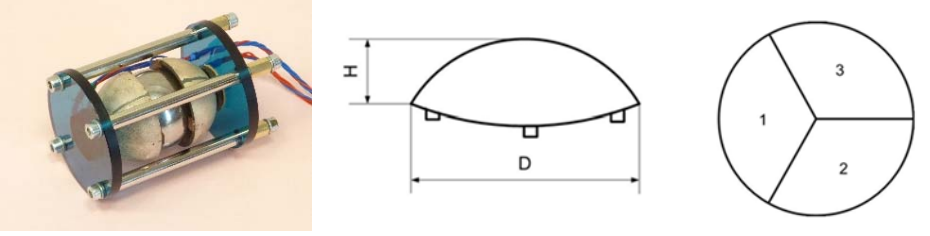

a) b) c)

S.3.3 pav. Nagrinėjama kinematinė pora ir elektrodų konfigūracija (hemisferinis pjezokeitiklis): a) nagrinėjamos dvi kinematinės poros – 2 hemisferos ir 1 sfera; b) hemisferinio pjezokeitiklio vaizdas iš šono; c) 1, 2, 3 – sferos paviršiuje išdėstyti elektrodai

Skaitinis modeliavimas atliktas vienu metu skirtingomis įtampomis žadinant 2 elektrodus, tuomet paskaičiuojamos kontaktinių taškų judėjimo trajektorijos. Darbe pateikiamas kontaktinių taškų judesio formavimo algoritmas, atsižvelgiant į elektrodų žadinimo schemas. Pirmajam pjezokeitikliui pasirinktos PZT-4 ir PZT-8 medžiagos, ant cilindro viršaus uždėta feromagnetinė sfera. Išorinis cilindro paviršius padengtas elektrodais, išdėstytais 120° vienas nuo kito, vidinis paviršius turi vieną elektrodą, kuris yra įžeminamas. Hemisferiniam pjezokeitikliui taikoma elektrodų schema pavaizduota S.3.3c paveiksle, pasirinkta medžiaga PZT-4.

Skaitinės analizės metu pirmiausia nustatomi tinkami geometriniai parametrai. Siekiama, kad didžiausi poslinkiai vyktų Z ašies kryptimi t.y. poslinkių amplitudės didžiausios, o antros pagal amplitudžių didumą – liestinės kontaktiniame taške kryptimi. Skaitinio modeliavimo seka, norint užtikrinti tinkamą pjezoroboto veikimą yra tokia:

- nustatyti rezonuojančius dažnius;
- apskaičiuoti dominavimo koeficientus, siekiant nustatyti tinkamas savąsias formas;
- nustatyti tinkamus geometrinius parametrus;
- nustatyti kontaktinių taškų judėjimo trajektorijas, kai elektrodai žadinami tam tikromis įtampomis;
- nustatyti kontaktinių taškų judėjimo trajektorijų kryptį;
- nustatyti tinkamas įtampų poras elektrodų žadinimui.

Pjezoelektrinio keitiklio baigtinio elemento matematinis modelis aprašomas lygtimis:

$$[\boldsymbol{M}]\{\ddot{\delta}\} + [\boldsymbol{H}]\{\dot{\delta}\} + [\boldsymbol{K}]\{\delta\} - [\boldsymbol{T}]\{\varphi\} = [\boldsymbol{F}] \tag{S.3.1}$$

$$[\boldsymbol{T}]'\{\delta\} + [\boldsymbol{S}]\{\varphi\} = \{\boldsymbol{Q}\},$$

čia $[\boldsymbol{M}], [\boldsymbol{K}], [\boldsymbol{T}], [\boldsymbol{S}]$ yra baigtinio elemento struktūrinės matricos (Kulvietis G. 1998):

$$\begin{aligned} [\boldsymbol{K}] &= \int [\boldsymbol{B}]'[\boldsymbol{c^E}][\boldsymbol{B}]\boldsymbol{dV}; \\ [\boldsymbol{T}] &= \int^{\boldsymbol{V}} [\boldsymbol{B}]'[\boldsymbol{e}]\,[\boldsymbol{C}]\boldsymbol{dV}; \\ [\boldsymbol{S}] &= \int_{\boldsymbol{V}}^{\boldsymbol{V}} [\boldsymbol{C}]'\,[\boldsymbol{\zeta^S}][\boldsymbol{C}]\boldsymbol{dV}, \end{aligned} \tag{S.3.2}$$

čia $[\boldsymbol{c^E}]$ standumo tenzorių matrica esant pastoviam elektriniam laukui, $[\boldsymbol{e}]$ – pjezoelektrinių konstantų matrica, $[\boldsymbol{\zeta^S}]$ – dielektrinių konstantų matrica esant pastovioms deformacijoms, $\{\delta\}$ – poslinių vektorius, $\{\varphi\}$ – elektrinio potencialo vektorius, $\{\boldsymbol{Q}\}$ – elektrinio krūvio vektorius. Pjezoroboto dinaminis užrašomas taip modelis (Kulvietis G. 1998):

$$P_i = \sum_{j=1}^{n} H_{ij}(q)\ddot{q}_j + \sum_{k=1}^{n}\sum_{l=1}^{n} C_{kl}^{i}(q)\dot{q}_k\dot{q}_l + g(q), \tag{S.3.3}$$

čia P_i is yra varomoji jėga jungtyje i; vektorius $\boldsymbol{q}$ apibūdina jungties koordinates; n – laisvės laipsnių skaičius. Pjezokeitiklio baigtinių elementų modelis aprašomas taip (Kulvietis G. 1998):

$$[M]\{\ddot{\delta}\} + [C]\{\dot{\delta}\} + [K]\{\delta\} = \{F(\delta, \dot{\delta}, q)\} + [L]\{u(t)\}, \quad \text{(S.3.4)}$$

čia $\{F(\delta, \dot{\delta}, q)\}$ – netiesinė kintanti laike varomoji jėga, $\{u(t)\}$ – išvesties valdymas, $\{\delta_i\} = \{\rho_i, \theta_i, z_i\}$ – mazgo *i* poslinkių vektorius cilindrinėse koordinatėse.

Dominavimo koeficientai skaičiuojami norint nustatyti tinkamus geometrinius parametrus ir rezonuojantį dažnį. Pilnutinė sistemos energija užrašoma kaip amplitudžių kvadratų suma visomis mazgo laisvės laipsnių kryptimis (Tumasoniene I. *et al.* 2007; Kulvietis G. et al. 2005; Kulvietis G. et al. 2006):

$$S_k^n = \sum_{i=1}^{r} (A_{ik}^n)^2, \quad \text{(S.3.5)}$$

čia *n* – sistemos savojo dažnio numeris*; k* – laisvės laipsnių skaičius mazge; A_{ik}^n – savosios formos vektoriaus reikšmė elementui *i*. Tuomet paskaičiuojamas santykis (Tumasoniene *et al.* 2007; Kulvietis *et al.* 2005; Kulvietis *et al.* 2006):

$$m_j^n = \frac{s_j^n}{\sum_{i=1}^{k} s_i^n}, \quad \text{(S.3.6)}$$

čia m_j^n – virpesių dominavimo koeficientas *n*-tajai savajai formai. Indeksas *j* parodo kuria kryptimi analizuojama energija yra didžiausia.

Judesys sukuriamas žadinant 2 elektrodus vienu metu. Įtampa pirmajam elektrodui yra pastovi, o antrojo keičiama. Kontaktiniai taškai juda elipsės trajektorija ir judesys perduodamas sferai. Nagrinėjamos trajektorijos, esančios plokštumoje einančioje per kontaktinį tašką, spindulį ir ašį Z. Viso sudaryta ir išnagrinėta 15 skirtingų cilindrinių pjezokeitiklių modelių, kurių aukštis bei diametrai skirtingi, o sienelės storis yra pastovus ir lygus 2.5 mm. Siekiama sužadinti tokius virpesius, kad didžiausi poslinkiai vyktų Z ašies kryptimi. Atlikta harmoninė analizė, kurios metu nustatyti rezonuojantys dažniai lemiantys didžiausias poslinkių amplitudes Z ašies kryptimi. Modalinės analizės metu nustatyti savieji dažniai, kurie atitinka dažnius atrinktus harmoninės analizės metu. Sekančiame etape apskaičiuoti dominavimo koeficientai, kurie leidžia nustatyti tinkamas savąsias formas. Tai būtina atlikti, kadangi pakeitus geometrinius parametrus, savieji dažniai gali pakeisti savo eiliškumą.

Kaip harmoninės analizės metu deformuojasi kūnas žadinant 2 elektrodus vienu metu pavaizduota S.3.4a paveiksle, S.3.4b paveiksle pavaizduota tinkama savoji forma (cilindras 14 mm × 16 mm × 21 mm). Šiuo atveju rezonuojantis dažnis buvo 80 250 Hz, o dominavimo koeficientai patvirtino, kad didžiausi poslinkiai vyksta Z ašies kryptimi ($m_2^n < m_1^n < m_3^n$). Cilindrinio pjezokeitiklio virpesių sužadinimui taikytos stačiakampė ir trikampė elektrodų schemos. Judesys sukuriamas vienu metu žadinant 2 elektrodus skirtingomis įtampomis. Pirmajam elektrodui įtampa yra visuomet pastovi ir lygi 100 V. Antrajam elektrodui įtampa kinta – 50 V, 75 V ir 100 V. Kontaktiniai taškai juda elipsės formos trajektorijomis ir suka sferą, esančią ant cilindro viršaus. Kontaktinės jėgos dydis nustatomas paskaičiuojant kontaktinių taškų atstojamojo poslinkių vektoriaus ilgį. S.3.5 paveiksle pavaizduotos kontaktinių taškų judėjimo trajektorijos 14 mm × 16 mm × 21 mm cilindrui, kai įtampų pora 100 V/50 V: a) pirmojo kontaktinio taško judėjimo trajektorija,

b) antrojo kontaktinio taško judėjimo trajektorija, c) kiekvieno kontaktinio taško poslinkių vektorius ir jų atstojamasis poslinkių vektorius.

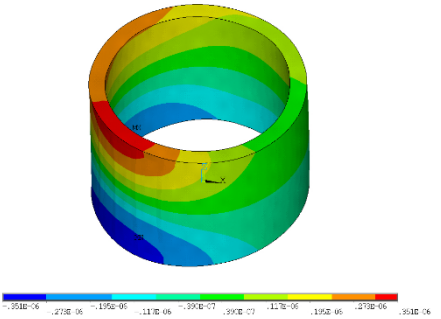

a)

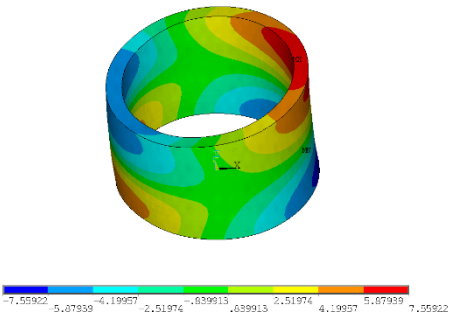

b)

S.3.4 pav. Harmoninės ir modalinės analizės rezultatai: a) rezonuojantis 80 250 Hz dažnis ir kūno deformacijos; b) tinkama savoji forma, esant 80 250 Hz rezonuojančiam dažniui

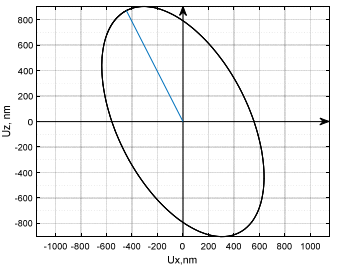

a)

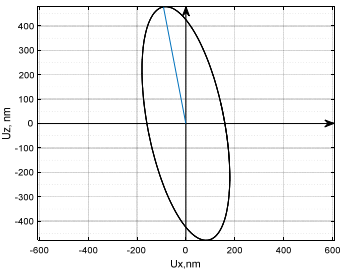

b)

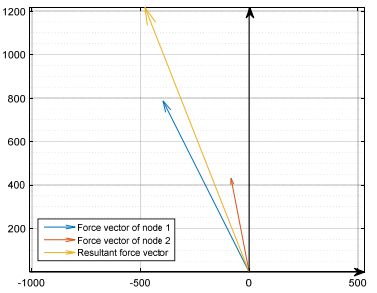

c)

S.3.5 pav. Kontaktinių taškų judėjimo trajektorijos *XZ'* plokštumoje: a) pirmojo taško; b) antrojo taško; c) atstojamasis jėgų vektorius

S.3.6a paveiksle pavaizduotos kūno deformacijos harmoninės analizės metu, S.3.6b paveiksle parodyta savoji forma ir dažnis atitinkantis harmoninės analizės metu nustatytą dažnį. Dominavimo koeficientai parodo, kad patys didžiausi poslinkiai nėra Z ašies kryptimi, tačiau forma yra tinkama. Hemisferinio pjezokeitiklio skaitinės analizės metu skaičiuojami dominavimo koeficientai negali vienareikšmiškai parodyti, kuris savasis dažnis yra tinkamas. Taip yra dėl to, kad hemisfera yra sudėtingesnis kūnas ir formos yra surištosios. Todėl paskaičiavus dominavimo koeficientus, būtina atsižvelgti į savąją forma t. y. nors Z ašies kryptimi poslinkiai gali nebūti didžiausi, tačiau gali būti tinkama savoji forma.

S.3.7 paveiksle pateiktos hemisferos 13.5 mm × 15 mm × 13 mm hemisfera kontaktinių taškų judėjimo trajektorijos, žadinant 2 elektrodus vienu metu, kai įtampų pora – 100 V/75 V: a) pirmojo kontaktinio taško judėjimo trajektorija, b) antrojo kontaktinio taško judėjimo trajektorija, c) atstojamasis poslinkių vektorius.

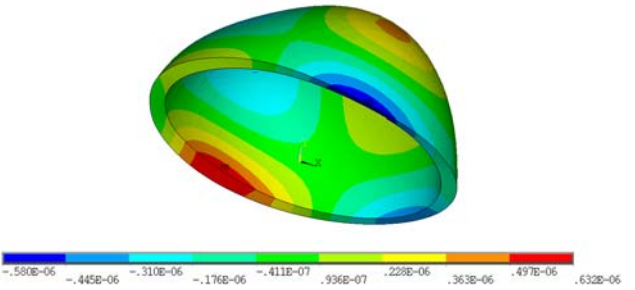

a)

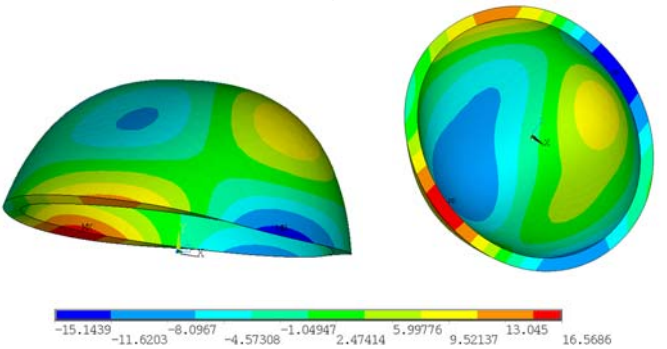

b)

$m_1^n = 0{,}207596$ $m_3^n = 0{,}376257$

$m_2^n = 0{,}416147$ $n = 18, FREQ = 37\,000\ Hz$

S.3.6 pav. Harmoninės ir modalinės analizės rezultatai: a) rezonuojantis 37 000 Hz dažnis ir kūno deformacijos; b) tinkama savoji forma, esant 37 000 Hz rezonuojančiam dažniui

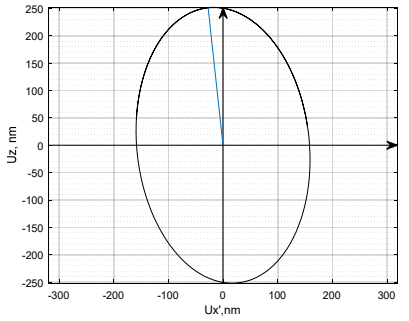

a)

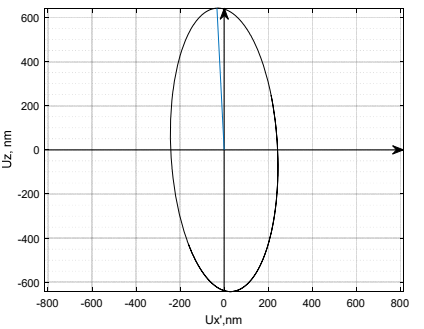

b)

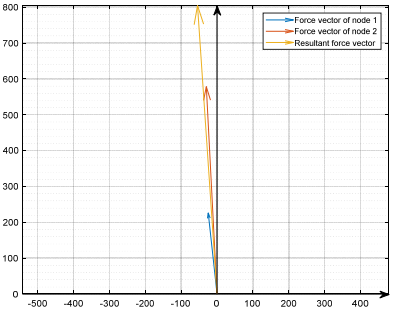

c) $r = 896.23\ nm\ \varphi = 93{,}85°$

S.3.7 pav. Kontaktinių taškų judėjimo trajektorijos *XZ'* plokštumoje ir atstojamieji jėgų vektoriai: a) pirmojo taško; b) antrojo taško; c) atstojamasis jėgų vektorius

Darbe viso išnagrinėta 30 cilindrinių pjezokeitiklių (15 taikant stačiakampę elektrodų schemą, 15 taikant trikampę elektrodų schemą) ir 15 hemisferinių pjezokeitiklių.

4. Kiekybinių charakteristikų analizė

Pjezoroboto judėjimas plokštuma ar sferos judėjimo trajektorija tiesiogiai priklauso nuo kontaktinių taškų judėjimo trajektorijų. Sėkmingam judesio valdymui užtikrinti reikia žinoti kokiomis įtampomis turi būti žadinami elektrodai ir koks yra atstojamojo poslinkių vektoriaus ilgis bei kryptis. S.4.1 paveiksle pateikta schema, kuri aprašo pjezorobotų trajektorijų planavimo problemos sudėtingumą. Kadangi vienu metu žadinami 2 elektrodai, skaičiuojamas atstojamasis poslinkių vektorius. Atstojamųjų poslinkių vektorių dydis ir kryptis nustatomi kiekvienos skaitinės analizės metu. Žinant, kokiomis įtampomis ir kada turi būti žadinami elektrodai, galima planuoti pjezoroboto judėjimą. MATLAB programinės įrangos trajektorijų planavimas yra integruotas į LabVIEW

programą. MATLAB modulis suformuoja sinusoidinį valdymo signalą, o pats signalas nustatomas pagal skaitinės analizės rezultatus. Atlikti eksperimentiniai tyrimai žadinant tiek vieną, tiek 2 elektrodus. Tyrimų rezultatai pristatyti recenzuojamuose mokslo žurnaluose (Grybas *et al.* 2016, Bansevičius *et al.* 2018, Bansevičius *et al.* 2016, Bansevičius *et al.* 2017, Janutėnaitė-Bogdanienė *et al.* 2017, Mačerauskas *et al.* 2017). Tinkami darbiniai dažniai, gauti eksperimentų metu buvo labai artimi gautiesiems skaitinės analizės metu (skirtumas buvo ne didesnis nei 6 %).

Cilindrinio pjezokeitiklio planuotos ir gautos trajektorijos pateiktos S.4.2 ir S.4.3 paveiksluose. Pjezoroboto skiriamoji geba ir greitis išmatuoti naudojant 3D lazerinę vibrometro sistemą OFV-5000/505, varža išmatuota varžos analizatoriumi Wayne Kerr 6500B, linijinis stiprintuvas P200 buvo naudotas pjezoroboto judesiui generuoti. S.4.4 paveiksle pateikta cilindrinio pjezokeitiklio virpesių vizualizacija su 3D lazeriniu vibrometru.

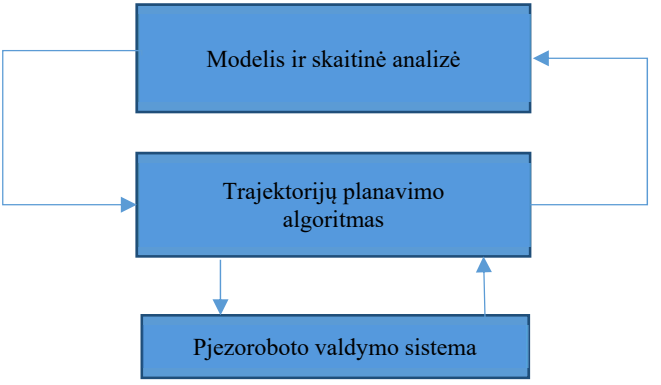

S.4.1 pav. Pjezoroboto trajektorijų planavimo schema: 1 – paskaičiuojamas reikiamo jėgos vektoriaus ilgis ir kryptis; 2 – randamas atstojamasis poslinkių vektorius; 3 – sinusoidinis valdymo dažnio signalas suformuojamas pagal skaitinės analizės rezultatus

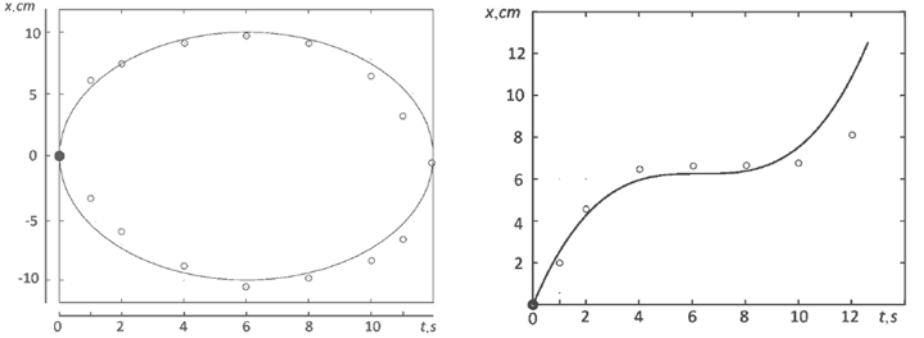

a) b)

S.4.2 pav. Pjezoroboto trajektorijos: a) elipsės trajektorija; b) kreivės trajektorija, čia ● – pradinė koordinatė, ○ – koordinatė diskrečiu laiko momentu, — – užprogramuotos koordinatės (Bansevicius *et al.* 2016a)

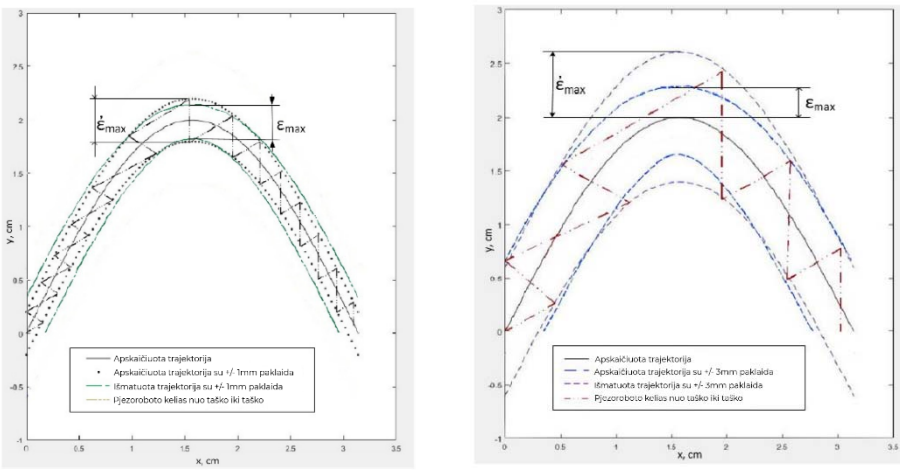

a) b)

S.4.3 pav. Pjezoroboto trajektorijos, gautos eksperimentų metu: a) ε_{max} – apskaičiuota paklaida; b) ε'_{max} – išmatuota paklaida (Janutenaite-Bogdaniene *et al.* 2017)

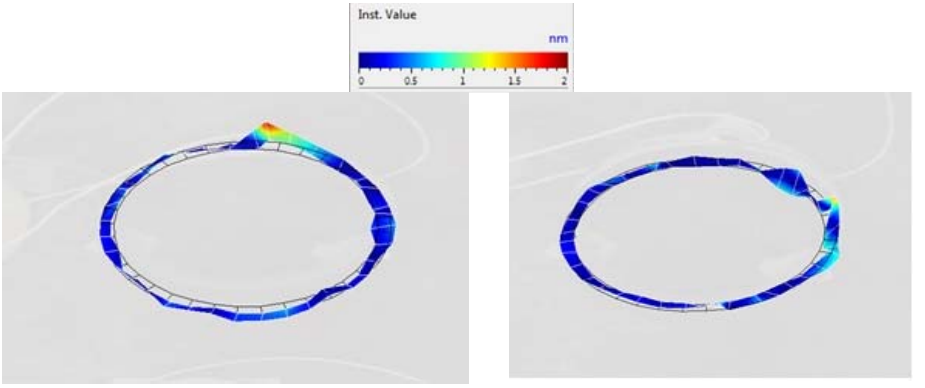

a) b)

S.4.4 pav. Deformacijų būsena: a) kontaktiniai taškai yra link analizuojamo paviršiaus; b) kontaktiniai taškai yra priešingai nuo analizuojamo paviršiaus (Bansevicius *et al.* 2018)

Taikyta trikampė elektrodų schema, S.4.4 paveiksle pateikta deformacijų būsena pjezoelektrinio cilindro krašte, esant 5 V žadinimo signalui ir 93,6 kHz darbiniam dažniui: a) žadinami elektrodai, kurių kontaktiniai taškai yra link analizuojamo paviršiaus, b) žadinami elektrodai, kurių kontaktiniai taškai yra priešingai nuo analizuojamo paviršiaus. S.4.5 paveiksle parodyta analizuojama kinematinė pora – pjezokeraminis cilindras ir feromagentinė sfera. Eksperimentai atlikti taip pat atlikti su hemisferiniu pjezokeitikliu – dvi kinematines poras sudaro hemisferos ir tarp jų esanti sfera.

S.4.5 pav. Pirmoji kinematinė pora – cilindrinis pjezokeitiklis su ant jo esančia feromagnetine sfera

Hemisferinių pjezokeitiklių prototipai pateikti S.4.6 paveiksle: a) skirtingų geometrinių parametrų pjezokeitikliai su judesį perduodančiais kontaktiniais taškais, b) hemisferinis pjezokeitiklis su ant jo uždėta sfera. Sukurti hemisferiniai pzejokeitikliai patikrinti eksperimentiškai, nustatyta kaip judesys per kontaktinius taškus perduodamas sferai.

a) b)

S.4.6 pav. Hemisferinių pjezokeitiklių prototipai: skirtingų geometrinių parametrų hemisferiniai pjezokeitikliai; b) hemisferinis pjezokeitiklis su sfera

Eksperimentų rezultatai parodė, jog pasiūlytasis pjezorobotų judesio formavimo algoritmas, atsižvelgiant į elektrodų žadinimo schemas, yra teisingas ir tokie pjezorobotai gali sėkmingai būti pritaikomi nanopalydovų stabilizavimui. Pasiūlytasis metodas gali būti naudojamas tolimesniems skaičiavimams ir tyrimams.

Bendrosios išvados

1. Pjezokeitiklių analizės metu nustatyta, kad pjezokeitikliai dėl savo išskirtinių savybių naudojami įrenginiuose, kuriuose būtinas didelis tikslumas. Kuriamų ir tiriamų tokių įrenginių analizė patvirtina pjezokeitiklių tinkamumą bei pritaikomumą.
2. Išanalizavus mokslinius šaltinius apie palydovus, nustatytos pagrindinės palydovų padėties stabilizavimo problemos. Išnagrinėtos pjezorobotų pritaikymo galimybės nanopalydovų padėties stabilizavimui, palydovo matmenų sumažinimui, išlaikant reikiamą funkcionalumą. Kadangi tradiciniai trajektorijų planavimo ir valdymo metodai nėra tinkami, nustatyti specialūs judesio formavimo metodai pjezorobotams.
3. Disertacijoje pateikti ir išanalizuoti du pjezorobotų variantai turintys šešis laisvės laipsnius. Skaitinės analizės rezultatai parodė, jog žadinant du elektrodus vienu metu, cilindrinis pjezorobotas juda plokštuma tolydžia trajektorija arba pasuka sferą, o hemisferinis pjezokeitiklis pasuka sferą. Norint nustatyti rezonuojančius dažnius, kurie lemia didžiausias poslinkių amplitudes Z ašies kryptimi, atliktos harmoninė ir modalinė analizės. Išanalizavus 45 skirtingų geometrinių matmenų pjezokeitiklių dinamiką, nustatyti tinkamų dažnių intervalai cilindriniam pjezokeitikliui 60 kHz–90 kHz, ir hemisferiniam 37 kHz–55 kHz. Nustatyta, kad rezonuojantis pjezokeitiklio dažnis ne visada lemia didžiausias poslinkių amplitudes, kadangi reikia rinktis dažnį kiek įmanoma artimą tinkamam savajam dažniui.
4. Skaitinės analizės metu nustatyta, kad keičiant pjezokeitiklio geometrinius parametrus, pasikeičia savųjų dažnių eilė. Siekiant išvengti netinkamo dažnio sužadinimo, kiekvieno pjezokeitiklio atveju apskaičiuoti dominavimo koeficientai ir parinkta tinkama pjezokeitiklio savoji forma. Nustatyta priklausomybė tarp geometrinių parametrų ir savojo dažnio pasikeitimo: didinant pjezokeitiklio aukštį savasis dažnis didėjo; didinant pjezokeitiklio spindulį savasis dažnis mažėjo.
5. Taikant disertacijoje aprašytą skaitinės analizės metodiką, galima nustatyti pjezokeitiklio kontaktinių taškų atstojamąjį poslinkių vektorių bet kuriuo laiko momentu, kai yra žinomas jėgos dydis ir kryptis. Taikant pjezoroboto trajektorijų planavimo algoritmą apskaičiuojama jėgą pagal kontaktinių taškų atstojamųjų poslinkių vektorius. Skaitinės analizės metu nustatytos kontaktinių taškų judėjimo trajektorijos keičiantis įtampai.
6. Eksperimentinės analizės rezultatai patvirtino skaitinės analizės tinkamumą pjezoroboto valdymo prognozavimui. Nustatyta, kad rezonuojantys dažniai gauti skaitinės analizės metu nesiskiria nuo eksperimentinės analizės metu gautų dažnių daugiau nei 6 %.
7. Skaitinė ir eksperimentinė analizės parodė, jog pjezorobotai yra valdomi ir veikia kaip numatyta trajektorijų planavimo algoritme. Dėl jų didelio tikslumo ir mažų matmenų pjezorobotai gali būti sėkmingai taikomi sprendžiant nanopalydovų padėties stabilizavimo problemas.

Annexes[1]

Annex A. Motion trajectories of contact points for cylindrical and hemispheric piezorobots

Annex B. MATLAB and ANSYS scripts

Annex C. Declaration of Academic Integrity

Annex D. The coauthors agreements to present publications for the dissertation defence

Annex E. Copies of scientific publications by the autor on the topic of the dissertation

[1]The annexes are supplied in the enclosed compact disc.

Jūratė JANUTĖNAITĖ-BOGDANIENĖ

CONTROL OF PIEZOROBOTS' TRAJECTORIES
FOR NANOSATELLITE STABILIZATION

Doctoral Dissertation

Technological Sciences,
Mechanical Engineering (T 009)

PJEZOROBOTŲ TRAJEKTORIJŲ VALDYMAS
NANOPALYDOVŲ STABILIZAVIMUI

Daktaro disertacija

Technologijos mokslai,
mechanikos inžinerija (T 009)

2019 10 15. 10,0 sp. l. Tiražas 20 egz.
Vilniaus Gedimino technikos universiteto
leidykla „Technika“,
Saulėtekio al. 11, 10223 Vilnius,
http://leidykla.vgtu.lt
Spausdino BĮ UAB „Baltijos kopija“
Kareivių g. 13B, 09109 Vilnius